List of contents

List of Figures

List of Tables

List of symbols

Symbols	Quantity	units
A	Amplitude	
a	Number of components	
	Defect size	mm
$\hat{a}_{dec}$	Decision threshold	-
$a_{0,..,m}$	Polynomial coefficient	-
B	Coefficient matrix	-
C	Thermal contrast	^{o}C
c_p	Heat capacity	J/kg K
$c_{p_{CFRP}}$	Heat capacity of CFRP	J/kg K
c_{p_T}	Heat capacity of teflon	J/kg K
C_1	First radiation constant	W.m^2
D	Diameter	mm
E	Residual matrix	-
e	Thermal effusivity	Ws$^{1/2}$/m^{2}K
F	Residual matrix	-
f	Frequency	Hz
f_n	nth frequency component	Hz
f_s	Sampling rate	Hz
f_c	Critical (Nyquist) frequency	Hz
f_b	Blind frequency	Hz
H	Height of the specimen	mm
h	Planck's constant	J.s
h_{conv}	Convection heat transfer coefficient	W/m^{2}K
Im	Imaginary part of the transform	-
i	Grid point (x axis)	-
j	Grid point (y axis)	-
	Imaginary number	
k	Grid point (z axis)	-
	Thermal conductivity	W/m.K
k_{CFRP}	Thermal conductivity of CFRP	W/m.K
k_T	Thermal conductivity of teflon	W/m.K
k_{xx}	Thermal conductivity (x axis)	W/m.K
k_{yy}	Thermal conductivity (y axis)	W/m.K
k_{zz}	Thermal conductivity (z axis)	W/m.K
L	Length of the specimen	mm
M	Number of vertical elements on a matrix	-
N	Number of horizontal elements on a matrix	-
	serial number of discrete data simple refractive index	
$N_{f.d}$	Number of false detected defect	-
$N_{m.d}$	Number of missed detected defect	-
$N_{r.d}$	numbers of true detected defect	-
N_t	Total number of images	-
N_x	Number of pixels per row	-

N_y	Number of pixels per column	-
n	Number of frequency component	-
	Total numbers of pixels of sound area	-
P	Loading matrix	-
Q	Thermal energy loading matrix	J
Re	Real part of the transform	-
S	Thermographic signal	-
S_a	Sound area	m^2
$\bar{S}$	Mean value of the signal	
T	Temperature score matrix	K, ^oC
T_{amb}	Ambient temperature	K, ^oC
T_c	Tanimoto criterion	
T_d	Defect area temperature	
T_{sa}	Sound area temperature	K, ^oC
T_0	Initial temperature	K, ^oC
t	Time score vector	s
t_{acq}	Acquisition (or observation) duration time	s
t'	A given value of time ranging between the time of flash pulse and the time at which the first defect becomes visible	s
u	Scan velocity	mm/s
W	Width of the specimen weights matrix	mm
X	Predictor matrix	
x	Cartesian coordinate	
x_i	Predicted value	
$x_{i,ref}$	Reference value	
Y	Matrix of responses	
y	Cartesian coordinate	
z	Depth cartesian coordinate	mm
α	Thermal diffusivity	m^2/s
β	Angle	rad, ^{o}
β_0	Intercept parameter	
β_1	Slope parameter	
γ	Angle	rad, ^{o}
δ	Thickness	mm
ε	Emissivity	
θ	Angle	rad, ^{o}
μ	Diffusion length mean	m
π	Pi	
ρ	Density	kg/m^3
ρ_{cfrp}	Density of CFRP	kg/m^3
ρ_T	Density of teflon	kg/m^3
σ	Stefan-Boltzman constant standard deviation	
φ	Phase	rad, ^{o}
φ_d	Phase of a defective pixel	rad, ^{o}
φ_s	Phase of non-defective pixel	rad, ^{o}
ω	Angular frequency (2 π f)	rad/s
Δ	Gradient (temperature or phase)	rad, ^{o}
∇	Gradient	rad, ^{o}

Acronyms

AET	Acoustic Emission Testing
CFRP	Carbon Fiber Reinforced Polymer
CFT	Continuous Fourier Transform
DAC	Differential Absolute Contrast
DFT	Discrete Fourier Transform
EOF	Empirical Orthogonal Function
ET	Electromagnetic Testing
FEM	Finite Element Method
FFT	Fast Fourier Transform
FIR	Far-Infrared
GFRP	Glass Fiber Reinforced Polymer
IR	Infrared
IRT	Infrared Thermography
LTM	Laser Testing Methods
LED	Light-Emitting Diode
LT	Lock-in Thermography
LWIR	Long-Wave-Infrared
MFL	Magnetic Flux Leakage
MLR	Multivariate Linear Regression
MWIR	Mid-Wave-Infrared
NDT	Nondestructive Testing
NDT&E	Nondestructive Testing and Evaluation
NIPALS	Nonlinear Iterative Partial Least Squares
NRT	Neutron Radiographic Testing
PC	Principal Component
PCA	Principal Component Analysis
PCT	Principal Component Thermography
PDE	Partial Differential Equation
PLSR	Partial Least Squares Regression
PLST	Partial Least Squares Thermography

PoD	Probability of Detection
PPT	Pulsed Phase Thermography
PSS	Pseudo-Static Sequence
PT	Pulsed Thermography
RT	Radiographic Testing
RMSE	Root Mean Square Error
SNR	Signal-to-Noise Ratio
SPCA	Supervised Principal Component Analysis
SVD	Singular Value Decomposition
SWIR	Short-Wave-Infrared
TSR	Thermographic Signal Reconstruction
UT	Ultrasonic Testing
VA	Vibration analysis
VT	Vibro-thermography
WT	Wavelet Transform

Introduction

Nondestructive testing (NDT) is a method of testing materials without destroying them. More specifically, these methods are used to evaluate and inspect processes and materials to identify the differences in characteristics and components for discontinuities. NDT methods are known as useful tools to determine ductility and impact resilience, fatigue strength, fracture, flaws, abnormal operations, etc. NDT is used in many industrial applications in order to evaluate the quality and integrity of components and equipment. For industrial systems, temperature monitoring is known as an important criterion to evaluate proper operation. Detection of abnormal temperature patterns is useful to avoid potential future problems [1].

In fact, various NDT and measuring techniques are applied in maintenance processes to determine equipment status and conduct repairs before a costly breakdown occurs [2]. For instance, NDT methods ensure that a large variety of equipment is maintained both safe and reliable. This includes electrical systems such as switchboards, distribution systems, mechanical systems, steam systems, boilers, motor controllers, diesel engines, power electronics, etc. [3]. The NDT technique is widely used in science and industry, especially since it has no damaging effect on materials [4, 5].

Chapters 1 and 2 presented a literature review on the popular NDT methods and their applications, Composite materials and specifications, instruments and infrared camera, and the horizons of thermography in 2050. Also, line scan thermography was introduced as an effective and fast approach to inspect the large composite material spcially in the sensitive industries such as aerospace and military. Chapter 2 is composed of a published literature review paper which was published in Quantitative Infrared Themrography Journal by Taylor & Francis Publications.

Chapter 3 presented a review on the most popular data processing algorithms in thermography applications. Thermographic signal reconstruction (TSR), Differential absolute contrast (DAC), Pulse Phase Thermography (PPT), Principal component analysis (PCA), and Partial least square Thermography (PLST) are the most important data processing algorithms which were investigated in terms of theory, application, effectiveness, properties, and advantages. Also, three evaluation criteria were introduced and investigated to evaluate and estimate the performance of data processing algorithms on the raw data.

Chapter 4 presented the step by step procedure to simulate the line scan thrermography using numerical approach in COMSOL Multiphysics. COMSOL Multiphysics employed finite element approach to solve the derivative equations. The simulation procedure includes geometry definition, material selection, mesh generation, solving, and result analysis. The most complex parts of the simulation is to define the CFRP material, light heat source, and linear motion of the source and camera. The results of 3-D simulation of line scan thermography were investigated in order to find the optimal value of the inspection parameters.

Chapter 5 investigated the performance of data processing and algorithms were evaluated and compared using Tanimoto criterion in the case of static thermography. This chapter includes a conference paper which was published in NDT in Canada 2015 Conference.

In chapter 6, the effect of different data processing algorithms in LST thermography were investigated and compared. The procedure of reconstructed raw matrix of LST was presented and used to generate the static data from LST data. The performance of of various data processing algorithms such as PPT, TSR, PCT, and PLSR were evaluated using PoD criterion. This chapter includes an original research paper which was published in the Journal of Nondestructive Evaluation (Springer).

In chapter 7, various data processing algorithms such as PPT, TSR, PCT and PLSR were employed to enhance the LST inspection quality. Different experimental data of LST was employed to evaluate the performance of data processing algorithms. To determine the performance of algorithms, signal to noise (SNR) criterion was used. This chapter includes a research paper which was published in 30th IEEE Canadian Conference on Electrical and Computer Engineering (CCECE).

In chapter 8, a systematic approach was proposed and developed to find the optimal parameters of LST inspection using a composition of analytical model, 3-D finite element simulation and experimental data. After parameter optimization, the signal to noise value was enhanced to 95%. Also, the detection depth in CFRP material increased up to 3.5 mm under the surface. This chapter includes an original research paper which was published to the Journal of Nondestructive Evaluation (Springer).

Chapter I

1.1 Infrared thermography

1.1.1 NDT methods and applications

Many useful NDT methods were introduced in the literature to detect the defects and delamination which has been used according to defect size and type, material, and defect location [6]. Some of the most commonly used NDT methods are: Acoustic Emission Testing (AET), Electromagnetic Testing (ET), Laser Testing Methods (LM), Magnetic Flux Leakage (MFL), Magnetic Particle Testing (MT), Neutron Radiographic Testing (NRT), Radiographic Testing (RT), Thermal/Infrared Testing (IR), Ultrasonic Testing (UT), Vibrothermography (VT) [7]. Among various NDT methods, infrared thermography is known as an effective technique, which is utilized on a wide range of materials. The infrared thermography has many advantages as a non-contact method, non-destructive and fast technique, does not emit any harmful radiation and etc. [8].

IR thermography is an interesting approach to analyze the thermal information obtained from a specimen. This technique detects energy emitted from the specimen under investigation and converts it to the temperature variation. The output is an image of temperature variation from the specimen. IR thermography refers to the radiations located between visible and microwave in electromagnetic bands [9-11]. Generally, IR bands are divided into four parts: short-wave-infrared (SWIR), mid-wave-infrared (MWIR), long-wave-infrared (LWIR), and Far-infrared (FIR), which are respectively from 0.75 to 3 μm, 3–5 μm, 8–12 μm, and 50–1000 μm [9]. IR radiation was unknown until more than 200 years ago when Herschel conducted the first experiment with a thermometer. He built a crude monochromator in which a thermometer was used to detect radiative energy under sunlight [12].

Infrared thermography has been divided into two main groups, which are passive and active thermography. This categorization refers to using or not using an external excitation in order to have a thermal contrast between the sound area (non-defect area) and defect area [13]. In IRT, to induce the thermal contrast, there are various types of energy sources, which can be used, in active thermography. The most common forms are divided into optical, mechanical, microwave and electromagnetic [14, 15]. In the mechanical excitation known as vibrothermography, the energy in the form of the ultrasound wave is injected into the specimen under investigation by a transducer. The energy is delivered into the specimen in the forms of Lock-in vibrothermography and burst vibrothermography [9, 14, 15]. A strong magnetic field or electric current is used in the electromagnetic testing such as eddy current testing, remote field testing, magnetic particle and ultrasonic [16]. In the microwave methods, the nondestructive testing method is applied electromagnetic wave or current signal with frequencies between a few hundred MHz and a few hundred GHz. The microwave NDT techniques are accurate, fast, low cost and the depth of penetration in non-metallic materials is high [17]. In optical methods, the energy is applied to the specimen by optical tools, via radiation heat transfer, such as photographic flashes (for heat pulsed stimulation) or halogen lamps (for periodic heating). The surface of the specimen absorbs the energy and the energy is transmited by conduction through the specimen and in the defect area. The energy propagates with a different rate of the sound area. During this time, hot or cold spots appear on the surface of the specimen [18]. Lock-in thermography uses a periodical energy to the specimen's surface. The temperature information obtained is transformed into the frequency domain [19].

In the optical class, one of the most interesting methods is pulsed thermography (PT). In this technique, energy is applied to the specimen in a short time. This time can be a few milliseconds

for high thermal conductivity materials and a few seconds for low-conductivity materials [9]. Using IR technology has many advantages such as the fact that it is a non-contact method, nondestructive and fast technique, which does not emit any harmful radiations, etc. [20, 21].

The specimen absorbs the energy of the pulse, and the surface temperature is rising while in the cooling time, the temperature of the surface will decrease uniformly in the non-defect areas and will appear abnormal temperature template in defect areas. This operation is recorded with an infrared camera. The defects which are large, and near the surface are easily observed in the raw thermal image but to detect the defects which are smaller and deeper must employ signal processing techniques [22, 23].

Automated inspection by infrared thermography provides an opportunity to optimize the inspection process especially in complex components shapes, which usually are found in the aerospace industry. Aerospace materials present great challenges because of their large surfaces and complex shapes. In the last few years, composites have been used in various fields.

1.1.2 Composite materials

A composite materials are the materials which are made from two or more constituent materials with significantly different physical or chemical properties that, when combined, produce a material with characteristics different from the individual components. Composites can be divided into two groups based on their structure: laminates and sandwich panels. Sandwich-type composites consist of two thin layers, commonly of Aluminum, fiberglass or carbon fiber, and a lightweight honeycomb core [24] and laminates are stacked and bonded fiber-reinforced sheets. These materials play a significant role in today's world due to their improved mechanical properties, such as high resistivity to fatigue and higher strength [25].

Carbon fiber reinforced polymer (CFRP) is one of the composites that is widely used for a variety of purposes such as in the aerospace field, aircraft industry, medical field, automobile industry, military and many others. CFRPs offer valuable properties to manufacture complex-shaped components with reduced manufacturing time [25-27]. Due to their interlaminar structure, CFRPs distribute the energy of the impact over a large area using a polymeric matrix. This characteristic makes them more resistant against low-velocity impacts, but it may increase the detection probability of internal defects that cannot be observed from the surface [25]. Therefore, due to the high probability of damaging composite materials, engineers must inspect and evaluate the components during the different steps of manufacturing, service, and maintenance.

1.1.3 Line scan thermography

Non-destructive testing (NDT) with infrared thermography techniques have been broadly applied to defect detection in specimens. Therefore, there is the need of advanced inspection methods that can provide results in a fast, accurate and reliable manner. Line scan thermography (LST) provides an alternative for these challenging situations. In this method – conversely, to static active thermography – the component of interest is inspected in motion and the acquired data can be organized as a pseudo-static sequence, similar to static data. LST is a dynamic active thermography technique and one of the emerging technologies aimed to solve key problems in the inspection of complex component (for instance, non-uniform heating due to the irregular shape of the surface under inspection). In LST, the inspection is performed by heating the component, line-by-line while acquiring a series of thermograms with an IR camera. The robotic arm—which carries an infrared camera and the heating source—moves along the surface while the specimen is motionless [28, 29]. The robotized LST provides some advantages in comparison to the static approaches. Robotized LST provides heating uniformity and allows image processing which enhances the

detection probability, allowing a large-scale component to be inspected without a loss of resolution. Using the LST approach, it is possible to inspect large areas at high scan speeds. Also, the inspection results are immediately available for analysis while the scanning process continues. The acquired data is then reorganized as a pseudo-static sequence (PSS) for further analysis and processing in a similar way as is done in the static configuration. Figure 1.1 illustrates a picture of the robotized line scanning setup. The infrared camera and heat source are installed on the robot arm. These components move in tandem, while the specimen remains fixed.

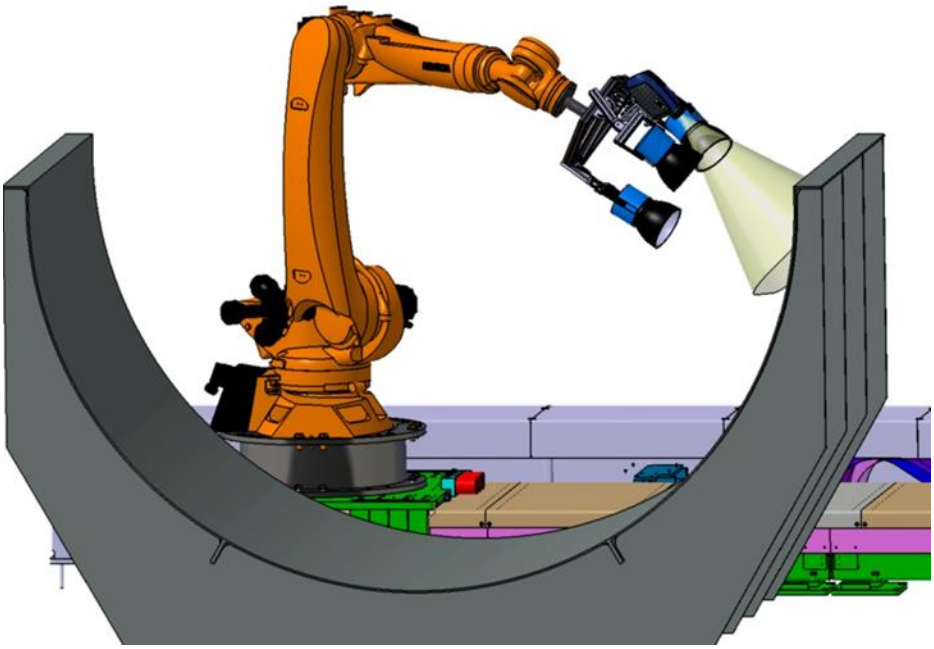

Figure 1.1: Robotized line scan thermography inspection [30]

There are numerous data processing techniques such as pulsed phase thermography (PPT) that are employed on LST thermal data in order to reduce the effects of the noise and enhance the test performance [9, 27, 31, 32], principal components thermography (PCT) [33-35], partial least squares thermography (PLST) [13, 36] and etc.

The data processing methods have advantages and disadvantages. There are some approaches to evaluate and compare these algorithms to reduce the noise such as the probability of detection (PoD), signal to noise (SNR), and etc.

In the last few years, numerical simulation has played an important role to increase the performance of NDT techniques. There are various approaches to analyze the LST method. Researchers employed analytical thermal model, finite elements method and compound methods to analyze the LST and increase the performance of the test. In this thesis, the 3D-FEM approach is used to estimate the optimum inspection parameters. COMSOL Multiphysics was the software used to model the problem and to solve the differential equations that govern the heat transfer process [37].

1.2 Research objective

The main objective of this thesis is to maximize the performance of line scan thermography for defect detection in laminated composite materials. In this project, different approaches and tools such as 3D finite elements simulation, data processing algorithms, experimental data and performance estimation criteria are employed to enhance the detection possibility in the composite material. This type of material is generally used in sensitive applications such as aerospace and military. Thus, it is very important to make an inspection with maximum reliability.

To achieve this goal, a series of specific objectives are defined which can be stated as follows:

1. Review the fundamental concepts of pulsed thermography
2. Utilization of various data processing techniques (PPT, PCA, PLS, SPCA) in order to optimize the capabilities of the LST inspection, to detect and characterize subsurface defects in laminated composites (especially in deeper defects).

3. It is important to define some criteria in order to evaluate and compare the performance of different data processing algorithms. The performance of these techniques was evaluated with the signal to noise ratio (SNR) and the probability of detection (PoD).
4. In this project, 3D simulation of composite materials and line scan thermography using COMSOL Multiphysics are used to find the optimum parameters to maximize the performance of defect detection such as scanning velocity, source, and the distance between the source and the specimen.

1.3 Thesis organization

This research concentrates to optimize the parameters of LST inspection in the case of CFRP materials. In order to achieve this objective, both theoretical and experimental approaches are employed. In the theoretical approach, the finite element model with COMSOL Multiphysics was used to simulate the LST inspection on composites. COMSOL Multiphysics was the software used to model the LST setup and to solve the differential equations that govern the heat transfer process [37]. An experimental LST inspection has been conducted in order to validate the numerical simulation and to verify the inspection parameters obtained through the finite element method (FEM) simulation. To simulate the LST inspection, the three-dimensional finite element method (3D-FEM) is employed to determine the thermal response of the composite specimen when a dynamic heat excitation is applied on its surface. The LST parameters must be adjusted to maximize the temperature variation on the material surface. COMSOL Multiphysics, was employed to model and simulate the LST inspection of the CFRP specimen. In order to simulate the LST thermography in COMSOL Multiphysics, the heat transfer module and multibody dynamics module are used. These modules allows the 3D transient energy equation to be modeled

and solved in order to obtain the temperature distribution in the CFRP specimen that contains subsurface defects.

In Chapter 1, the history of static thermography approaches was presented. An introduction to linear scan thermography and CFRP materials were presented. Also, the main and secondary objectives of this thesis were explained.

Chapter 2 provides the infrared thermography history, applications and its future horizon in the NDT is explained.

Chapter 3 presents a review of various data processing algorithms such as TSR, PCT and PLS in thermal non destructive testing and explain their theory, advantage and disadvantages. In chapter 4 presents the experimental setup and the data processing algorithms are employed on CFRP data. In this part, the Tanimoto criterion [38] was used to compare the capabilities of the different signal processing methods for qualitative defect detection.

Chapter 5 and 6 are concerned with the line scan thermography inspection and on using data processing algorithm on LST images to enhance the detection probability. In these chapter, for theoretical analysis, the LST inspection was simulated using a mathematical formulation based on the 3D heat conduction equation in the transient regime. Finally, the performance of each signal processing technique was evaluated using the POD and SNR approach.

In chapter 7, the main Ph.D. objectives are developed. The main objective of this dissertation is to maximize the performance of the line scan thermography for defect detection in laminated composite materials. In this chapter, an innovative optimization procedure has been employed using analytical model, 3-D simulation using COMSOL Multiphysics, experimental setup and signal processing algorithms. The goal is to maximize the detection depth and signal to noise value as the criteria to evaluate the inspection quality and performance. The proposed algorithm starts

by searching the optimization of the variable of the robotized LST such as scanning speed, source power and distance considering all technical and mechanical constraints.

1.4 Conclusion

In this chapter, an introduction to non-destructive test methods and the composite materials and their characteristics was presented. In the first section, a short literature review on the common NDT methods and their applications was presented. Then, the composite materials with the specifications and application was explained. Also, the most popular investigation tools to study the composite and thermal process were introduced. Line scan thermography was introduced as an effective NDT method to inspect the large composite material in the manufacturing and maintenance time. Finally, the research objectives of this thesis were explained.

Chapter II

Infrared thermography and NDT: 2050 horizon

2.1. Résumé

Dans le marché concurrentiel d'aujourd'hui, les essais non destructifs (END) jouent un rôle important pour maintenir et accroître la part de marché. Les essais non destructifs (END) sont une méthode utile pour tester les matériaux sans les détruire. Il existe de nombreux tests, qui peuvent être effectués sur des matériaux parmi lesquels nous pouvons nommer les matériaux d'évaluation, le processus d'inspection, les différences dans les caractéristiques et les composants pour les discontinuités. Ces tests sont utilisés pour identifier les propriétés des matériaux. Les tests non destructifs garantissent la sécurité, la fiabilité et la rentabilité des composants mécaniques. Cette technique est largement utilisée dans la science et l'industrie et n'a aucun effet dommageable sur les matériaux [5, 8]. Les tests non destructifs ont été divisés en deux groupes principaux: la thermographie active et la thermographie passive. Cette classification représente l'utilisation de la source de chaleur externe ou non. La thermographie infrarouge (IRT) est l'une des méthodes actives les plus courantes et les plus utiles dans les tests non destructifs grâce à ses avantages tels que la méthode sans contact, facile à utiliser, en temps réel, etc. La thermographie infrarouge est l'analyse des informations thermiques obtenues. d'un spécimen. Cette technique détecte l'énergie infrarouge émise par l'échantillon et la convertit en variation de température [13]. Cet article fournit une revue de l'histoire de l'END et de la thermographie infrarouge, et tente de montrer le futur potentiel d'IRT-NDT.

2.2. Summary

In today's competitive market, non-destructive testing (NDT) plays an important role to maintain and expand the market share. Non-destructive testing (NDT) is a valuable method of testing materials without destroying them. There are many tests, which can be performed on materials among which we can name evaluating materials, the process of inspecting, differences in characteristics, and components for discontinuities. These tests are used to identify the properties of materials. Non-destructive testing keeps the function of mechanical components safe, reliable, and cost-effective. This technique is used widely in science and industry and it does not have any damaging effect on materials [5, 8]. Non destructive testing has been divided into two main groups: active thermography and passive thermography. This classification represents the usage of the external heat source or not. Infrared thermography (IRT) is one of the most common and useful active methods in non-destructive testing due to its advantages such as non contact method, easy to use, real time and etc. Infrared thermography is the analysis of thermal information obtained from a specimen. This technique detects the infrared energy emitted from the specimen and converts it to temperature variation [13]. This paper provides a review of the NDT and infrared thermography history, and attempts to show the potential future of IRT-NDT.

Infrared thermography and NDT: 2050 horizon

Fariba Khodayar, Saeed Sojasi and Xavier Maldague

Computer vision and Systems laboratory, electrical and Computer engineering department, université laval, Quebec City, Canada

ABSTRACT

Society is changing fast, new technologies and materials have been developed which require new inspection approaches. Infrared thermography (IRT) has emerged in the recent years as an attractive and reliable technique to address complex non-destructive testing (NDT) problems. Companies are now providing turn-key IRT-NDT systems, but the question we ask now is 'What is next?'. Even though the future is elusive, we can consider the possible future developments in IR NDT. Our analysis shows that new developments will take place in various areas such as: acquisition, stimulation, processing and obviously an always enlarging range of applications with new materials which will have particular inspection requirements. This paper presents the various developments in the field of IRT which have evolved to lead to the current situation, and then examines the potential future trend in IRT-NDT.

1. Introduction

Infrared thermography (IRT) is an attractive method to analyse the thermal information obtained from a specimen. This technique detects energy emitted from the specimen under investigation and converts it to temperature variation. The output is an image of temperature variation from the specimen. IR refers to the radiations located between visible and microwave in electromagnetic bands.[1–3] Generally, IR bands are divided into four parts: short-wave-infrared (SWIR), mid-

wave-infrared (MWIR), long-wave-infrared (LWIR), and Farinfrared (FIR), which are respectively from 0.75 to 3 μm, 3–5 μm, 8–12 μm, and 50–1000 μm. [1] IR radiation was unknown until more than 200 years ago, when Herschel conducted the first experiment with a thermometer. He built a crude monochromator in which a thermometer was used to detect radiative energy under sunlight.[4]

Non-destructive testing (NDT) is a method for testing materials without destroying them. More specifically, these methods are used to evaluate and inspect processes and materials so as to identify the differences in characteristics, and components for discontinuities. The NDT methods are attractive and useful to determine ductility and impact resilience, fatigue strength, fracture, flaws, abnormal operations, etc. NDT is used in many industrial applications in order to evaluate the quality and integrity of parts and equipment. For industrial systems, temperature monitoring is known as one of the most important criteria to evaluate proper operation. Detection of abnormal temperature patterns is useful to avoid potential future problems.[5]

In fact, various NDT and measuring techniques are applied in maintenance processes to determine equipment status and conduct repairs before a costly breakdown occurs.[6] For instance, NDT methods ensure that a large variety of equipment is maintained both safe and reliable. This includes: electrical systems such as switchboards, distribution systems, mechanical systems, steam systems, boilers, motor controllers, diesel engines, power electronics, etc.[7] The NDT technique is widely used in science and industry, especially since it has no damaging effect on materials.[8,9] IR thermography is one of the useful techniques that has been used in NDT. Using IR technology has many advantages such as the fact that it is a non-contact method, non-destructive and fast technique, which does not emit any harmful radiations, etc.[10,11] The current paper will offer insight into the future developments of IR thermography based on an overview of literature from

the past to the present, including IR applications, progress and processing, and IR markets. The vision of IRT and future trends in IRT will be examined based on an overview of the developments which have led to the current situation in the field. IR thermography strives towards using equipment offering high performance, high accuracy and low cost. IR thermography may soon involve the use of robots in dangerous environments, which will be discussed as well. The new technologies and advances in IR thermography have created new markets such as: intelligent building, automotive and environment control.[12]

2. Background and history

2.1. Short history of IR thermographic technology

The development of IR began after the discovery of IR light in 1800, and the establishment of important laws such as Stefan-Boltzmann's Law and Planck's law.[13–15] After the discovery of the transistor in 1947, the emergence of the first cryogenic cooled IR detectors led to a revolution in IR thermography (typical coolant was liquid nitrogen maintained at 77 K – 196.15 °C in a Dewar vessel). These detectors were based on various technologies such as lead selenide (PbSe), lead telluride (PbTe), indium antimonide (InSb) or mercury cadmium telluride (HgCdTe) with good spectral detectivity D* (expressed in mW−1 Hz1/2) in the spectral range 3–5 μm (8–14 μm for HgCdTe).[15] Such technological development in detectors was shortly followed by the availability of the first (1965) commercial IR cameras featuring a single detector coupled to an optical-mechanical scanning mechanism to acquire the scene images. During that period, the role of IRT as an effective tool in NDT became more prominent.[16] In the 1970–1980s decades, the first bidimensional arrays were produced and cooled Focal Plane Arrays (FPA) with more pixels have started to appear on the market in the 1990s (nowadays largest arrays are 2048 × 2048). In that time, the uncooled FPA technology based on microbolometers emerged with acceptable

performances. With respect to cooled FPA IR cameras, uncooled FPA IR cameras have a lower D* (at least lower by an order of magnitude) and a lower cost since the cryogenic unit (often a stirling engine nowadays) is replaced by a cheaper temperature stabilisation heat sink (generally based on a Peltier element). The 'revolution' in thermal imaging has really been the emergence of uncooled IR arrays based on thermal detectors with the ability to work at room temperature.

Thermal detectors had been used before in scanning imagers, but they had a slow response. With a low bandwidth, these thermal detectors were useful for example for scanning 2D electronic arrays.[4] Nowadays arrays of thermal detectors achieve interesting capabilities hence opening new application prospects.

The other main technology is IR photodetector technology which underwent rapid development in the last decades of the twentieth century. Two IR detectors were especially well developed: indium antimonide (InSb) and mercury cadmium telluride (HgCdTe-based) detectors. They are now commercially available and their developments have continued to progress over the last few years.[17] Molecular beam epitaxy was used in the growth of mercury cadmium telluride (MCT) detectors in 2000. At that time, most of the published research covered two main subjects: MCT on silicon substrates and LWIR detectors. LWIR detection was an extension of SWIR and MWIR.[17,18] Towards 2010, IR community users have devoted more attention to portable equipment in the field of active thermography.[18,19] Ongoing research has improved the performance of room-temperature devices in terms of improved detectivity.[2,13] Table 1 summarises the history of IR development.

2.2. Thermography: a multifaceted technique for NDE

IRT is an engineering discipline with a combination of stimulation, acquisition, and thermal information analysis. In general IRT approaches have been divided into two main groups, which

are passive and active thermography. This categorisation refers to using or not using an external excitation in order to have a thermal contrast between the sound area (non-defect area) and defect area.[23] To induce a significative thermal contrast, various types of energy sources can be used in active thermography, the most common forms being divided into optical, mechanical (vibrothermography), and electromagnetic (microwaves, terahertz …).[23,24] There are two main classical types of active thermography techniques if we consider the way to deliver the energy, which are pulsed thermography (PT), and modulated or lock-in thermography (LT).[1]

PT is one of the most attractive and popular methods in the field of NDT. The use of PT in NDT had increased in 1996 due to progress in IR camera technology.[25–27] PT is a very fast and effective technique which utilises a high power laser, flash lamp or microwave heating source to heat the specimen in a short time. The duration of the pulse is from a few milliseconds (2–15 ms using flashes) to a few seconds (using lamps).

Modulated thermography (MT) or LT, proposed by Carlomagno and Berardi [28] was pioneered by several groups leaded by Busse [29–32] and by other groups.[33–35] Dynamic precision contact thermography was applied as a first LT technique with the temperature sensitivity below 1mK and with a spatial resolution of approximately 30 μm.[36,37] The use of LT was developed, and in 2005, frequency modulated thermal wave imaging (FMTWI) was proposed by Mulaveesala and Tuli. This approach was a combination of the advantages of modulated and pulse phase thermography (PPT) techniques. PPT is itself a combination of pulsed and LT, developed by Maldague and Marinetti in 1996. In the FMTWI method, the thermal waves stimulate the specimen in a desired range of frequencies, while the phase information from the observed thermal response is extracted.[38]

Vibro-thermography is a mechanical excitation which is also used to inspect the specimen (often metallic). In the late 80s, Hennecke et al. proposed this method and almost twenty years later, VT was propagated by several groups.[39–43] In this method, the mechanical energy is transformed into thermal energy due to the acoustical damping. A IR camera is used to measure the temperature which rises in the surface close to the defects.[44]

Table 1. the history of ir development.[20–22]

Date	IR event
1800	in england, William herschel discovers ir rays
1833	development of thermopile consisting of 10 in-line Sb-Bi thermal pairs by l. nobili and m. melloni
1835	formulation of the hypothesis that light and electromagnetic radiation are of the same nature by a. m. ampère
1859	relationship between absorption and emission by g. Kirchoff
1864	theory of electromagnetic radiation by J.C. maxwell
1873	discovery of photoconductive effect in selenium by W. Smith
1880	Study of absorption characteristics of the atmosphere through a pt bolometer resistance by S.p. langley
1883	Study of transmission characteristics of ir-transparent materials by m. melloni
1884	thermodynamic derivation of the Stefan law by l. Botzmann
1887	observation of photoelectric effect in the ultraviolet by h. hertz
1890	J. elster and h. geitel constructed a photoemissive detector consisting of an alkali-metal cathode
1894–1900	derivation of the wavelength relation of blackbody radiation by J.W. rayleigh and W. Wien
1900	discovery of quantum properties of light by m. planck
1903	temperature measurements of stars and planets using ir radiometry and spectrometry by W.W. Coblentz
1917	t.W. Case developed the first ir photoconductor from substance composed of thallium and sulphur
1930	ir direction finders based on pbS quantum detectors in the wavelength range 1.5–3.0 μm for military applications (gudden, görlich and Kutscher), increased range in World War ii to 30 km for ships and 7 km for tanks (3–5 μm)
1934	first ir image converter
1955	mass production start of ir seeker heads for ir guided rockets begins in the uSa (pbS and pbte detectors, later inSb detectors for Sidewinder rockets)
1957	discovery of hgCdte ternary alloy as ir detector material by W.d. lawson, S. nelson, and a.S. young
1961	discovery of extrinsic ge:hg and its application (linear array) in the first lWir flir systems
1977	discovery of the broken-gap type-ii inas/gaSb superlattices by g.a. Sai-halasz, r. tsu and l. esaki
1980	development and production of second generation systems [cameras fitted with hybrid hgCdte (inSb)/ Si(readout) fpas]. first demonstration of two-colour back-to-back SWir gainasp detector by J.C. Campbell, a.g. dental, t.p. lee, and C.a. Burrus
1985	development and mass production of cameras fitted with Schottky diode fpas (platinum silicide)
1990	development and production of quantum well ir photoconductor (QWip) hybrid 2nd generation systems
1995	production begins of ir cameras with uncooled fpas (microbolometer-based and pyroelectric fpas)
2000	development and production of third generation ir systems
2000–2010	multicolour functionality and other on-chip functions (mems fpas, two-colour type-ii fpas, two-colour Qdip fpas, two-colour megapixel fpas,147 megapixel fpas)
2013	on february 14 researchers developed a neural implant that gives rats the ability to sense ir light which for the first time provides living creatures with new abilities, instead of simply replacing or augmenting existing abilities

3. IR detectors

An IR detector is sensitive to IR radiation energy and reacts to this energy and converts it into a quantifiable form. A review of IR detectors indicates that there have been three significant developments in IR detectors: the first one dealt with scanning systems, the second one was staring array systems and the third involved multicolour detectors.[45] Some consequential parameters which affect the performance of IR detectors are signal to noise ratio, spectral detectivity D*, noise equivalent temperature difference, spectral response and acquisition time.[46,47] There are different types of IR detectors, which can be classified according to different criteria such as wavelength, sensitivity, power dissipation, and bandwidth.[48] A certain type of classification divides IR detectors into two general types: the first type is thermal or bolometer detectors, which are low-cost and do not depend on wavelength, but they have inferior performance with high production volume. Their cost is dependent on the cooling system to a significant extent (they are often temperature stabilised using Peltier elements). The second type is the quantum type or the photon detector that is dependent on wavelength, requires expensive cryogenic cooling mechanisms and has a lower production volume with high cost. Their sensitivity and response time are typically higher than bolometer detectors.[2,22,46,47,49,50]

3.1. Current IR detectors

Nowadays, IR detectors are based on three important technologies; one of them is MCT, an expensive technology. The indium antimonide (InSb) detector is another type of detector, which is photovoltaic, and where the indium antimonide requires periodic recalibration. The InSb detector is a function of thickness near the band edge photons and it has 100% internal quantum efficiency.[2,49,50] Quantum-well infrared photodetectors (QWIPs) represent another existing IR technology which is dependent on the wavelength range and can cover a wide range of

wavelengths. Since this technology operates at low temperature and requires cryogenic systems, it is expensive: but in comparison with MCT, it has a lower cost.[2,49–51]

3.2. Future developments

Recent research on IR thermal detector technologies has focussed on the following goals: lower cost, higher performance, larger detectivities, portable devices, the use of focal plane array to obtain the highest number of pixels, the ability to work at higher temperatures and elimination of cryogenic cooling.[2,15,49,50,52–54] One of the new technologies is quantum dot based infrared detectors (QDIPs), which perform well in the MWIR as well as the LWIR range.[55] They are very similar to QWIPs but with some advantages such as: normal incident detection, low dark current, high absorption coefficient, ability to work at higher temperatures, multicolour detection, and lower cost.[2,49,50,56,57]

Looking to the future, IR thermal detector technologies will continue to aim for higher sensitivity, higher efficiency and better performance at a lower cost. These detectors will be further developed to increase their operating temperature, reduce power dissipation and eliminate cooling system and cryogenic components. Future work will be directed towards increasing pixel density, embedding detectors with smart algorithms, improving response time, increasing spatial resolution, reducing non-uniformity and pixel size, as well as enabling multispectral capabilities. One important issue is however the (huge) investment required by the industry. In that sense we might see a reduced pace to performances related to the necessity to first provide a return on investments with the current technology.

4. Smart sensors

Smart sensors are defined as sensing elements with embedded intelligence.[58] They can perform many functions such as: data conversion, logic function, decision-making, bidirectional communication, signal detection, signal processing, and data interpretation.[58,59] Applications of smart sensors are divided into the following groups: optical sensors, IR detector arrays, accelerometers, multisensory integration, etc.[47,59]

IR thermography involves very small signals, which are very sensitive to noise.[47,59] IR temperature measurement could be combined with digital technology through smart IR sensors.[60] Smart sensors have several advantages such as: high reliability, simplified design, high performance, minimum cost and small size. Smart Sensing has led to considerable developments in consolidated Solid State Very Large Integration Microcircuits VLSI including MEMs technology [61] and in the new emerging nanotechnology. Nanotechnology allows sensors to be smaller, smarter and less costly.[61] These new sensors are being developed with carbon nanotubes, graphenes and nanoparticles.[55] Future trends in thermal detectors indicate an increasing usage of intelligent sensors. Smart sensors will be able to extract signals, conduct signal processing and select information. The Smart sensors of the future will provide higher accuracy, higher performance with increased speed at a lower cost. [47,62,63]

5. Multi-band detector

A critical issue for capability development of active and passive remote sensing in the uV to FIR spectroscopy is the development of multi-band detectors.[64] Multi-band detectors are used in numerous applications such as medical imaging, military, remote sensing, etc. A multi-band detector is formed of a stacked arrangement of different materials in which the longer wavelength detector has been located below the shorter wavelength detector. [64] The shorter wavelength

detector absorbs the shorter wavelength, and the longer wavelength detector absorbs only the longer wavelength.[64] In other words, the desired wavelength band is absorbed by a suitable detector and the rest of the spectrum, without significant losses, is transmitted to and absorbed by other appropriate detectors. Inspecting a component at various wavelengths provides more information about it and its behaviour under test conditions. In that sense, multi-band detectors enable a more complete inspection, especially when coupled with data fusion of the recorded signals.

6. Terahertz technology

Recent works in optical NDT technology have improved sensitivity, the accuracy of detection, signal multiplexing, in addition to finding solutions for eliminating electromagnetic interference. Among these advances, the term 'terahertz' (THz) has been used to refer to a part of the electromagnetic spectrum which is located between IR light and microwaves (frequency range: 300 GHz to 3 THz with corresponding wavelength range: 1 mm–100 μm). There are various THz systems which can be divided into two principal kinds: continuous wave (CW) and picosecond pulses. CW could be generated by two near IR lasers of adjacent wavelengths which are spatially overlapped. This technique has some advantages such as: high resolution, spectral selectivity, and superior signal-to-noise ratio (SNR) values.[65] Femtosecond lasers generate Pulsed terahertz radiation. The ultrashort (ultrafast) laser pulses produce a fast current transient. This laser emits electromagnetic waves in the terahertz range.[66] In the last few years, terahertz detectors and sources have been developed considerably and used as one of the new NDT technologies.

By analysing changes in the THz signal, the internal structure of the object can be determined and the defects can be identified.[67–69] In comparison to other NDT techniques, THz has the particular advantage of being able to detect internal defects in non-metallic materials. THz

radiation penetrates clothing and many other opaque materials; it is also selectively absorbed by water and organic substances. These unique qualities make THz radiation interesting and informative. When a source with a fixed-frequency and a single detector is applied, the CW terahertz does not have the capability of providing any depth, frequency-domain or time-domain information. CW imaging is less complex than a pulsed THz system, since the CW imaging does not require a pump probe system, and also it is a compact, simple system.[69] Terahertz is safe to use on living organisms (non ionising radiation) and has a shorter wavelength and higher spatial resolution than microwave radiation. It is increasingly been used in a large range of fields such as spectroscopy, medicine, NDT, chemistry, agriculture, food industry, materials science, biology and pharmacy.[69–74]

This technique has been used through fibre stretchers with kilohertz acquisition rates,[69] and also, with porous polymer fibres designed to guide terahertz radiation. One of the particularities of THz detection methods is using semiconductor quantum dot detectors to detect a single THz photon. Two detection technologies which use THz cameras have been improved in the recent years: (1) plasma-wave detectors and arrays (2) uncooled bolometer detectors and arrays.[75] In the last few years, THz has been increasingly applied in the field of NDT, for example in the aerospace industry for defect detection, and stress damage evaluation in airplanes and spacecrafts.[67]

Some companies such as Terasense and NeTHIS are developing THz technology and reaching interesting performance, simply, and in a less expensive fashion. Terasense proposes plasmonic detectors in the terahertz range which have high sensitivity and low cost.[76] The detector in the array measures the dispersion of magnetoplasma and plasma excitations (resonance) in an electron system whose edges are formed by a voltage applied to a metallic gate.[67] For generation, they use an IMPATT (IMPact ionisation Avalanche Transit-Time) diode which is a high-power diode

used in microwave electronics and sub-THz devices (frequency range 3–400 GHz). Another example of innovation is the TeraCam camera which is produced by NeTHIS. This camera is a Multispectral camera (IR and terahertz). The TeraCam has been designed for laser beam metrology, 2D and 3D imaging, and NDT of insulating materials.[77] NeTHIS uses a transfer process in which THz radiation heats a surface imaged by the IR camera, the IR camera being fitted with a 'photothermal converter' type of adapter. [78]

In the future, THz technologies will strive toward cost reduction, increased spatial resolution, with real-time capability imaging.[68,69,74,79] The development of THz technology will continue as the technology evolves to reach a certain threshold, upon which the mature technology will most certainly attract considerable attention.[80]

7. Data processing algorithms for IRT-NDT

One of the most important steps in IR imaging is data processing to extract the desired information. Data processing involves a series of advanced mathematical operations which are performed on the data to transform it into useful information. IR images are strongly influenced by vignetting, spectrometer drift, radial distortion, environment reflections, emissivity variation, non-uniform radiation, fixed pattern noise, etc.[81,82] The purpose of signal processing is to eliminate unwanted signals and noise.[83] There are many data processing algorithms and the selection of the method depends on the objectives of the research. Some of the most useful techniques are [83–97]: thermographich signal reconstruction (TSR), differential absolute contrast (DAC), pulsed phase thermography (PPT), principal component thermography (PCT), partial least square thermography (PLST), supervised principal component analysis (PCA) and machine learning techniques can be used for the inspection performance in order to detect the deeper defects in the composite material. These methods are summarised below.

Thermographic signal reconstruction (TSR) was proposed by Shepard [98]. The TSR is known as an efficient processing technique which uses PT data: a low order polynomial function is fitted over the data from PT inspection in order to reconstruct the temperature evolution. The most important advantages of using this method with respect to PT raw data is its simplicity and noise reduction capabilities (due to the fitting procedure) which lead to an improved accuracy of the quantitative data inversion, improvement of the contrast between non-defective and defective areas (thanks to its ability to produce time derivative images).[86,97,99,100] Calculation of the first and second time derivatives from synthetic data reduces blurring present in temperature raw data.[93,99,101]

DAC is also known as a classical processing technique which is generally utilised to eliminate the requirement of selecting a sound area when performing classical thermal contrast computations.[86,102] It is one of the first techniques developed as an alternative to the classical thermal contrast computations and its poor handling of non-uniform heating, emissivity variations, and environmental reactions.[91,103] The DAC method provides an alternative to the selection of a sound area temperature through the local (pixel per pixel) 1D solution of the Fourier equation for homogeneous and semi-infinite materials stimulated with a Dirac impulse. This model, in its simplest form, does not include the sample thickness. Therefore, the DAC accuracy decreases as time elapses when the heat front reaches the opposite sample face and heat losses (by convection) becomes dominant with respect to the initial heating pulse.[93,104]

One of the most popular data processing methods is the PPT method which is based on Fourier Transform (FT).[105] In a sense, PPT is a combination of PT, for which data acquisition is fast and LT, for which depth retrieval is relatively straightforward. The FT extracts thermal waves from a thermal pulse, each one at a specific frequency, amplitude, and phase delay. [88,106,107] The

FT is one of the different transform algorithms which is used to extract amplitude and phase information in PPT. It is possible to use other algorithms such as the Wavelet Transform (WT) which have additional advantages with respect to FT. The WT algorithm keeps the time information while it is lost in the FT due to the infinite nature of the sine and cosine used in the decomposition [−, +]. Wavelets are periodic waves of finite duration. They enable a better reproduction of a transient signal and usage of different scales or resolutions.[108,109] However WT requires challenging parameters to be adjusted (scaling and translation factors) precluding its spreading use. In that sense PPT is still one of the most popular approaches since results are readily obtained, directly from the FT.

PCA, was initiated by Pearson in 1901 and developed by Hotelling in 1933. It finds applications in various fields such as system and control theory, communications, face recognition, remote sensing, image compression and in fact in fields with datasets of high dimensions. PCT was derived from PCA and enables the extraction of features while reducing undesirable information in thermographic sequences. Basically, PCA decomposes the data-set in its various elements of orthogonal variance. The first element will contain the element with the highest variance, the second one with the highest variance in what is remaining, etc. For a PT experiment, the first element in the PCT decomposition will be related to the non-uniform heating.[110]

Partial least square (PLS) is a statistical decomposition method which originated from social science and was proposed by Herman Wold in the 1960s.[111] PLS enables relations to be made between sets of observed variables by means of latent variables. PLS comprises regression and classification tasks as well as dimension reduction techniques and modelling tools.[112,113] As a regression method, it seeks to model a dependent variable Y (predicted) in terms of an independent

variable X (predictor). PLS generalises and combines features of two techniques: principal component regression and multivariate linear regression. [95,114,115]

PLS thermography (PLST) decomposes the data-set similarly to PCT with the difference that the time information is kept so that the data-set can later be reconstructed from the decomposed elements (called loadings).[95] This decomposition-reconstruction process makes the PLST attractive because one can play with the loadings. For example, as for PCT, the first loading is related to non-uniform heating in PLST and can be omitted in the reconstruction process. Once reconstructed other techniques can be applied for various needs such as PPT (for quantitative inversion), DAC (defect visibility enhancement), etc. All this makes this processing technique versatile indeed.[102]

IRT-NDT data processing techniques have some advantages and limitations such as defect detection enhancement on one hand, but sometimes exhibit slow computing or require interactions with an operator to select algorithm parameters on the other hand (ex: selection of a non-defect area which could affect final results). The performance of these techniques can be evaluated quantitatively with methods such as: signal to noise ratio, Tanimoto criterion and probability of detection (PoD). PoD is very important for industry since it is a quantitative accepted measurement of reliability. In the future, these techniques will likely see enhancements while others will be proposed (such as PLST which has been known in the field of economics for decades but was only proposed recently in IR-NDT). A brief overview of these methods is provided below.

The SNR is an effective criterion to characterise the performance of signal processing techniques. using the quantification of the SNR, it is possible to analyse the relationship between the desired signal strength and the level of background noise at the maximum signal contrast. This quantification helps to determine and qualify the advantages and limitations of each processing

technique based on the inspection parameters, thermal properties of the material and aspect ratio of defects.[86,116]

The heuristic approach to qualitative defect detection can be illustrated with the so-called Tanimoto criterion which is used for data comparison.[20] The missed and false defects are combined in the Tanimoto criterion.[21] Defect detection is performed by an operator or an automatic device. Operators are guided by some heuristic rules which are not well understood even if it is clear that pixel amplitudes, defect pattern size, and shape are crucial in decision-making.[21] The PoD analysis is a quantitative measuring approach which is utilised to evaluate the inspection limit and reliability of an NDT technique. It provides the probability that a flaw of given size is detected, i.e. it could be detected reliably by the NDT technique, in given conditions.[117,118]

Quantitative extraction of information is still on the agenda in IRT and has seen considerable efforts. It is expected that advances in that direction will be achieved through the coupling of IRT image processing as described above, coupled with appropriate thermal models of the studied processes. An example was shown recently using a thermal quadrupole based model whose parameters were adjusted recursively by non-linear least square minimisation enabling the computation of local thermal diffusivity.[119]

8. IRT applications: NDT and more

In the few past years, IR thermography has been considerably developed and has found applications in analysis, detection in various fields such as medicine, industry, military, civil engineering, animal and veterinary sciences, sports, surveillance and security, etc.[120] Some of the most important applications of IR thermography include the following [121, 122]: inspections for predictive maintenance, non-destructive evaluation of thermal and mechanical properties, building science, military reconnaissance and weapons guidance, and medical imaging.

- IR thermography is widely used in NDT, both in industry and R&D, to detect a wide variety of defects. NDT and Condition Monitoring are tools used to locate defects in materials and machinery, to investigate and control materials and processes without causing any damage. The quality of engineering materials and the safety of engineering structures can be evaluated with NDT. A new trend is that NDT can also be used virtually in industry to ensure that final products do not have any defects related to possible difficulty of assembly on the production line. Virtual NDT inspection proceeds at the design stage of the component enabling the anticipation of how (well) a given part could be verified by NDT.[123] This is very important in airplanes and engines, nuclear plants, ships and satellites, etc.[122]
- For the first time, Hippocrates used the sense of touch to detect the anomalies of skin temperature for the diagnosis of a patient's pain and illness,[124] or localised the centre of a pleurisys by the obervation of the heating rate and the subsequent change of colour of a mud poultice put on the back of a patient.[125] Today, thermal imaging is used in medicine as a monitoring tool for the diagnosis of different types of diseases due to temperature change in the body's surface (i.e. the skin). It is applied to the diagnosis and monitoring of pain, human body tumours, breast cancer diagnosis, Raynaud's disease, arthritis, heart failure, chronic fatigue, stress, toxicity, etc. However medical applications of IRT are challenging due to the many factors that affect skin temperature such as: environment factors (ambient temperature, room size, atmosphere pressure, etc.), individual factors (sex, age, skin emissivity, metabolic rate, etc.), and technical factors (camera features, statistical analysis, etc.).[126] Figure 1 shows two examples of the use of IR images in the field of medicine.

- Recently, thermal imaging has been applied to measure the skin temperature of ath-letes during the matches and different types of exercise. It is useful to detect potential injuries, manage injury evolution, understand of human body thermal interactions, etc.[120,127,128]
- IR thermography is widely used in civil engineering. IR thermography is a powerful tool for the detection of defects and damage in various cases such as buildings and construction. For example, IR techniques are used to determine moisture content, to conduct quality control of buildings, to identify the exact position of heating pipes, to investigate hardened concert, etc.[131,132] In the Figure 2, the specified region near the windows in the IR image, indicate moisture penetration.

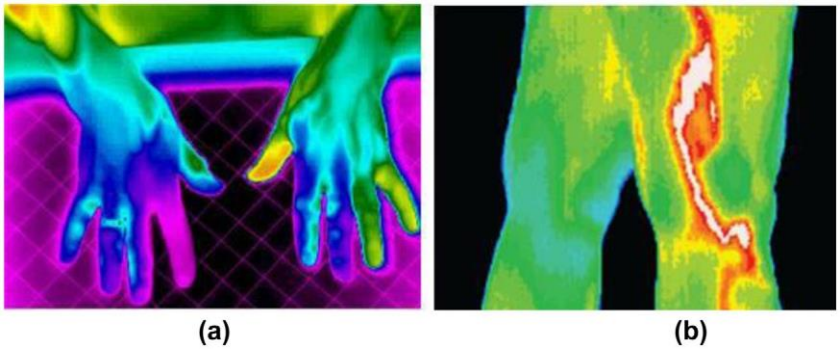

Figure 1. (a) the diagnosis of raynaud's syndrome, (b) the diagnosis of a vascular inflammatory condition. [129,130]

Figure 2. (a) a rgB photo, (b) a ir image that shows moisture penetration near the window.[133]

Figure 3. (a and b) thermal cameras show the temperature differences in race cars.[134]

- A nother recent application of IR technology is in race cars to manage the car temperatures to ensure the reliability, assess the efficiency of brakes, engine components, tyres, etc.[134] In Figure 3, the use of IR systems in racing cars is shown.

IR imaging is also used in other fields such as: in the military (military surveillance, target tracking, night vision, etc.), in industry (analysing the thermal efficiency of processes and machinery, inspection in industry, monitoring the environment, etc.), in agriculture (measuring the nitrate-state nitrogen in fresh leaves, analysis of soil nutrient status, plant growth and soil water deficit, etc.),[135,136] in the environment (to acquire information about climate, to monitor water pollution, to acquire information about landfill sites, etc.,[124] in remote sensing (to predict climate change, to locate materials, etc.), in art and cultural heritage (to preserve the state of the artefacts, to monitor musical wind instrument's temperature, to monitor the conservation status of paintings in museums over time, to detect the temperature anomalies on ancient monuments such as the pyramids of Egypt, etc.[120]), in chemical industries (to identify molecular structure and composition and their emission and absorption, etc.) [121,122] among other applications. With the falling price of IR cameras and computers even more applications of IRT will emerge, in any field where a non-contact change of temperature witnesses a phenomenon of interest. Figure 4 shows two applications of thermography technology such as the state inspection for cultural heritage (Figure 4(a)) and the monitoring of ocean features (Figure 4(b)).

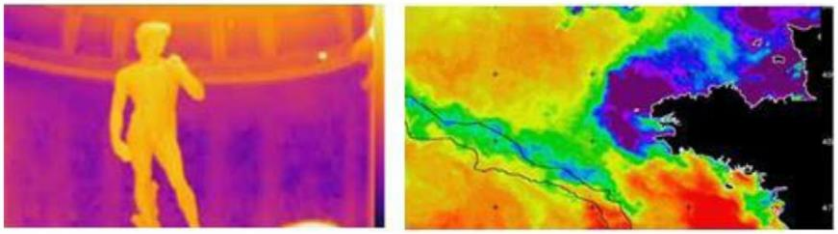

Figure 4. examples of application fields for thermography: (a) cultural heritage conservation [137]; (b) remote sensing from space.[138]

9. Recent and new IR technologies

Future IR technologies strive to develop detectors which are portable and have a high sensitivity, lower cost, high resolution, etc.[56] Some of the new systems and devices are described below.

The first is the Heat-Wave, which is a 3D device combined with a thermal camera, colour camera and a range sensor (RGB-D camera and single additional thermal camera). The fact that the Heat-Wave is a light-weight thermal IR camera is a great advantage.

All sensors in this device have a closed format and are mounted on an ergonomic handle for portable deployment.[139] The various viewpoints recorded improve the accuracy. The Heat-Wave can be used in different applications such as: energy efficiency monitoring, energy losses, mechanical and electrical assessment, construction monitoring, fire detection, first responders and non-invasive medical diagnosis, etc.[139–141] This system can also be used in NDT, since it can locate sources of energy losses in buildings and can identify faulty components with abnormal temperatures in industry.[139–141] Figure 5 shows a 3D thermal map of a chiller water pump system and a HeatWave 3D thermography device. In Figure 5(a), the top right photo shows a RGB image, the middle-right photo illustrates a thermal image, the (b) right image represents an operator working with a HeatWave 3D thermography device, and the extreme left image is a 3D thermal

map. In these applications the advantage is obviously the projection of thermal data on the 3D shape of the object, enabling a better understanding of the IR signature.

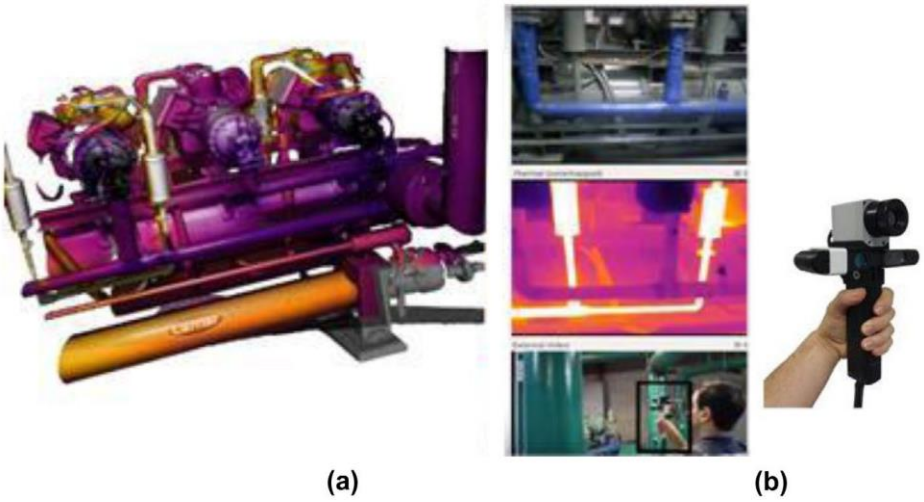

Figure 5. (a) 3d thermal map of a chiller water pump system using the iron-bow colour palette. (b) heatWave 3d thermography device.[139–142]

Other interesting systems are small low cost IR detectors.[55] One of the new areas of interest in IR technologies is the panoramic IR technology, which is designed to capture 360° images.[55] In the future, this technology could be used in low cost and low resolution systems in vehicles and boats to increase safety, especially at night or in conditions of poor visibility (smoke conditions, etc.). High-resolution systems which are more expensive would be suitable for use in ships and submarines. In a panoramic system, the frame rate is very important.[55] If the frame rate of the scanned system which rotates to provide a photo is too slow, the camera would not be able to recognise the target and enable the tracking.[55] In some instances, a ‘pyramidal-shaped’ mirror can be used in front of the IR camera to acquire a 360° image at once. Such images are however distorted and need correction before being displayed. This technology can be very useful in the field of NDT, in the field of medicine, because it can be applied to cylindrical objects and offers a global internal thermal view.

Robots have recently been combined with other IR technologies, in a variety of applications (see Figure 6). Robots can be used in automated NDT, in complex geometries, and in hazardous areas.[143] In the future, the robotic technology will produce humanoid robots, similar to the one shown in Figure 6(b) which could hold an IR camera in one hand and a heat source in the other, and inspect a variety of specimens. In the next 25 years, NDT robots will be equipped with a thermal camera, a colour camera and a range sensor in their 'eyes'. The robot's vision system will detect the defects with the help of an analytical system using data processing algorithms, all embedded in the robot's 'brain'.[144] This is in fact the new trend of the so-called Industry 4.0 and the Internet of things (IOT), seen by some as the next industrial revolution.[145] IOT is the network of physical objects or 'things' including robots, IR cameras embedded with electronics, software, sensors and connectivity to enable the IOT network to achieve greater value and service by exchanging data with the manufacturer, operator and/or other connected devices.[146] IR-NDT will exploit these novelties as well, as explained briefly below.

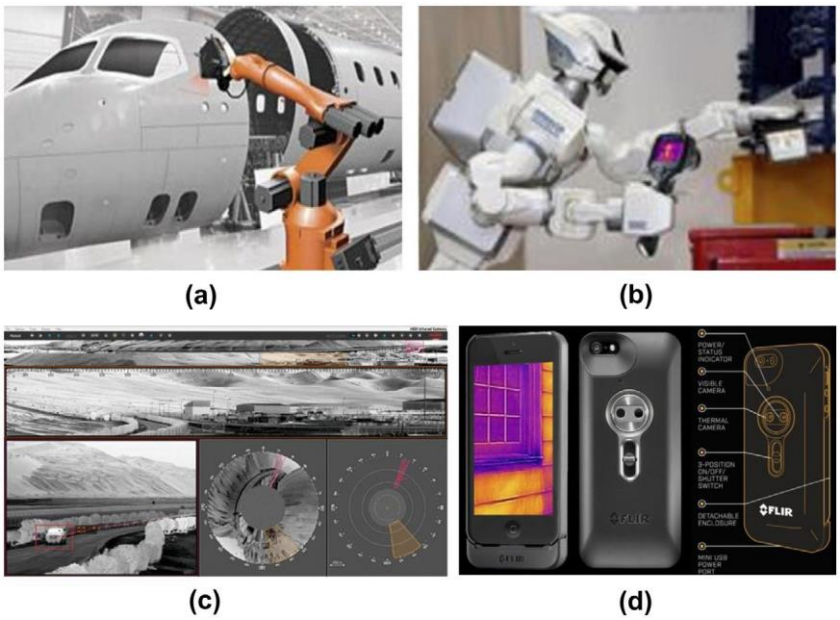

Figure 6. (a and b) the robots in NDT, (c) panoramic IR image, (d) FLIR one IR camera (image courtesy of FLIR).[26,149]

Today, microbolometers arrays are becoming more popular. Their launch price was over ten thousand dollars, but elementary complete systems could be purchased for several hundred dollars in 2015.[55] Such systems have been used in thermography, automotive applications, and other fields for a few years already, and low-cost arrays have increased the popularity of thermal imaging (e.g. FLIR Lepton – see below – offered in kits on popular microcontroler platforms such as Raspberry Pi or Arduino). Another recent example is the FLIR One which is a thermal imager for smartphones that was unveiled in January 2014 (see Figure 6(d)). Its cost is $350 and includes a visible camera and a microbolometer camera that is presented on the smartphone screen.[55] The small thermal camera in this case is a very low-cost microbolometer-based core (called Lepton). The Lepton is an 80-by-60-pixel array with 17 μm pitch detectors. Its sensitivity band is in the range of 8–12 μm (LWIR) and the fitted lens has a 50-degree horizontal field of view.[55] FLIR One can be used to locate warm or cold air leaks in homes, heat losses through windows and insulation, identify moisture in buildings, detect overloaded electrical connections, locate pipes behind walls and under floors and control radiant floor heating and even more applications depending on the user's imagination [147].

Therm-App from Opgal Optronic is another thermography application which was released for the android phones. using this Therm-App, an Android phone becomes an attractive thermography tool.[148] Therm-App offers many advantages such as: easy to use, lightweight (138 g), small size (55 × 6565 × 40 mm), low power consumption (less than 0.5 W), with resolution (384 × 288 pixels) and long range (see Figure 7).[148]

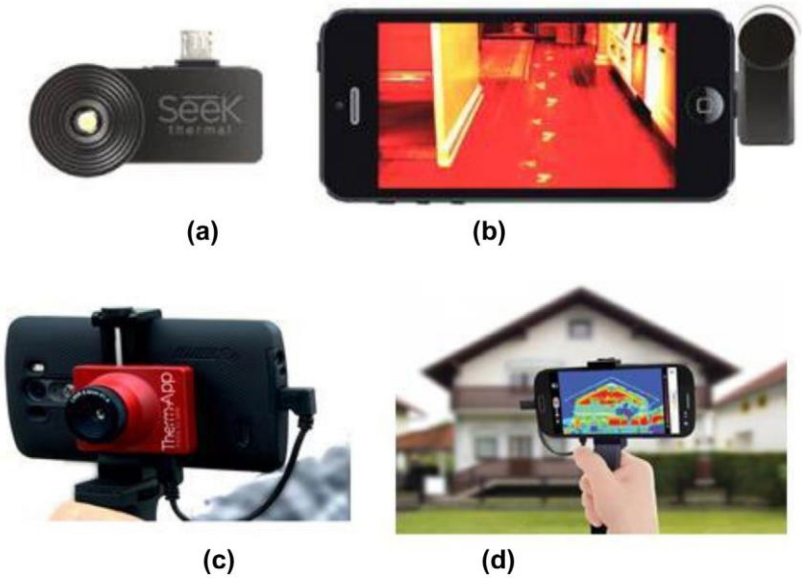

Figure 7. (a) front-view of Seek thermal camera for smartphone, (b) the camera plugged into a smartphone, showing the achieved miniaturisation and the quality of the obtained thermal image,[149] (c) therm-app ir camera for android,[150] (d) a building inspection by therm-app.[151]

The Seek thermal camera is another thermal imaging camera which uses more than 32,000 (206 × 156) thermal pixels to create a IR image displayed on iOS and android devices (see Figure 7). This type of camera is very small and has a plug adaptor for USB ports. This camera does not require batteries or special cables. The software is similar to that of FLIR One. This camera has a spot metre function to display surface temperatures.[149]

The reduction in price of IR sensors (and in the price of more powerful pocket size computers) will enable the emergence of ‘stand-alone dedicated IR systems’. For example, PC computers are now available on a USB key (ex: Intel’s ‘Compute Stick’. The same for IR sensors with an uSB interface: a full system including Bluetooth, WI-FIis thus available for a minimum hardware cost of less than 350 $ (PC: 149$ + IR: 199 $).

The price will most likely continue to decrease in the years ahead. Such USB-IRT-PC could be loaded with IR image processing software for special applications such as in monitoring overheating in electric cabinets, detection of subsurface defects on production lines, etc. WIFI

could be used to communicate automated diagnosis to a central unit and, in case of IR-NDT, activate stimulating sources (such as pulse heating). In the competitive environment of IR thermography and IR imaging, there are many companies with different market shares such as: FLIR systems, Fluke, InfraTec, IRIsys, IRnova, Jen Optik, Opgal, Seek thermal, Telops, Xenics, etc. Due to the competitive environment, companies attempt to increase their market shares by producing IR cameras with higher resolution, lower weight, smaller size and lower price.[152]

In the future, at even lower cost, size and weight, these systems could even be deployed permanently inside critical (electrical cabinets, etc.) components for continuous check-up following the previously discussed IOT trend. All technologies related to IR are developing very rapidly.[43] Today with changes in detectors, camera sensors, and IR systems, it is important to have high resolution, high performance, and low cost systems. These goals will become even more obvious in the future as illustrated in Figure 8 which shows the expected reduction in IR camera cost accompanied by an increase in pixel capability.

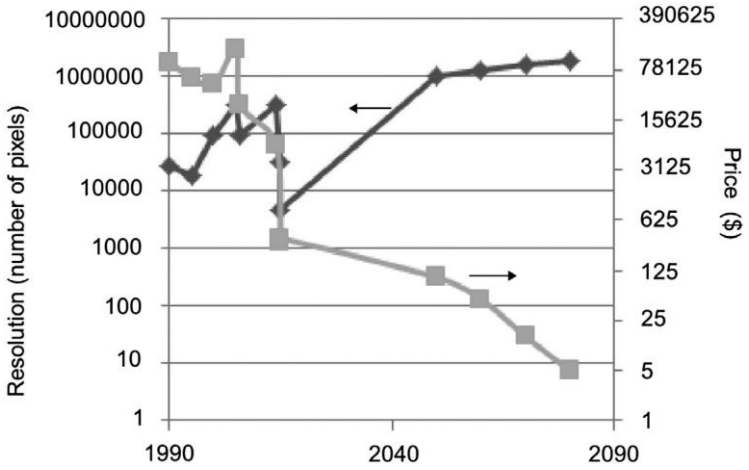

Figure 8. Diagram of the changes of ir camera cost and resolution from 1990 to 2080.

10. Conclusion

In the future, with respect to detectors, IRT will continue to develop with higher resolution and lower cost due to the continuous development of uncooled FPAs (microbolometers) and cooled FPAs (photonics, quantum detectors for high-end applications). With regard to image processing, IRT has evolved from digital functional imaging to pattern analysis, detection and quantitative analysis. Further developments are expected as well especially since new processors will be able to handle more complex algorithms (such as real-time thermal quadrupoles manipulation or complex thermal models for instance). IOT will also revolutionise IRT with a widespread use of internet connected low-cost smart IR sensors distributed in many places for a given application, in NDT and other fields. These improvements in IRT will lead to a greater acceptance in industry and elsewhere (even by the general public) and a variety of 'hot applications' will emerge. This will for instance include humanoid robots which will be fitted with IRT as well.

References

[1] Maldague X. Theory and practice of infrared technology for nondestructive testing. New york (Ny): Wiley; 2001.
[2] Andersson Jy, Karim A. Infrared detectors: Advances, challenges and new technologies. In: Ford Lumban Gaol, et al. editors. IOP Conference Series: Materials Science and Engineering. Vol. 51. IOP Publishing; 2013. p. 12001–12008.
[3] Ness S, Sherlock CN, Moore PO, et al. Non-destructive testing overview. Columbus (OH): American Society for Nondestructive Testing; 1996.
[4] Rogalski A. Infrared detectors: status and trends. Prog. Quantum Electron. 2003;27:59–210.
[5] Bagavathiappan S, Lahiri B, Saravanan T, et al. Infrared thermography for condition monitoring – a review. Infrared Phys. Technol. 2013;60:35–55.
[6] Preventive and Predictive Maintenance. Web [cited 2016 Feb 15]. Available from: https://www. lce.com/pdfs/The-PMPdM-Program-124.pdf
[7] Predictive Maintenance Technologies. Web [cited 2016 Feb 15]. Available from: https://www1. eere.energy.gov/femp/pdfs/om_6.pdf
[8] About ASNT. Introduction to nondestructive testing. Web [cited 2015 Apr 12]. Available from: https://www.asnt.org/MinorSiteSections/AboutASNT/Intro-to-NDT
[9] NDT and Training. N D T and NDT online training – 218-270-3182 – Hutchinson and Brainerd and MN NDT and training, NDT and NDT online training – 218-270-3182 – Hutchinson and Brainerd and MN. Web [cited 2015 Apr 12]. Available from: http://trainingndt.com/
[10] Avdelidis N, Gan TH, Ibarra-Castanedo C, et al. Infrared thermography as a non-destructive tool for materials characterisation and assessment. In: Proc. SPIE 8013, Thermosense: Thermal Infrared Applications XXXIII; 2011; Orlando, Fl, uSA. p. 801313.
[11] Meola C, Carlomagno G. The role of infrared thermography in NDT. In: Büyüköztürk O, et al. editors. Nondestructive testing of materials and structures. Netherlands: Springer; 2013. p. 91–96.

[12] Corsi C. New frontiers for infrared. Opto-Electron. Rev. 2015;23:3–25.
[13] Corsi C. Infrared: a key technology for security systems. In: Compagnone D, et al. editors. Sensors. Springer; 2014. p. 37–42.
[14] Riley RS, Ben-Ezra JM, Massey D, et al. Digital photography: a primer for pathologists. J. Clin. Lab. Anal. 2004;18:91–128.
[15] Righini GC, Tajani A, Cutolo A. An introduction to optoelectronic sensors. Hackensack (NJ): World Scientific Publishing; 2009.
[16] T hajeel H. Numerical modeling of infrared thermography techniques via ANSyS [master thesis]. Columbia (SC): Missouri university of Science and Technology; 2013.
[17] Downs C, Vandervelde TE. Progress in infrared photodetectors since 2000. Sensors. 2013;13:5054– 5098.
[18] Vavilov V. Thermal NDT: historical milestones, state-of-the-art and trends. Quant. InfraRed Thermogr. J. 2014;11:66–83.
[19] yakushev M, Brunev D, Varavin V, et al. HgCdTe heterostructures on Si (310) substrates for midinfrared focal plane arrays. Semiconductors. 2011;45:385–391.
[20] Vavilov V, Burleigh DD. Review of pulsed thermal NDT: physical principles, theory and data processing. NDT & E Int. 2015;73:28–52.
[21] Vavilov V, Thermal non destructive testing: short history and state-of-art. QIRT Conference 1992. Paper QIRT 1992-028; 1992. Paris, France. Available from QIRT Open Archives: http://www.qirt.org/archives/qirt1992/papers/028.pdf
[22] Rogalski A. History of infrared detectors. Opto-Electron. Rev. 2012;20:279–308.
[23] Ibarra-Castanedo C, Genest M, Piau J-M, et al. Active infrared thermography techniques for the nondestructive testing of materials. In: Chen CH, editor. ultrasonic and advanced methods for nondestructive testing and material characterization. World Scientific; 2007. Chapter XIV; p. 325–348.
[24] Chen C. ultrasonic and advanced methods for nondestructive testing and material characterization: World Scientific Publishing Company Incorporated. Hackensack (NJ): World Scientific; 2007.
[25] Vavilov V, Ivanov A. Pulse thermal testing of multilayer specimens. Sov. J. NDT. 1984;6:39–47.
[26] Hogan H. For IR imaging, better swap beckons. Photonics.com; 2016. Available from: http://www.photonics.com/Article.aspx?AID=57610
[27] Balageas DL, Krapez J-C, Cielo P. Pulsed photothermal modeling of layered materials. J. Appl. Phys. 1986;59:348–357.
[28] Carlomagno G, Berardi PG, editors. unsteady thermotopography in non-destructive testing. Proceedings of the 3rd Biannual Exchange; 1976; St Louis, MO, uSA.
[29] Busse G, Wu D, Karpen W. Thermal wave imaging with phase sensitive modulated thermography. J. Appl. Phys. 1992;71:3962–3965.
[30] Busse G. Optoacoustic and photothermal material inspection techniques. Appl. Opt. 1982;21:107– 110.
[31] Wu D, Rantala J, Karpen W, et al. Applications of lockin-thermography methods. In: Thompson DO, Chimenti DE, editors. Review of progress in quantitative nondestructive evaluation. Plenum press (Ny): Springer; 1996. p. 511–518.
[32] Wu D, Busse G. NDT of materials using lock-in thermography. NDTnet. 1997;2. Available from: http://www.ndt.net/article/dresd97/wu/wu.htm
[33] Kuo P, Feng Z, Ahmed T, et al. Parallel thermal wave imaging using a vector lock-in video technique. In: Hess P, Pelzl J, editors. Photoacoustic and photothermal phenomena. Springer; 1988. p. 415–418.
[34] Beaudoin JL, Merienne E, Danjoux R, et al. Numerical system for infrared scanners and application to the subsurface control of materials by photothermal radiometry. In: 1985 International Technical Symposium/Europe. International Society for Optics and Photonics; 1986; Cannes, France. p. 285–292.
[35] Breitenstein O, Langenkamp M. Lock-in contact thermography investigation of lateral electronic inhomogeneities in semiconductor devices. Sens. Actuators, A. 1998;71:46–50.
[36] Breitenstein O, Iwig K, Konovalov I. Evaluation of local electrical parameters of solar cells by dynamic (lock-in) thermography. Phys. Status Solidi A. 1997;160:271–282.
[37] H uth S, Breitenstein O, Huber A, et al. Lock-in IR-thermography – a novel tool for material and device characterization. In: Raineri V, Priolo F, Kittler M, Richter H, editors. Diffusion and defect data part B solid state phenomena. Vols. 82–84. Dürnten: Trans Tech Publications; 2002. p. 741–746. http://dx.doi.org/10.4028/www.scientific.net/SSP.82-84.741
[38] Mulaveesala R, Tuli S. Digitized frequency modulated thermal wave imaging for nondestructive testing. Mater. Eval. 2005;63:1046–1050.
[39] Zweschper T, Dillenz A, Busse G. ultrasound lock-in thermography – a defect-selective NDT method for the inspection of aerospace components. Insight. 2001;43:173–179.
[40] Szwedo M, Pieczonka L, uhl T, editors. Application of vibrothermography in nondestructive testing of structures. In: Boller Ch., editor. Proceedings of the Sixth on Structural Health Monitoring; 2012 Jul 3–6; Dresden, Germany: DGZfP e.V Publisher.
[41] Henneke E II, Reifsnider KL, Stinchcomb WW. Thermography – an NDI method for damage detection. JOM. 1979;31:11–15.

[42] Favro L, Han X, Ouyang Z, et al. Infrared imaging of defects heated by a sonic pulse. Rev. Sci. Instrum. 2000;71:2418–2421.
[43] Balageas D, Maldague X, Burleigh D, et al. Thermal (IR) and other NDT techniques for improved material inspection. J. Nondestr. Eval. 2016;35:1–17.
[44] Sojasi S, Khodayar F, Lopez F, et al. Infrared testing of CFRP components: comparisons of approaches using the Tanimoto criterion. NDT in Canada; 2015; Edmonton, Canada.
[45] Rogalski A. Infrared detectors. Boca Raton (FL): Taylor & Francis; 2010.
[46] Hyseni G, Caka N, Hyseni K. Infrared thermal detectors parameters: semiconductor bolometers versus pyroelectrics. WSEAS Trans. Circuits Syst. 2010;9:238–247.
[47] Corsi C. History highlights and future trends of infrared sensors. J. Mod. Opt. 2010;57:1663–1686.
[48] What is an infrared detector, IR detectors, photodetector – future electronics. Web [cited 2015 Apr 12]. Available from: http://www.futureelectronics.com/en/optoelectronics/infrared-detector. aspx
[49] Rogalski A. Recent progress in infrared detector technologies. Infrared Phys. Technol. 2011;54:136– 154.
[50] Rogalski A. Infrared detectors for the future. Acta Phys. Pol., A. 2009;116:389–406.
[51] Rogalski A, Antoszewski J, Faraone L. Third-generation infrared photodetector arrays. J. Appl. Phys. 2009;105:091101.
[52] Wolfe WL, Kruse PW. Thermal detectors. OSA handbook of optics. New york (Ny): McGraw-Hill; 2004 (sponsored by the Optical Society of America).
[53] Kylili A, Fokaides PA, Christou P, et al. Infrared thermography (IRT) applications for building diagnostics: a review. Appl. Energy. 2014;134:531–549.
[54] Driggers RG. What's new in infrared systems? San Diego (CA): SPIE Professional; 2014 Apr.
[55] Dhar NK, Dat R, Sood AK. Advances in infrared detector array technology. In: Pyshkin SL, Ballato JM, editors. Optoelectronics – advanced materials and devices. Rijeka: Intech; 2013. p. 1–27.
[56] M artyniuk P, Antoszewski J, Martyniuk M, et al. New concepts in infrared photodetector designs. Appl. Phys. Rev. 2014;1:041102.
[57] Tsao S, Razeghi M. Quantum dots. In: Andrews DL, editor. Photonics. Vol. 2, Nanophotonic structures and materials. Hoboken (NJ): Wiley-Science Wise Co Publication; 2015. p. 169–260.
[58] Hunter GW, Stetter JR, Hesketh PJ, et al. Smart sensor systems. Electrochem. Soc. Interface. 2010;19:29–34.
[59] Corsi C. Smart sensors. Infrared Phys. Technol. 2007;49:192–197.
[60] Cook R. Smart infrared temperature sensors: Making sense of the new generation. Sensors. 2000;17:48–55.
[61] Corsi C. Smart sensors: Why and when the origin was and why and where the future will be. In: SPIE OPTO. San Francisco (CA): International Society for Optics and Photonics; 2013. p. 899302.
[62] Kanoun O, Trankler H-R. Sensor technology advances and future trends. IEEE Trans. Instrum. Meas. 2004;53:1497–1501.
[63] Suryadevara NK, Mukhopadhyay SC. Smart homes: design, implementation and issues. Vol. 14, Smart sensors, mesurement and instrumentation. New Zealand: Springer; 2015.
[64] Abedin MN, Bhat I, Gunapala SD, et al. The future of single-to multi-band detector technologies: Review. Crete: 2006 Advanced Research Workshop-Future Trends in Microelectronics up the Nano Creek; 2006.
[65] T erahertz Technology – Sources and THz Generation/Detection Methods. Web [cited 2015 May 2]. Available from: http://www.toptica.com/products/terahertz_generation/terahertz_ technologysources_and_thz_generation_methods.html
[66] Terahertz Technology Pulsed Terahertz Generation. Web [cited 2015 May 2]. Available from: http://www.toptica.com/products/terahertz_generation/terahertz_technologysources_and_ thz_generation_methods/pulsed_terahertz_generation.html
[67] Gubarev SI, Dremin AA, Kozlov VE, et al. Plasma waves in a two-dimensional electron system laterally screened by a metallic gate. JETP Lett. 2009;90:539–543.
[68] Rogalski A, Sizov F. Terahertz detectors and focal plane arrays. Opto-Electron. Rev. 2011;19:346– 404.
[69] Karpowicz N, Zhong H, Xu J, et al. Comparison between pulsed terahertz time-domain imaging and continuous wave terahertz imaging. Semicond. Sci. Technol. 2005;20:S293–S299.
[70] Jansen C, Wietzke S, Peters O, et al. Terahertz imaging: applications and perspectives. Appl. Opt. 2010;49:E48–E57.
[71] Ok G, Kim HJ, Chun HS, et al. Foreign-body detection in dry food using continuous sub-terahertz wave imaging. Food Control. 2014;42:284–289.
[72] Pradere C, Caumes J, Palomo E, et al. use of SVD decomposition to increase signal and noise ratio on THz imaging measurements. QIRT Conference 2014. Paper QIRT 2014-198; 2014; Bordeaux, France. Available from: QIRT Open Archives: http://www.qirt.org/archives/qirt2014/QIRT2014. html
[73] Abina A, Puc u, Jeglič A, et al. Applications of terahertz spectroscopy in the field of construction and building materials. Appl. Spectrosc. Rev. 2015;50:279–303.
[74] Hochrein T. Terahertz technology is advancing-change from pure scientific to commercial use observed. Opt. Photonik. 2015;10:4–10.
[75] Nagatsuma T. Terahertz technologies: present and future. IEICE Electron. Exp. 2011;8:1127–1142.

[76] Terahertz & Sub-THZ Imaging Technology. Web [cited 2015 May 2]. Available from: http:// terasense.com/terahertz-technology
[77] New Terahertz Imaging Systems. Web 2015 May 2. Available from: http://www.nethis-thz.com/ en/nethis-products/nethis-teracam
[78] Pradere C, Caumes J-P, Balageas D, et al. Photothermal converters for quantitative 2D and 3D real time terahertz imaging. Quant. InfraRed Thermogr. J. 2010;7:217–235.
[79] Karasik BS, Sergeev AV, Prober DE. Nanobolometers for THz photon detection. IEEE Trans. Terahertz Sci. Technol. 2011;1:97–111.
[80] Mittleman DM. Frontiers in terahertz sources and plasmonics. Nat. Photonics. 2013;7:666–669.
[81] Ibarra-Castanedo C, Piau J-M, Se Guilbert, et al. Comparative study of active thermography techniques for the nondestructive evaluation of honeycomb structures. Res. Nondestr. Eval. 2009;20:1–31.
[82] Ibarra-Castanedo C, Gonzalez D, Klein M, et al. Infrared image processing and data analysis. Infrared Phys. Technol. 2004;46:75–83.
[83] Hidalgo-Gato R, Andrés J, López-Higuera JM, et al. Quantification by signal to noise ratio of active infrared thermography data processing techniques. Opt. Photonics J. 2013;3:20–26.
[84] Maldague XP. Introduction to NDT by active infrared thermography. Mater. Eval. 2002;60:1060– 1073.
[85] Maldague X, Galmiche F, Ziadi A. Advances in pulsed phase thermography. Infrared Phys. Technol. 2002;43:175–181.
[86] Lopez F, Ibarra-Castanedo C, Maldague X, et al. Pulsed thermography signal processing techniques based on the 1D solution of the heat equation applied to the inspection of laminated composites. Mater. Eval. 2014;72:91–102.
[87] Ibarra-Castanedo C. Quantitative subsurface defect evaluation by pulsed phase thermography: depth retrieval with the phase [PhD dissertation]. Quebec: university of Laval; 2005.
[88] Ibarra-Castanedo C, Gonzalez D, Galmiche F, et al. Discrete signal transforms as a tool for processing and analyzing pulsed thermographic data. In: Proc. SPIE 6205, Thermosense: Thermal Infrared Appl. XXVIII; 2006; Orlando, FL, uSA. p. 620514.
[89] Maldague X, Marinetti S. Pulse phase infrared thermography. J. Appl. Phys. 1996;79:2694–2698.
[90] Madruga F, Ibarra-Castanedo C, Conde O, et al. Automatic data processing based on the skewness statistic parameter for subsurface defect detection by active infrared thermography. QIRT Conference 2008. Paper QIRT 2008 – 12_16_16; 2008; Krakow, Poland. Available from: QIRT Open Archives: http://www.qirt.org/archives/qirt2008/QIRT2008.html
[91] Lopez F, Ibarra-Castanedo C, Maldague X, et al. Analysis of signal processing techniques in pulsed thermography. In: Proc. SPIE 8705, Thermosense: Thermal Infrared Appl. XXXV; 2013; Baltimore, MD, uSA. p. 87050W.
[92] Benitez HD, Ibarra-Castanedo C, Bendada A, et al. Defect quantification with reference-free thermal contrast and artificial neural networks. In: Proc. SPIE 6541, Thermosense: Thermal Infrared Appl. XXIX; 2007; Orlando, FL, uSA. p. 65410V.
[93] Benitez H, Ibarra-Castanedo C, Bendada A, et al. Modified differential absolute contrast using thermal quadrupoles for the non-destructive testing of finite thickness specimens by infrared thermography. In: 2006 IEEE Canadian Conference on Electrical and Computer Engineering, CCECE'06; 2006; Ottawa, Canada. p. 1039–1042.
[94] B ai L, Gao B, Tian S, et al. A comparative study of principal component analysis and independent component analysis in eddy current pulsed thermography data processing. Rev. Sci. Instrum. 2013;84:104901.1–104901.11.
[95] Lopez F, Nicolau V, Maldague X, et al. Multivariate infrared signal processing by partial least-squares thermography. Proceedings of the VIIth International Workshop Advances in Signal Processing for NDT, Non-Destructive Evaluation of Materials; 2013; Quebec, Canada.
[96] Bin J, Ai FF, Liu N, et al. Supervised principal components: a new method for multivariate spectral analysis. J. Chemom. 2013;27:457–465.
[97] Balageas D. Thickness or diffusivity measurements from front-face flash experiments using the TSR (thermographic signal reconstruction) approach. QIRT Conference 2010. Paper QIRT 2010011; 2010; Quebec, Canada. Available from: QIRT Open Archives: http://www.qirt.org/archives/ qirt2010/QIRT2010.html
[98] Shepard SM, Lhota JR, Rubadeux BA, et al. Reconstruction and enhancement of active thermographic image sequences. Opt. Eng. 2003;42:1337–1342.
[99] Balageas D, Chapuis B, Deban G, et al. Quantitative assessment of the improvement of the detection of defects by pulse thermography thanks to the TSR approach in the case of a smart composite repair patch. Quant. InfraRed Thermogr. J. 2010;7:167–187.
[100] Balageas DL. Defense and illustration of time-resolved pulsed thermography for NDE. Quant. InfraRed Thermogr. J. 2012;9:3–32.
[101] Oswald-Tranta B, Maier A, Schledjewski R. Defect depth determination in a CFRP structure using TSR technique. QIRT Conference 2014. Paper QIRT 2014-061; 2014; Bordeaux, France. Available from: QIRT Open Archives: http://www.qirt.org/archives/qirt2014/QIRT2014.html
[102] Lopez F, Maldague X, Ibarra-Castanedo C. Enhanced image processing for infrared nondestructive testing. Opto-Electron. Rev. 2014;22:245–251.
[103] Susa M, Benítez HD, Ibarra-Castanedo C, et al. Phase contrast using a differentiated absolute contrast method. Quant. InfraRed Thermogr. J. 2006;3:219–230.

[104] Ibarra-Castanedo C, Sfarra S, Ambrosini D, et al. Diagnostics of panel paintings using holographic interferometry and pulsed thermography. Quant. InfraRed Thermogr. J. 2010;7:85–114.
[105] Mulaveesala R, Tuli S. Theory of frequency modulated thermal wave imaging for nondestructive subsurface defect detection. Appl. Phys. Lett. 2006;89:191913-1–191913-3.
[106] Ibarra-Castanedo C, Maldague X. Pulsed phase thermography reviewed. Quant. InfraRed Thermogr. J. 2004;1:47–70.
[107] Ibarra-Castanedo C, Maldague XP. Interactive methodology for optimized defect characterization by quantitative pulsed phase thermography. Res. Nondestr. Eval. 2005;16:175–193.
[108] Olbrycht R, Więcek B, Gralewicz G, et al. Comparison of Fourier and wavelet analyses for defect detection in lock-in and pulse phase thermography. Quant. InfraRed Thermogr. J. 2007;4:219–232.
[109] Ibarra-Castanedo C, Genest M, Servais P, et al. Qualitative and quantitative assessment of aerospace structures by pulsed thermography. Nondestr. Test. Eval. 2007;22:199–215.
[110] Marinetti S, Grinzato E, Bison PG, et al. Statistical analysis of IR thermographic sequences by PCA. Infrared Phys. Technol. 2004;46:85–91.
[111] Abdi H. Partial least square regression (PLS regression). In: Neil Salkind, editor. Encyclopedia for research methods for the social sciences; 2003. Thousand Oaks (CA): Sage. p. 792–795.
[112] Rosipal R, Kramer N. Overview and recent advances in partial least squares. In: Craig Saunders, Marko Grobelnik, Steve Gunn, John Shawe-Taylor, editors. Subspace, latent structure and feature selection. Berlin: Springer; 2006. p. 34–51.
[113] Lopez F, Ibarra-Castanedo C, Nicolau V, et al. Comparative study of thermographic signal reconstruction and partial least-squares thermography for detection and evaluation of subsurface defects. QIRT Conference 2014. Paper QIRT 2014-095; 2014; Bordeaux, France. Available from: QIRT Open Archives: http://www.qirt.org/archives/qirt2014/QIRT2014.html
[114] Lopez F, Ibarra-Castanedo C, de Paulo Nicolau V, et al. Optimization of pulsed thermography inspection by partial least-squares regression. NDT E Int. 2014;66:128–138.
[115] Barshan E, Ghodsi A, Azimifar Z, et al. Supervised principal component analysis: visualization, classification and regression on subspaces and submanifolds. Pattern Recogn. 2011;44:1357– 1371.
[116] Albendea P, Madruga FJ, Cobo A, et al. Signal to noise ratio (SNR) comparison for pulsed thermographic data processing methods applied to welding defect detection. QIRT Conference 2010. Paper QIRT 2010-004; 2010, Quebec, Canada. Available from QIRT Open Archives: http:// www.qirt.org/archives/qirt2010/QIRT2010.html
[117] Duan y. Probability of detection analysis for infrared nondestructive testing and evaluation with applications including a comparison with ultrasonic testing [PhD dissertation]. Quebec: university of Laval; 2014.
[118] Duan y, Servais P, Genest M, et al. ThermoPoD: a reliability study on active infrared thermography for the inspection of composite materials. J. Mech. Sci. Technol. 2012;26:1985–1991.
[119] Ospina JE, Florez JF, Benitez HD, et al. Thermal diffusivity estimation with quantitative pulsed phase thermography. In: Proc. SPIE 9485, Thermosense: Thermal Infrared Appl. XXXVII; 2015; Baltimore, MD, uSA. p. 948512-1–948512-8.
[120] Vollmer M, Möllmann K-P. Infrared thermal imaging: Fundamentals, research and applications. Weinheim: Wiley; 2010.
[121] Uses, Applications and Hazards of Infrared Radiation. Web [cited 2015 Apr 12]. Available from: http://hubpages.com/hub/uses-Hazards-and-Applications-of-Infrared-Radiation
[122] Future of NDT in uK economy. Web [cited 2015 Apr 12]. Available from: http://www.bindt.org/ downloads/Materials-KTN-Future-of-NDT-in-uK-economy.pdf
[123] D'Ans G, Ripak P, Cerckel P, et al. Some applications of virtual instrumentation in NDT. Laborelec university of Brussels; 2001. Available from: http://www.ulb.ac.be/polytech/laborulb/athens/ papere.pdf
[124] Meola C, Carlomagno GM. Recent advances in the use of infrared thermography. Meas. Sci. Technol. 2004;15:R27–R58.
[125] Otsuka K, Togawa T. Hippocratic thermography. Physiol. Meas. 1997;18:227–232.
[126] Fernandez-Cuevas I, Marins JCB, Lastras JA, et al. Classification of factors influencing the use of infrared thermography in humans: a review. Infrared Phys. Technol. 2015;71:28–55.
[127] Arfaoui A, Popa C, Polidori G, et al. Infrared thermography in sports activity. In: Prakash RV, editor. In infrared thermography; Rijeka: InTech; 2012; Chapter 7. p 141–168.
[128] ThermoHuman. Applied thermography in sports science and health. Web [cited 2016 Feb 16]. Available from: http://www.thermohuman.com/
[129] Medical-thermography.com. New Page 1. Web [cited 2016 Feb 16]. Available from: http://www. medical-thermography.com/DyNAMIC%20THERMOGRAPHy/dynamic%20thermography.htm
[130] Wholebodywellness.co.uk. Medical thermal imaging. Web [cited 2016 Feb 16]. Available from: http://wholebodywellness.co.uk/diti.html
[131] Wild W. Application of infrared thermography in civil engineering. Proc. Estonian Acad. Sci. Eng. 2007;4:436–444.
[132] Rao P. Infrared thermography and its applications in civil engineering. Indian Concr. J. 2008;82:41– 50.
[133] Moisture Detection with Infrared Cameras. Web [cited 2016 Feb 16]. Available from: https://www. youtube.com/watch?v=4gbQQWlFu5I
[134] FLIR Systems. Thermal imaging for sports. Web [cited 2016 Feb 16]. Available from: http://www. flir.com/corporate/display/?id=68275

[135] Hashimoto A, Suehara K, Kameoka T. Applications of infrared spectroscopic techniques to quality evaluation in agriculture and food process. Adv. Infrared Technol. Appl. 2015;72–75.
[136] Ishimwe R, Abutaleb K, Ahmed F. Applications of thermal imaging in agriculture – a review. Adv. Remote Sens. 2014;3:128–140.
[137] FLIR Systems. Thermal imaging cameras help preserve italy's cultural heritage. Web [cited 2016 Feb 16]. Available from: http://www.flir.com/thermography/americas/ca/view/?id=54523
[138] The NERC Remote Sensing Data Analysis Service. Web [cited 2016 Mar 16]. Available from: https://rsg.pml.ac.uk/papers/groom_nercnews96/
[139] Moghadam P, Vidas S. Heatwave: the next generation of thermography devices. In: Proc. SPIE 9105, Thermosense: Thermal Infrared Appl. XXXVI; 2014; Baltimore, MD, uSA. p. 91050F.
[140] Vidas S, Moghadam P. HeatWave: a handheld 3D thermography system for energy auditing. Energy Build. 2013;66:445–460.
[141] Vidas S, Moghadam P, Bosse M. 3D thermal mapping of building interiors using an RGB-D and thermal camera. In: 2013 IEEE International Conference on Robotics and Automation (ICRA). Karlsruhe: IEEE; 2013. p. 2311–2318.
[142] HeatWave: 3D Thermography System. Web [cited 2016 Feb 16]. Available from: https://www.youtube.com/watch?v=wZWN1frZ7mo
[143] Mineo C, Herbert D, Morozov M, et al. Robotic non-destructive inspection. In: 51st Annual Conference of the British Institute of Non-destructive Testing; 2012; Daventry, uK. p. 345–352.
[144] Guizzo E. A robot in the family. Spectrum IEEE. 2015;52:29–58.
[145] A lbert M. 7 things to know about the internet of things and industry 4.0. Modern machine shop. Web [cited 2015 Dec 29]. Available from: http://www.mmsonline.com/articles/7-things-to-knowabout-the-internet-of-things-and-industry-40
[146] Internet of things.wikipedia.org. Web [cited 2015 May]. Available from: https://en.wikipedia.org/wiki/Internet_of_Things
[147] For your life. FLIR Systems. Available from: www.flir.com. Web [cited 2015 Apr 12].
[148] Therm-App. Therm-App. Web [cited 2016 Feb 16]. Available from: http://therm-app.com/thermapp/
[149] Thermal imaging camera. Seek thermal. Web [cited 2015 Apr 12]. Available from http://www.thermal.com
[150] Therm-App. Therm-App. Web [2016 Feb 16]. Available from: http://therm-app.com/
[151] Therm-App IR camera for Android. Web [cited 2016 Feb 16]. Available from: http://www.swisssale.ch/orientation-measuring/thermal-cameras/therm-app-ir-camera-for-android::2362. html?language=en
[152] New Market Research On The World Market For Commercial and Dual-use Infrared Imaging and Infrared Thermometry. Web [2016 Feb 16]. Available from: http://www.prnewswire.com/ news-releases/

Chapter III

Data processing algorithms in pulsed thermography

3. 1. Introduction

Data processing algorithms are employed to eliminate the noise from thermal inspections and enhance the quality of the inspection. There are several data processing algorithms which could help to increase the detection probability. The selection of data processing algorithm depends on the objectives of the research. Some of the most popular and useful techniques which are used in thermography inspection are: Thermographic signal reconstruction (TSR) [39, 40], Differential absolute contrast (DAC) [41], Pulsed phase thermography (PPT) [9, 31], Wavelet transforms (WT) [9], Principal component thermography (PCT) [33], and Partial least square thermography (PLST) [36]. Data processing techniques in NDT provide some advantages such as defect detection enhancement, but sometimes lead to slow computing or require interactions with an operator to select algorithm parameters on the other hand [8]. These methods are further discussed in the following.

3. 2. Thermographic signal reconstruction (TSR)

Thermographic signal reconstruction (TSR) [40] is known as an effective processing technique which is used in PT data. It is important to note that TSR is a patented teqnique and what is discussed below is refered to the basic-TSR. The most important advantages of using this method

over PT raw data is the simplicity and accuracy of quantitative measurement, increase of temporal and spatial resolution, reduction of high frequency noise and the ability to produce time derivative images [13]. As it name implies, TSR uses a low order polynomial function in order to reconstruct the temperature evolution curve which obtained from a PT inspection [42].

Considering that the temperature decay of a defect-free region behaves in a similar manner as the solution of the 1D heat diffusion equation, the temperature evolution of a non-defective area can be written in logarithmic form as [13]:

$$\ln(T - T_0) = \ln\left(\frac{Q}{e}\right) - \frac{1}{2}\ln(\pi . t) \tag{3.1}$$

In Eq. (3.1) T_0 is the initial temperature whereas T is the variable temperature; Q is the applied heat energy as external stimulation, e is the thermal effusivity of the material and t is the time [13]. We can transform Eq. (3.1) to a linear polynomial equation:

$$\ln(T - T_0) = a_0 + a_1 \ln(t) + a_2[\ln(t)]^2 + \cdots + a_m[\ln(t)]^m \tag{3.2}$$

There is an important point in Eq. (3.2), in order to select the factor m. For isotropic materials, a good correspondence between acquired data and fitted values can be achieved setting m to 4 or 5. Nevertheless, when working with anisotropic materials such as carbon and glass fiber reinforced polymers, the number of coefficients should be carefully selected in order to avoid higher residuals between fitted and experimental data [13]. Calculation of the first and second-order derivatives using synthetic data leads to improve the signal due to reduction of blurring effect present in temperature raw data (blurring effects are inherent to the lateral heat diffusion at later times). This is because the times at which occur changes at the first (rate of cooling) and second time (rate of change in the rate of cooling) derivative are shorter than in raw thermal images [35, 42].

3. 3. Differential absolute contrast (DAC)

Differential absolute contrast (DAC) is known as a classical processing technique which is generally used to eliminate the downside of selecting a sound area (S_a) when performing classical thermal contrast computations [13, 43]. It is one of the first techniques developed as an alternative to the classical thermal contrast computations and all the inherent problems that brings with it (non-uniform heating, emissivity variations, and environmental reflections) [42].

Based on the solution of the 1-D Fourier heat equation, DAC looks for the T_{sa} at the time t, which is computed locally assuming that on the first few images all points behave as a sound area [43]. The thermographic data obtained from a PT experiment can be approximated by the 1-D solution of heat equation through the following expression [43, 44]:

$$\Delta T_{DAC} = T(t) - \sqrt{\frac{t'}{t}}\, T(t') \tag{3.3}$$

Definition of t' is the first step in the calculation of the DAC method as a given time value between the instant when the external thermal source is applied, and the precise moment when the first defective spot appears on the thermogram [13, 35].

The differentiated absolute contrast (DAC) method was developed to perform a more convenient computation of the sound area temperature through the 1-D solution of the Fourier equation for homogeneous and semi-infinite materials stimulated by a Dirac impulse. This model, however, does not include the sample thickness. Therefore, the DAC accuracy is dependent on the time and it decreases for a long time after heating when the heat front reaches the sample face opposite to irradiation.

3. 4. Pulsed phase thermography (PPT)

One of the most popular data processing methods is the pulsed phase thermography (PPT) method which is based on the Fourier transform. It is a combination of pulsed thermography, for which data acquisition is fast and lock-in thermography, for which depth retrieval is easy and simple.

The Fourier Transform is used to extract a certain number of thermal waves from a thermal pulse, each one having a different frequency, amplitude, and pulse delay [31, 45].

In PPT, the data is transformed from the time domain to the frequency domain using the 1-D discrete Fourier transform [31, 46]:

$$F_n = \Delta t \sum_{k=0}^{N-1} T(k\Delta t) e^{(-\frac{j2\pi nk}{N})} = Re_n + Im_n \tag{3.4}$$

where Δt is the sampling interval, n determins the frequency increment $(n = 0,1, \dots N)$; and Re and Im are the real and the imaginary parts of the transformation, respectively [31].

The amplitude and the phase delay of the transformation are calculated with the real and imaginary parts of equation (4). They are calculated as follows [31]:

$$A_n = \sqrt{Re_n^2 + Im_n^2} \tag{3.5}$$

$$\phi_n = \tan^{-1}(\frac{Im_n}{Re_n}) \tag{3.6}$$

Phase profiles of the surface temperature are anti-symmetric, providing redundant information in both sides of the frequency spectra. In the following, only the positive part of the frequency spectra is used whilst the negative frequencies can be safely discarded [31, 47, 48].

Phase-grams are very interesting aspects in NDT, because they are insensitive to emissivity variations in the surface, reflection from the environment, surface geometry, and non-uniform

heating, therefore, defect contrast improves, but phase is affected by the noise, especially at high frequencies [31, 47, 48].

The absolute phase contrast $\Delta\varphi$ can be defined as:

$$\Delta\varphi = \varphi_d - \varphi_s \tag{3.7}$$

where φ_d is the phase of a defective pixel, and φ_s is the phase of non-defective pixel [48]. Phase contrast depends on four important factor; thermal properties of the material, the subsurface structure of the sample, the modulation frequency and the subsurface heat transfer coefficient [49]. Phase contrast computation is very important for determining blind frequencies. The blind frequency corresponds to the corresponding frequency at which the defect becomes visible for the first time [49]. These parameters are presented in the figure 3.1.

The inverse square root of the blind frequency $f_b^{-\frac{1}{2}}$ has a linear relationship with defect depth z, as given by [49]:

$$z = C_1\sqrt{\frac{\alpha}{\pi f_b}} \tag{3.8}$$

In this equation, α is the thermal diffusivity of the material, and C_1 is a constant (the value of C_1 is 1 when working with amplitude, and between 1.5 and 2 for phase data, with the value of 1.8 frequently adopted [50].

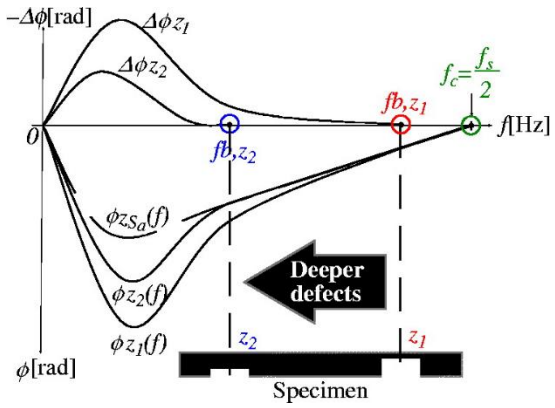

Figure 3.1: Depth retrieval from the PPT phase for the case of thick defects [Castanedo, C.I.: Quantitative subsurface defect evaluation bypulsed phase thermography: depth retrieval with the phase, Ph.D. thesis, Universite Laval (2005)]

The Fourier transform is one of the important and effective transformation algorithms that is used to extract amplitude and phase information in PPT. It is possible to use other algorithms such as wavelet transforms, which has additional advantages compared to FFT. The wavelet transform keeps the time information while it is lost in the Fourier transform. Wavelets are periodic waves of short duration that allow a better reproduction of a transient signal and these of different scales or resolutions [47, 51].

3. 5. Principal component thermography (PCT)

Principal component analysis (PCA), is presented by Pearson in 1901 and is developed by Hotelling in 1933 [52]. It is used in various fields such as system and control theory and communication, face recognition, remote sensing, image compression, and summarizing data of high dimension [52, 53].

One of the interesting techniques which is used to extract features and reduce the undesirable information in thermographic sequences is the principal component thermography (PCT). It is applied in NDT for defect detection and depth estimation of defects [33, 54].

PCT uses singular value decomposition (SVD) to extract the spatial (Empirical Orthogonal Functions or EOFs) and temporal (principal components PCs) information from thermogram matrix. In the principal component, the characteristic variability of the first component is more important than the second component and has the largest variance. The second component contains the second most important variability, and so on. Using the first few (most important), principal components helps to reduce the dimensionality of the data [33, 54-57].

For example, a thermographic 3-D ($N_x \times N_y \times N_t$ with $N_t =$ total number of images and N_x and N_y are the number of pixels per row and column of the IR camera) matrix A is reshaped to 2D ($M \times N$ where $M = N_x . N_y$ and $N = N_t$) matrix as illustrated in figure 3.2:

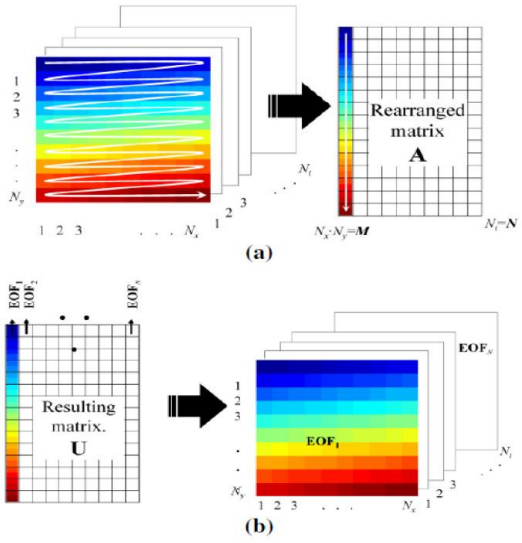

Figure 3.2: .(a) Thermographic data is rearranged from a 3D matrix to 2D a matrix in order to apply SVD, and (b) Rearrangement of 2D U matrix into a 3D matrix containing the EOFs [57]

After this step, the SVD is applied to the 2-D matrix as follows:

$$A = USV^T \tag{3.9}$$

where matrix U is a $M \times N$ orthogonal matrix so that its columns represent the EOFs associated with data spatial values. The rows of V^T corresponds to the principal components, which represent the temporal variations. Also, S is a diagonal $N \times N$ matrix [48]. The singular values in the matrix

S are the eigenvalues for the corresponding eigenvectors in the matrix V. The eigenvalues in S are reordered to arrange them in descending order of their value [58].

Generally; it is possible to represent the original data with only a few EOFs. Typically, a 1000 thermogram sequence can be replaced by 10 or fewer EOFs [55, 58]. In PCT, the first two or three empirical orthogonal functions generally contain nearly 90 percent of the variability of the image data and the remaining variability is presented in the corresponding functions which can be neglected due to huge computation requirements [33, 58].

3. 6. Partial Least-Squares thermography (PLST)

Partial least square is a statistical method which was introduced in social science by Herman Wold in the 1960's [59]. Partial least square (PLS) is used in various fields such as social science, chemometric, bioinformatics, neuroscience and etc. [60]. When this is a need to predict dependent variables from a large set of independent variables (predictors), it is a useful tool [59, 60].

Partial least square (PLS) is composed of a wide class of methods in order to establish the relations between a set of observed variables by means of latent variables. This involves regression and classification tasks as well as dimension reduction techniques and modeling tools. Using this method, irrelevant and unstable information is discarded and only the most relevant part of the thermal data is used for regression. Furthermore, since all variables are projected down to only a few linear combinations, simple plotting techniques can be used for analysis. As a regression method, partial least square regression (PLSR) seeks to model a dependent variable Y (predicted) in terms of an independent variable X (predictor) [61, 62]. PLS generalizes and combines features of two techniques: principal component regression (PCR) and multivariate linear regression (MLR) to achieve this aim [61, 62].

While in PCR factors that capture the greatest amount of variance in the predictor (X) variables are found, in MLR the aim is to find a single factor that best correlates predictor (X) with predicted (Y) variables [61, 62].

3.6.1. Mathematical formulation of PLSR

PLSR decomposes the matrix of zero-mean variables X(n $\times$ N , that is the matrix of predictors) and the matrix of zero-mean variables Y(n $\times$ M , that is matrix of responses) into a combination of loadings, scores and residuals. The PLS model is given by [61-63]:

$$X = TP^T + E \tag{3.10}$$

$$Y = TQ^T + F \tag{3.11}$$

In equations (3.10) and (3.11), $T(n \times a)$ is known as the scores matrix and its elements are denoted by $t_a(a = 1,2,3, \dots, A)$. The scores can be considered as a small set of underlying or latent variables responsible for the systematic variations in X. Matrices $P(N \times a)$ and $Q(M \times a)$ are called loadings (or coefficients) matrices and they describe how the variables in T relate to the original data matrices X and Y. Finally, matrices $E(n \times N)$ and $F(n \times M)$ are called residuals matrices and they represent the noise or irrelevant variability in X and Y, respectively [61, 62].

The scores are orthogonal and are estimated as linear combinations of the original variables X_k with the coefficients, called weights, W_{ka} (a $=$ 1,2, … , A). Thus, the scores matrix T is expressed by [61]:

$$T = XW \tag{3.12}$$

Once the scores matrix T is obtained, the loadings matrices P and Q are estimated through the regression of X and Y onto T. Next, the residual matrices are found by subtracting the estimated

versions of TP^T and TQ^T from X and Y, respectively. Finally, the regression coefficients for the model are obtained using equation (3.13) [61-63]:

$$B = WQ^T \tag{3.13}$$

which yields the regression model [61-63]:

$$Y = XB + F = XWQ^T + F \tag{3.14}$$

It is important to note that in PLS the weight column vectors are orthogonal to each other, while the loadings vectors (P and Q) and Y-scores are not. The columns of the PLS scores matrix T are also orthogonal to each other. The parameters of equations (3.10) and (3.11) can also be obtained by using different forms of PLS such as the nonlinear iterative partial least squares (NIPALS) [61-63].

3.6.2. Application of PLSR to pulsed thermography inspection

As a statistical correlation method, some researchers proposed the partial least squares thermography (PLST) as an advanced technique for the treatment of thermographic images. Using PLSR, it is possible to link time and temperature data, in a similar manner as TSR (or the linking of frequency and phase-lag in PPT), allowing the extraction of the most important variations while discarding the unnecessary information present in the original thermal sequence. The application of partial least squares regression to the pulsed thermography data is achieved by decomposing the raw thermal data into multiple PLS components, each component being orthogonal to each other [61-64]. It is possible to identify through the PLS components different phenomena affecting the overall thermal regime. Each of the PLS components is characterized by its variance .The thermal images captured from the PT inspection are typically arranged in a 3D matrix, whose x and y-axis are represented, respectively, by i and j pixels, while the z-axis corresponds to the frame number.

N_x and N_y correspond to the total numbers of pixels in the x and y directions while N_t is the total number of frames [61-64].

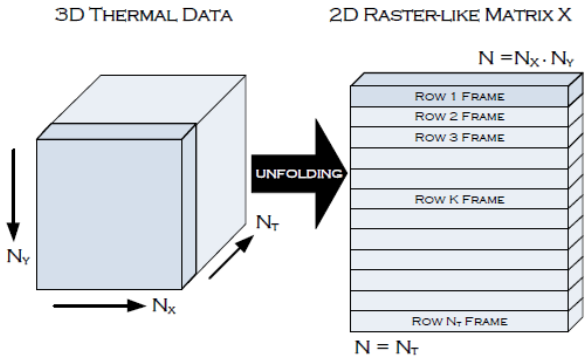

Figure 3.3: Transform the 3D thermal data into 2D matrix [62]

To perform the decomposition of the thermal data sequence into PLS components, the 3-D thermal data must be transformed into a 2-D raster-like matrix, as shown in Figure 3.3 [62]. This transformation is known as unfolding. The unfolded X matrix (corresponding to the thermal sequence) has dimensions $N_T \times N_x . N_y$ and physically represents N_T observations (or samples) of $N_x . N_y$ variables (or measurements). On the other hand, the dimension of the predicted matrix Y is defined by the observation time during which the thermal images were captured is $N_T \times 1$ [61-64]. It is necessary to select the appropriate number of PLS components to perform the decomposition of the thermal sequence matrix (which in a fact is a regression). To this aim, two parameters must be taken into account: RMSE (root mean square error) and the percentage variance explained in X matrix. The RMSE is expressed by [61-64]:

$$RMSE = \sqrt{\frac{\sum_{i=1}^{n}\left(x_i - x_{i,ref}\right)^2}{n}} \tag{3.15}$$

where n is the number of samples, $x_{i,ref}$ is the reference value and x_i is the predicted value. From Eq. (3.15) in order to find the best fits the X data it is possible to estimate the number of components. Lower RMSE values does not necessarily mean that the selected number of

components was the most appropriate for the regression model. In some cases, the RMSE tends to decrease as the number of components is increased. However, as mentioned earlier, increasing smaller components will introduce noise oscillations into the regressed data. The use of Eq. (3.15) to predict the number of latent variables should be carried out in conjunction with the analysis of the percentage of variance explained by each component [61-64].

One of the main attractions of PLST is the separation of physical effects. This is because of the orthogonality between each latent variable obtained from the decomposition of the thermal sequence [64].

The performance of these techniques can be evaluated quantitatively with different methods such as signal to noise ratio (SNR), Tanimoto criterion and probability of detection (PoD).

3. 7. Tanimoto criterion

The heuristic approach to qualitative defect detection can be illustrated with the so-called Tanimoto criterion. This is used for data comparison. Defect detection is performed by an operator or an automatic device [38]. Operators are guided by some heuristic rules which are not well understood even if it is clear that pixel amplitudes, defect pattern size, and shape are crucial in decision making [38, 65].

The Tanimoto criterion has been defined as follows [38]:

$$T_C = \frac{N_{r.d} - N_{m.d}}{N_{r.d} + N_{f.d}} \tag{3.16}$$

In this equation $N_{r.d}, N_{m.d}, N_{f.d}$ represent the numbers of true, missed and false defects which were detected by different data processing methods [38].

3. 8. Signal to noise ratio (SNR)

The signal-to-noise ratio (SNR) is an effective criterion to characterize the performance of the signal processing techniques. Using the quantification of the SNR, it is possible to analyze the relationship between the desired signal strength and the level of background noise at the maximum signal contrast [66]. This quantification helps us to determine and qualify the advantages and limitations of each processing technique based on the inspection parameters, thermal properties of the material and aspect ratio of defects. SNR is calculated using the following expression [13, 36, 62]:

$$SNR = \frac{C^2}{\sigma^2} \tag{3.17}$$

In Eq. (3.17), C^2 ($C = T_d - T_{sa}$) and σ^2 are respectively the amplitude of the signal and background noise. The signal amplitude is calculated from the contrast or temperature difference between defective and sound areas. Defective and sound areas are computed using the following expressions [62]:

$$T_d(t) = \sum_{i=1}^{nx}\sum_{j=1}^{ny}\frac{T(i,j)_d}{nx.ny} \tag{3.18}$$

$$T_{sa}(t) = \sum_{i=1}^{nx}\sum_{j=1}^{ny}\frac{T(i,j)_{sa}}{nx.ny} \tag{3.19}$$

where $\mathrm{T_d(t)}$ and $\mathrm{T_{sa}(t)}$ correspond to the temperature signals of the defective and non-defective regions. $\mathrm{T_d(t)}$ is computed as the mean value over the entire defective region. In a similar manner, $\mathrm{T_{sa}(t)}$ is computed as the mean value over the surroundings of the defective area. The area over which $\mathrm{T_{sa}(t)}$ is calculated is twice the lateral size of the defective region. Background noise is determined from the variance over the entire sound area. The variance is calculated using the following expression [36, 62]:

$$\sigma^2 = \frac{\sum_{i=1}^{n}(S_i - \bar{S})^2}{n-1} \tag{3.20}$$

In Eq. (3.20), $\bar{S}$ is the mean value of the signal and n is the total number of pixels that comprise the sound area. Eq. (3.17) can also be expressed in logarithmic decibels. In decibels, the SNR is defined as [36, 62]:

$$SNR = 10.\log_{10}\left(\frac{C}{\sigma}\right)^2 = 20.\log_{10}\left(\frac{C}{\sigma}\right) \tag{3.21}$$

It is important to note that each calculation using equations (3.17) to (3.21) is performed on every frame [36, 62].

3. 9. Probability of detection (PoD)

The probability of detection (PoD) analysis is a quantitative measuring method used to evaluate the inspection quality and the reliability of a NDT&E technique. This criterion is widely used for the traditional NDT&E techniques [67]. PoD tries to recognize the minimum flaw depth that can be reliably detected by the NDT technique. This is best done by plotting the accumulation of flaws detected against the flaw depth of all of the flaws "detected" or that produce a response over a threshold. Based on the PoD result, all defects which are deeper than a critical depth are not detected while others are detected. The tool most commonly used for PoD description is the PoD curve [68]. It was proved that the Log-Log distribution was the most acceptable [69, 70]. The mathematical expression to describe the PoD function is written below [68]:

$$PoD(a) = \frac{e^{\frac{p}{\sqrt{3}}\left(\frac{lna-\mu}{\sigma}\right)}}{1 + e^{\frac{p}{\sqrt{3}}\left(\frac{lna-\mu}{\sigma}\right)}} = \frac{e^{(a+\beta lna)}}{1 + e^{(a+\beta lna)}} \tag{3.22}$$

$$\ln\left(\frac{PoD(a)}{1-PoD(a)}\right) = a + \beta lna \tag{3.23}$$

where $\mu = -\frac{a}{\beta}$ and $\sigma = \frac{\pi}{\beta\sqrt{3}}$.

The following formula is commonly used to model the relation between a that is defect characterization and $\hat{a}$ as the maximum thermal/phase contrast [67, 71]:

$$\ln\hat{a} = \beta_0 + \beta_1 \ln(a) \tag{3.24}$$

where β_0 and β_1 are respectively intercept and slope which can be estimated by maximum likelihood. The PoD (a) function will be calculated as [67, 71]:

$$\text{PoD(a)} = \text{Probability}(\ln\hat{a} > ln\hat{a}_{dec}) \tag{3.25}$$

where $\hat{a}_{dec}$ is a decision the threshold [67, 71].

Finally, the PoD function is written based on the continuous cumulative distribution function.

$$\text{PoD(a)} = 1 - \text{F}\left(\frac{ln\hat{a}_{dec} - \beta_0 + \beta_1 \ln(a)}{\sigma}\right) = \text{F}(\frac{\ln(a) - \mu}{\sigma}) \tag{3.26}$$

where F is the continuous cumulative distribution function which has the cumulative log-normal distribution [67, 71].

3. 10. Conclusion

In this chapter, a literature review on the most popular data processing algorithms which are used in thermography applications. Thermographic signal reconstruction (TSR), Differential absolute contrast (DAC), Pulse Phase Thermography (PPT), Principal component analysis (PCA), and

Partial least square Thermography (PLST) are the most important data processing algorithm which were explained in this chapter. The performance of these methods depends on the application, material properties, camera resolusion and defect size. In order to evaluate the performance of data processing algorithms in each application, Tanimoto criterion, Signal to noise (SNR), and Probability of detection (PoD) were introduced and investigated as criteria of inspection performance. In the next chapter, the numerical 3-D simulation of line scan thermography and CFRP material using the finite elements method is investigated.

Chapter IV

Three dimensional simulation of Line scan thermography using COMSOL Multiphysics

4.1. Introduction

Thermal simulation is very popular in mathematic engineering science. Various analytical models of thermal distribution in materials have been introduced and developed in the literature. The proposed analytical models present different preciseness in comparison to the reality. Emergance of fast computers has provided the possibility of solving the thermal distribution using advanced numerical equations. Today, using fast computers, it is possible to simulate the very complex engineering issues before implementation. It has become as an essential part of science and engineering. A computer simulation environment is simply a translation of real world physical laws into their virtual form. It would be very useful to understand how much simplification takes place in the translation stage, and then it helps determining the accuracy of the resulting model [72].

4.2. COMSOL Multiphysics software

COMSOL Multiphysics is a very advanced finite element analysis environment, simulation software / FEA Software package for solving systems of time-dependent or stationary second order in space partial differential equations (PDEs) in one, two, and three dimensions. It is possible to make an interface between COMSOL Multiphysics and MATLAB and its toolboxes for a large variety of programming, preprocessing and post-processing possibilities. In addition to

conventional physics-based user-interfaces, COMSOL Multiphysics also allows for entering coupled systems of partial differential equations (PDEs) [72, 73].

4.3. Definition of a new model in COMSOL

The most important steps in order to create a thermal model in COMSOL are [72, 73]:

1. Work through the COMSOL Model to select the coordinate system for the model, the relevant physics to the problem, and the type of study you wish to perform (Time-dependent or stationary).
2. Define the parameters, equations and variables pertinent to the model (subdirectory (Global definitions).
3. Define the geometry of the model (Geometry).
4. Select the materials you wish to use in your model (Materials).
5. Select the boundary, bulk and initial conditions for your system for each physics you are using (This will be entered separately for each different physics you are using e.g. you will need to enter these for Laminar Flow and again for Heat Transfer if you are using both)
6. Choose the element size to be used (Mesh).
7. Adjust solver parameters and compute (Study).
8. Display the desired results in the most meaningful way (Results).

COMSOL Multiphysics provides sophisticated and convenient tools for geometric modeling. For many standard problems, it is possible to use provided templates in order to hide much of the complex details of modeling by equations. This is really helpful for the end user [72, 73].

4.4. Numerical Simulation of LST

In this thesis, the 3D finite elements method is employed to simulate the robotized LST inspection to determine the thermal distribution on the CFRP specimen. The linear scan thermography is composed of thermal equations and dynamic equations which must be considered at the same time. In order to simulate LST thermography in COMSOL Multiphysics, the heat transfer module and multibody dynamics module are employed. There are three important parts in this model: the dynamic heat excitation, CFRP component, and mechanical movement.

The heat transfer module simulates the dynamic heat excitation process that solves the 3D transient thermal equations using the finite elements approach in order to compute the energy and temperature distribution in the interlaminar structure of CFRP that contains subsurface defects. In this model, the heat transfer by conduction, convection, and radiation (surface to ambient and surface to surface) are considered. Figure 4.1 illustrates the schematic of the CFRP specimen with the participating of the heat fluxes.

The external excitation is applied by radiation heat transfer. Part of the incident energy is absorbed and the rest is reflected by the material surface. Due to the sudden increase in temperature caused by the thermal excitation, a thermal front is created and this propagates through the rest of the material by heat conduction. Heat transfer by convection and radiation also take place between the material surfaces and the environment. Internal discontinuities are resistive defects: regions of the material with different thermal properties which affect the heat flux rate [36]. The LST parameters must be adjusted to maximize the temperature variation on the material surface.

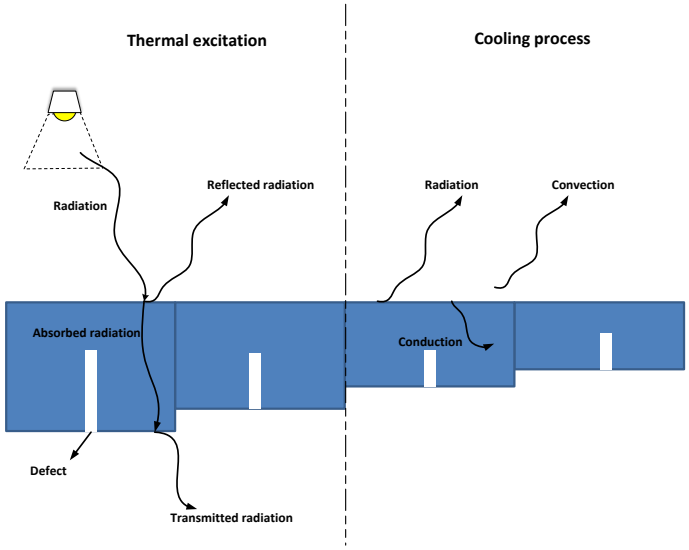

Figure 4.1: A schematic of the specimen with the heat fluxes participating

One of the primary and important steps in model definition is to create the precise geometry for the model. There are different ways to generate the geometry (each of them has some advantages and disadvantages) such as: draw the geometry, import an external CAD file, use one of the LiveLin products and import mesh data from an external file and etc.

Because of the complexity of composite structure, the next important step is to define the 3D model geometry of the CFRP specimen which consists 10 sections with various internal layers (progressively increasing from 6 to 22 plies) and in each layer, the fiber orientation has been considered (see figure 4.2-4.4). The number of layers, the defect position, and size and the composite interlaminar direction are the most important parameters in the implementation. The defects details are represented in table 4.1.

Table 4.1: Depths (mm) and diameter to depth ratios corresponding to the 30 at-bottom-holes of the reference panel

Line	section	1	2	3	4	5	6	7	8	9	10
A	D=6mm	0.88	0.86	0.63	0.69	0.94	0.99	0.42	0.86	0.54	0.65
		6.8	7.0	9.5	8.7	10.6	6.1	14.1	7.0	11.0	9.2
B	D=8mm	1.2	1.4	1.7	2.0	2.2	2.4	2.6	2.9	3.1	3.5
		6.5	5.7	4.7	4.1	3.6	3.3	3.1	2.7	2.6	2.3
C	D=10mm	1.5	2.1	2.6	3.2	3.5	3.7	4.2	4.9	5.5	6.1
		6.6	4.7	3.9	3.2	1.7	2.7	2.4	2.0	1.8	1.6

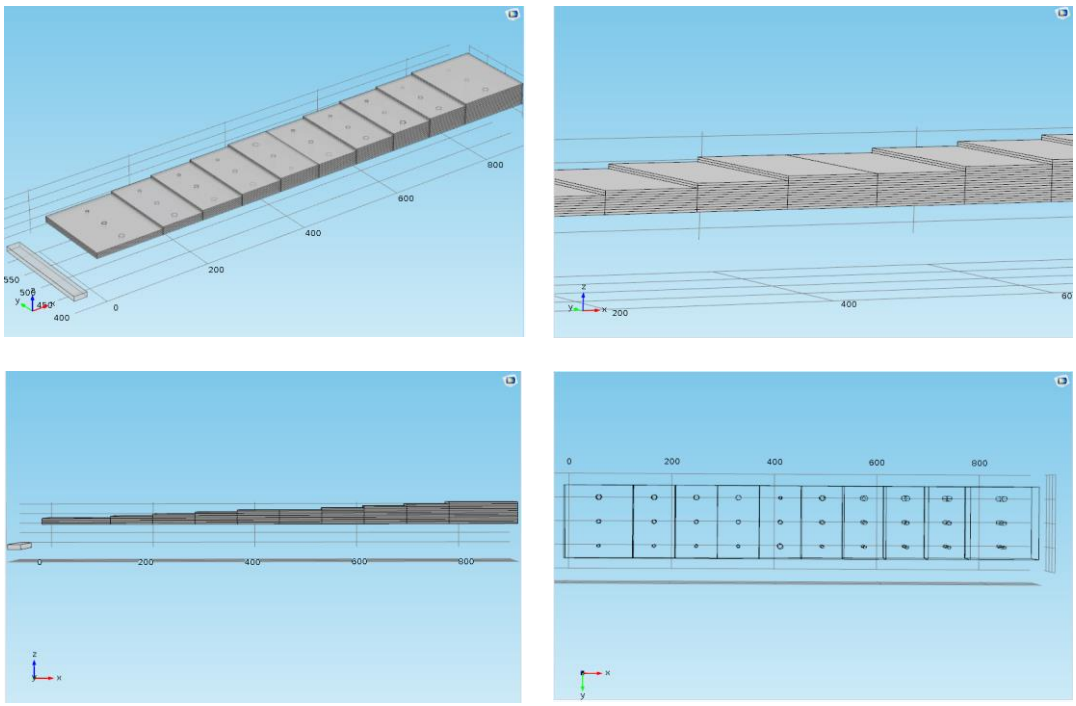

Figure 4.2: the Computational geometry of the specimen developed in COMSOL.

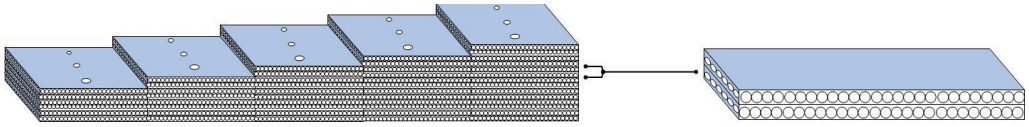

Figure 4.3: The specimen with bi-directional woven carbon fiber layers (in the left side photo, the half of the specimen is illustrated and in the right-side photo, two layers of the specimen are magnified)

One of the key steps in the simulation process is to generate the optimal mesh size. The size of the mesh is a trade-off between simulation time and result accuracy. Hence, finding the optimal mesh size is important to achieve better results. In the case of simple models, the result accuracy is verified using an analytical model, but for a the complex model, the accuracy of the analytical model is not sufficient to verify the result accuracy. In this case, a systematic mesh sizing procedure is employed to achieve the optimal mesh size. In this method, the size of the mesh is increased progressively and the accuracy is verified with the previous step until it converges [74].

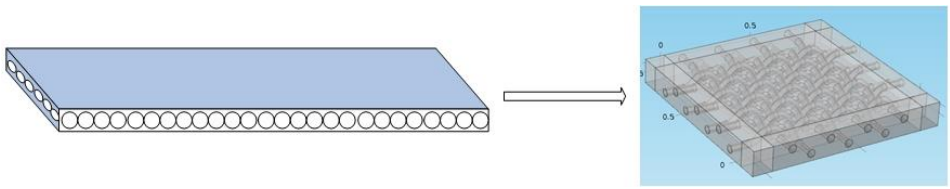

Figure 4.4: Fiber orientation in each layer

Researchers proposed various solutions to reduce model complexity and enhance the solution time. One of the popular solutions permitting to reduce model complexity is to define the model using smaller dimensions. Reducing the problem from 3-D to 2-D when possible, the model becomes significantly simpler and thus less demanding in terms of numerical solution treatment. The most often used elements in the 2-D case are the triangular elements since they account for a simpler domain partition, whereas in 3-D tetrahedral elements are used. Each of the elements is defined by its end points, called mesh vertices or geometric nodes. In the case of 2-D and 3-D elements, triangle and tetrahedron sides are also called edges, while triangles forming the boundaries of the tetrahedron are named element faces [74, 75]. Elements also differ in terms of the type of the conditions imposed on the solutions they provide. The simplest case is the so-called Lagrange elements, which are defined as to assure the continuity of the solution on the edges of the element. Unlike for example Argyris element, which also assures that the continuity of the solution first derivative on the element edges, and Hermite element, which assures that the continuity of the solution first derivative on the element node Lagrange elements provide a significant reduction in the model complexity while at the same time imposing sufficient preconditions for the solution stability to be obtained in applications such as transient heat conduction in solids where calculation of the velocity field is not needed [74].

As a result, these last remarks invite the users of FEM to pay attention when deciding on the compromise between the accuracy of the results and the model complexity. While increasing the

order of the Lagrange elements, as well as increasing number of mesh elements, contribute to the solution accuracy, they also increase drastically the number of degrees of freedom (DOF) for which the system is solved for and with it the numerical simulations more demanding in terms of calculation time and memory requirements [74].

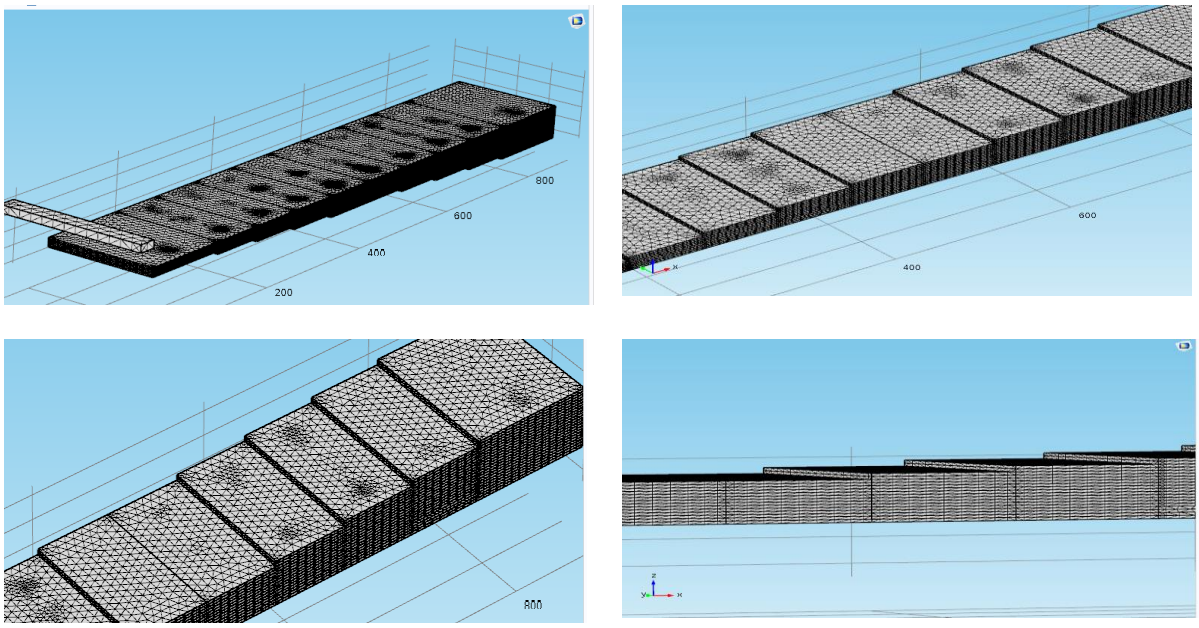

Figure 4.5: The generated 3D mesh in COMSOL

The mesh size is important due to a trade-off between accuracy of the results and simulation time. Using a finer mesh size increases the accuracy; while, it intensely increases the simulation time and requires more advanced computer hardware. Due to the anisotropy of the composite material, it may be difficult to generate the mesh in the intersections and therefore it may be difficult to achieve the convergence. The generated mesh has been shown in figure 4.5.

The most important parameters of line scan thermography setup are the source power, scanning speed and the distance between the specimen and the source. To find the optimal values, the 3-D simulation has been done using a range of values for each parameter. The 3-D heat conduction equations are solved by the finite element method in COMSOL. In this thesis, the absolute thermal

contrast (the difference of temperature between a non-defective and a defective area of the specimen) is calculated to evaluate defect visibility.

4.5. Mathematical model of the heat transfer

The temperature distribution in the specimen due to the thermal excitation in the 3-D geometry is modeled using the transient heat conduction equation, expressed in Eq, (4.1):

$$\rho c_p \frac{\partial T}{\partial t} = \frac{\partial}{\partial x}\left(k_{xx}\frac{\partial T}{\partial x}\right) + \frac{\partial}{\partial y}\left(k_{yy}\frac{\partial T}{\partial y}\right) + \frac{\partial}{\partial z}\left(k_{zz}\frac{\partial T}{\partial z}\right) \tag{4.1}$$

where ρ is the density, c_p is the specific heat capacity, T is the temperature field at coordinates x, y and z and t is the variable.The thermal conductivity is given by k, to simplify the calculation of thermal conductivity of an anisotropic sample that is related to the orientations of the principal axes of the thermal conductivity tensor (k_{xx}, k_{yy}, k_{zz}), it can be given as:

$$k = \sqrt{k_{xx}k_{yy}cos^2\gamma + k_{xx}k_{zz}cos^2\beta + k_{yy}k_{zz}cos^2\theta} \tag{4.2}$$

where θ, β, γ are, respectively angles between the line source axis and the principal axes of thermal conductivity x, y and z.

Considering that whole the specimen was at ambient temperature at the beginning of the inspection, the initial condition is given by the following expression:

$$T(x, y, z, t_o) = T_{amb} \tag{4.3}$$

The following equation presents the heat transfer by convection and radiation between the surfaces of the specimen and the ambient:

$$n \cdot (k\nabla T) = h_{conv}(T_{amb} - T) + \sigma\varepsilon(T_{amb}^4 - T^4) \tag{4.4}$$

where h_{conv} is the convective heat transfer coefficient, ε is the emissivity of the material and σ is the Stefan-Boltzmann constant.

To simulate the linear scanning thermography, there are two procedures to implement: (1) moving the specimen under the fixed heat source and camera (2) moving the heat source and camera with a fixed specimen. In this work, the second strategy is selected due to the experimental setup. Figure 4.6 Shows the motion of the heat source at a different time on the specimen by using the multibody dynamic module.

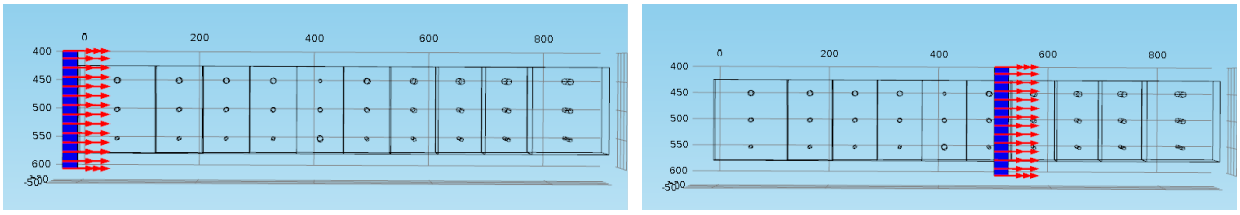

Figure 4.6: The motion of heat source on the specimen

Table 4.2: Simulation parameters used in the numerical simulation

Symbol	Simulation parameters	value
T_{amb}	Ambient temperature	293.15 K
T_0	Initial temperature	293.15 K
$H \times L \times W$	Specimen dimension	$(\delta \times \text{number of layers}) \times 900\text{mm} \times 150\text{mm}$
δ	Ply thickness	2 mm
u	Velocity	5-40 mm/sec
h	Convection heat transfer	9.1
ρ_{CFRP}	Density (CFRP)	500-2000 kg/m^3
$C_{p_{CFRP}}$	Specific heat (CFRP)	1000 J/(kg.K)
k_{CFRP}	Thermal conductivity (CFRP) $(k_{xx} = k_{yy} = k_{zz})$	24 W/(m.K)
ρ_T	Density (Teflon)	2200 kg/m^3
C_{p_T}	Specific heat (Teflon)	1050 J/(kg.K)
k_T	Thermal conductivity (Teflon)	0.25 W/(m.K)
ε	Emissivity	0.98

In this work, different values of velocity, heat source and distance are simulated in order to find the optimal parameters. The simulation parameters, as well as the thermophysical properties of the

specimen, are listed in Table 4.2. The 3D simulation results to different scanning speeds at different time values are shown in figure 4.7. Figure 4.7 shows that with increasing speed, the defect visibility decreases. The scanning speed has an impact on the observation time as well as on the amount of energy that is delivered to the specimen.

The observation time is dependent on the scanning speed. Since the scanning speed increases, the observation time decreases and the amount of energy that is delivered to the specimen decreases with reducing the observation time. Figure 4.7 illustrates the temperature variation of defect B4 at three different scanning speeds (10 to 30 mm/s) using a constant power of heat source (500W).

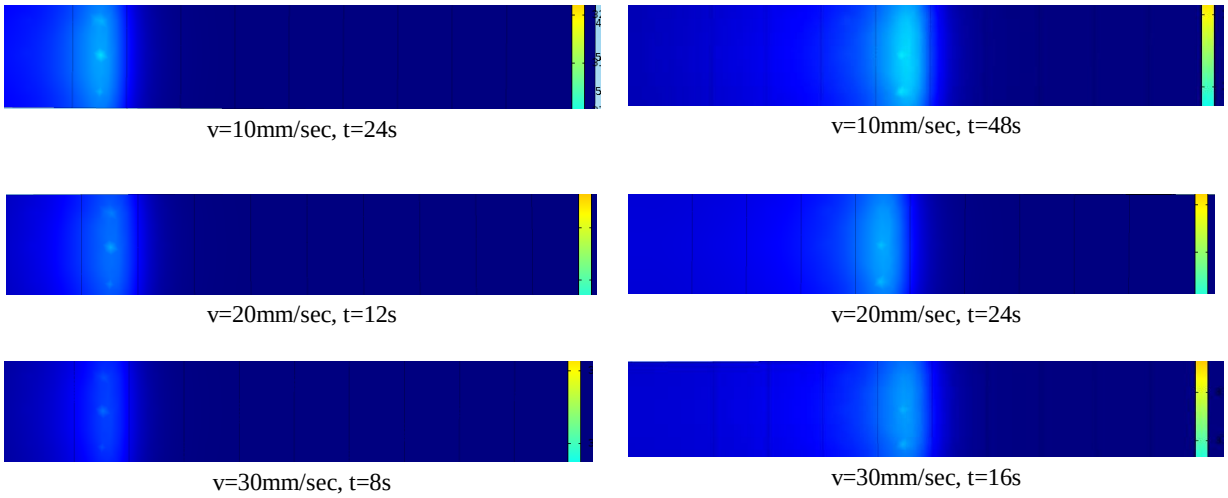

Figure 4.7: The surface temperature variation in the different scanning speed

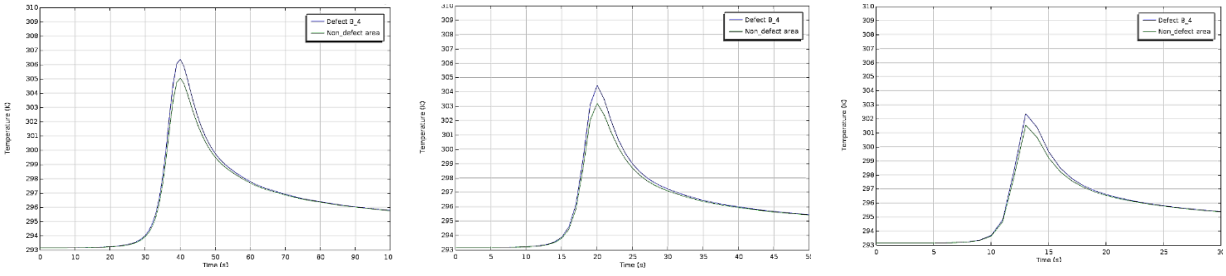

(a) v=10mm/sec (b) v=20mm/sec (c) v=30mm/sec

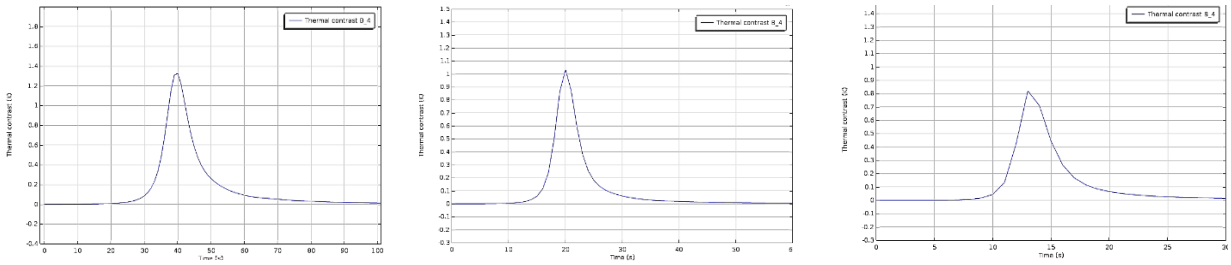

(d) v=10mm/sec (e) v=20mm/sec (f) v=30mm/sec

Figure 4.8: The thermal profiles (a-c) and thermal contrast (d-f) of Defect B4, using three scanning speeds, 10,20 and 30 mm/s (from left to right), power heat source is constant (500 W)

Figure 4.8 shows that the specimen receives more energy from the line source in the lower scanning speed and produces a higher thermal contrast. The detectability level of defects has a direct relationship with thermal contrast. This means that as thermal contrast increases, defect visibility increases. To calculate thermal contrast, the average of some pixels is selected (see figure 4.9). The thermal contrasts of three defects (A4, B4 and C4) with progressively increasing scanning speed from 10 mm/sec to 30 mm/sec were compared in figure 4.10.

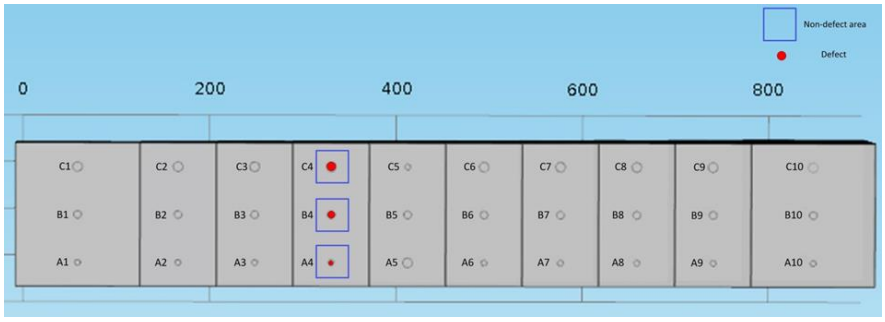

Figure 4.9: Selected defects area (red circles) and non-defects area (blue squares)

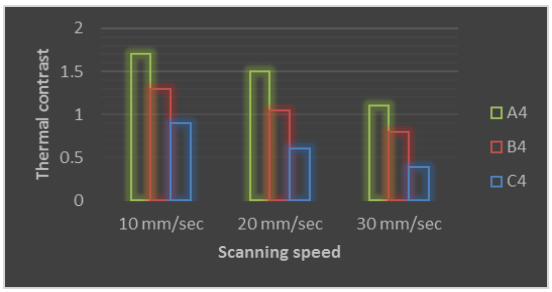

Figure 4.10: The comparison of maximum thermal contrasts (A4 with D/z=8.7, B4 with D/z=4.1 and C4 with D/z=3.2) with different scanning speeds

According to the simulation results, it is possible to detect almost all of the defects with a different level of visibility using the LST approach. The simulation results using different scanning speeds prove that a longer heating time (lower scanning speed) increases the defect visibility due to the time during which energy is delivered to the specimen surface.

In this chapter, the analytical model of LST was presented to study how the optimum inspection parameters could be set. The LST inspection is simulated using the 3D-FEM approach. COMSOL Multiphysics was the attractive and strong software used to simulate the model. The first step has defined the geometry. This step is important due to the anisotropy of the woven carbon fiber. Selecting the mesh size was the next significant step according to a trade-off between the accuracy of the results and the simulation time. There are many sub-steps to complete the model such as defined parameters and functions, adding materials, selecting the modules and their sub nodes and etc. Finally, the results of simulation is employed to enhance the defect visibility with finding the best parameters.

4.6. **Conclusion**

In this chapter, the 3-D simulation of line scan thermography using COMSOL Multiphysics was presented and explained. The simulation is composed of thermal equations and dynamic equations.

The heat source and CFRP material are important parts of the simulation. The CFRP material has a complex interlaminar structure which leads to a high number of mesh at the edge. The 3-D model of CFRP specimen was implemented in COMSOL. A light heat source has employed in simulation to warm the specimen. The optimal size of the mesh was selected according to a systematic procedure. The simulation was done using different heat source and scanning speeds. The result was investigated and compared in different heat source and scanning speed.

The main contribution of this chapter is to indentify the important parameters of line scan thermography which affect the performance of inspection. The simulation results show that the material characteristics, source power, scan speed, and distance between the specimen and the source are the most important parameters in LST inspection. Regarding the simulation results, lower scanning speed enhances the thermal contrast.

Chapter V

Infrared Testing of CFRP Components: Comparisons of Approaches using the Tanimoto Criterion

5. 1. Résumé

De nos jours, les matériaux composites sont largement utilisés dans divers domaines. Le polymère renforcé de fibres de carbone (PRFC) est l'un des composites qui joue un rôle important dans différents domaines tels que l'aérospatiale, l'aéronautique, le nucléaire, l'industrie civile, l'industrie automobile, les équipements sportifs, militaires et bien d'autres. capacités telles que poids léger, résistance thermique élevée, rigidité élevée, résistance élevée à la corrosion, résistance à la fatigue élevée, conductivité électrique élevée, résistance mécanique, chimique et de température élevée. Le composite de fibre de carbone a une faible résistance à l'impact et à la compression. Il peut être affecté par différents dommages, défaillances et défauts de diverses manières. Normalement, les dommages aux composites ne sont pas visibles. La thermographie IR est l'une des méthodes utiles pour la détection des défauts et des dommages. Dans cet article, quatre approches de traitement des données sont utilisées pour inspecter l'échantillon: thermographie pulsée et Lock-in, vibrothermographie et LED. De plus, un certain nombre de techniques avancées de traitement du signal ont été utilisées pour traiter les données brutes obtenues à partir de l'inspection d'un composant en PRFC, qui contient 25 défauts internes de différentes tailles situés à différentes

profondeurs sous la surface. Pour évaluer la capacité de chaque technique à réduire le bruit, le critère de Tanimato est utilisé.

5. 2. Summary

Nowadays, composite materials are widely used in various fields. Carbon fiber reinforced polymer (CFRP) is one of the composites that plays an important role in different fields such as in the aerospace field, aircraft industry, nuclear field, civil industry, automobile industry, sport equipments, military and many others due to its specific capabilities such as low weight, high thermal strength, high rigidity, high corrosion resistance, high fatigue strength, high electrical conductivity, high mechanical, chemical, and temperature resistance. Carbon fiber composite has a low resistance to impact and compression. It can be affected by different damages, failures, and defects in various ways. Normally, the damages to composites are not visible. IR thermography is one of the useful methods for detection of defects and damages. In this paper, four data processing approaches are employed to inspect the specimen: pulsed and Lock-in thermography, vibrothermography and LED. And also, a number advanced signal processing techniques have been used to process raw data obtained from the inspection of a CFRP component, which contains 25 internal defects with different sizes that located at different depths under the surface. To evaluate the ability of each technique to reduce the noise, Tanimato criterion is used.

Infrared Testing of CFRP Components: Comparisons of Approaches using the Tanimoto Criterion

Saeed SOJASI [1], Fariba KHODAYAR [1], Fernando LOPEZ [1], Clemente IBARRA-CASTANDO[1], Xavier MALDAGUE[1], Vladimir P. VAVILOV[2], Arseny O. CHULKOV[2]
Electrical and Computing Engineering Dept., Université Laval, Quebec City (Quebec), Canada
Phone: +11 418656 2962, Fax: +11 418 656 3594 e-mail: saeed.sojasi.1@ulaval.ca, fariba.khodayar.1@ulaval.ca, ferlopezro@gmail.com,Clemente.Ibarra-Castanedo@gel.ulaval.ca, Xavier.Maldague@gel.ulaval.ca Institute of Non-destructive Testing, Tomsk Polytechnic University; Tomsk, Russia; e-mail: vavilov@tpu.ru, chulkovao@tpu.ru

Abstract

In the last few years, composites increasingly have been used in various fields. Carbon fiber reinforced polymer (CFRP) is one of the composites that is widely used for a variety of purposes such as in the aerospace field, aircraft industry, medical field, automobile industry, military and many others. Non-destructive testing (NDT) with infrared thermography techniques have been broadly applied to defect detection in specimens. In the later, excitations sources from mechanical, convective, optical, or induction sources are typically employed. In this paper, the capabilities of different approaches such as conventional pulsed and Lock-in thermography, vibrothermography and LED illumination have been compared in order to detect artificial Teflon inserts between CFRP plies. For this purpose, Tanimoto criterion has been used on acquired images by different methods. A 3D finite element method (FEM) with COMSOL Multiphysics has been used in parallel to simulate and optimize the parameters of experiments.

Keywords: pulsed thermography, Lock-in thermography, vibrothermography, non-destructive testing, carbon fiber composite

1. Introduction

In the recent years, carbon fiber reinforced plastic (CFRP) has been considered one of the most popular composite materials and has been increasingly used in different fields such as aerospace industry, civil engineering, renewable energy, sport tools, and many others due to its specific capabilities such as low weight, high thermal strength, high rigidity, high corrosion resistance, high mechanical, chemical, and temperature resistance. Carbon fiber composite has a low resistance to impact and compression. It can be affected by different damages, failures and defects in various ways. Normally, the damages to composites are not visible.

Non-destructive testing (NDT) is one of the useful methods for the detection of defects in different materials [5, 6, 7]. This technique does not have any negative effect on the specimens. The various techniques of nondestructive testing are used in different fields to ensure accuracy, verify integrity, reduce production costs and detect defects. There are many useful NDT methods to detect the flaws and delamination which have been used according to defect size and type, material, and defect location.

One of the attractive methods in NDT is infrared thermography, which is divided into two main groups: active and passive thermography, which depends on use or not of an external source [13]. There are many sources in active thermography, which are selected according to material physical properties, size and shape of specimens, the thermal properties, and etc. They can be divided into mechanical (vibrothermography) and optical sources (photographic flash and halogen lamps) [16]. In addition, light emitting diode (LED) technology has been developed in recent years. In comparison with incandescent lamps, it has some advantage such as: more compact, low power, and little radiation. These characteristics of the LED make them a potential candidate for

thermographic NDE applications to test specimens. High power light emitting diode (LED) has been used for long pulse and lock-in thermography [14]. The powerful LEDs are used to reduce reflection of radiation. These types of techniques are based on the principle of a 'dark field' which can be used for detecting limits for structural defects [15]. In this paper, the specimen is stimulated by pulsed thermography (PT), lock-in thermography (LT), vibrothermography (VT) and a light emitting diode (LED) to detect the defects. Normally, the raw images are not perfect for analysis. Therefore, data processing methods have been used for defect detection and characterization [17]. In this work, a number of techniques have been used to process the images such as: Thermographic signal reconstruction (TSR), Differential absolute contrast (DAC), Pulsed Phase Thermography (PPT), principal component thermal (PCT), Partial least squares (PLS). These techniques are described in the following sections.

2. Thermography

2.1 Pulsed thermography

Pulsed thermography (PT) is a very fast technique in the NDT field. In this technique, energy is applied to the specimen in a short time. This time can be a few milliseconds (2-15 ms) for high thermal conductivity materials and a few seconds for low-conductivity materials. Pulsed thermography (PT) uses a power optical source to submit a short heating pulse on the specimen surface [8]. Pulse energy increases the temperature of the specimen surface. After the pulse heating, the surface temperature will decrease [9]. The surface temperature will decrease with a uniform rate for non-defect areas and with a non-uniform rate for defect areas. The IR camera will

record the abnormal temperature patterns. Therefore, the defect can be detected. The flaw depth can be estimated by thermal propagation time and thermal properties of the materials.

$$t = \frac{z^2}{\alpha} \quad (1)$$

$$\alpha = \frac{K}{c.p} \quad (2)$$

In equation (1) and (2) z is the thickness of the material and α is the thermal diffusivity, k is the thermal conductivity, c is the specific heat and ρ is the density. In a complex structure, a specimen's calibration is used to estimate location of the flaws [18].

2.2 Lock-in thermography

Lock-in Thermography (LT) [2] is based on thermal waves which are generated inside a specimen by periodic deposition of heat on a specimen's surface [1]. In the lock-in thermography (LT), sometimes called modulated thermography, thermal waves are injected into the specimen periodically by one or several heating sources such as halogen lamps. Internal defects change amplitude and phase of the response signal on the surface. The response signal is recorded by an infrared camera. In this technique sinusoidal waves are usually employed although use of other periodic waves is also possible. Sinusoidal waves are suggested as input in lock-in thermography because the amplitude and phase can be changed, while the frequency and shape of response signal are preserved [3]. Generally, the phase information (which is related to the propagation delay of the thermal waves) is of interest since being related to the travel propagation of the thermal waves inside the specimen. This propagation is obviously affected by the presence of subsurface defects.

2.3 Vibrothermography (VT)

Vibrothermography is another method of active thermography. This technique evaluates heat that is produced by vibration or ultrasonic in the specimens [4]. Under the effect of mechanical vibration, heat is released by friction at defect locations (such as cracks). Vibrothermography can be employed in acoustic thermography, elastic-wave-activated thermography, ultrasonic infrared thermography, sonic IR, thermal vibration method (vibroIR) [4]. Vibrothermography is a very fast and sensitive technique [8]. For the detection of defects which are located in the deeper layer or cracks, vibrothermography is superior to optical methods. To compare VT with optical methods, thermal waves travel half the distance from the defect to the surface in VT (waves produced in the defect) while in optical methods these waves (reflection) have to travel from the surface to the defect and the return to the surface. VT is more appropriate for small objects. The limitation of vibrothermography in comparison to optical methods is that it needs a coupling media between the sample and the transducer [3]. In this study the vibration frequency was set to 20 kHz in all cases. The modulation frequencies are 0.125 Hz, 0.250 Hz, and 0.500 Hz. The percentage of energy are 00-50 pct, 20-50 pct, and 30-50 pct, the amplitude is varied between these two values.

2.4 LED optical excitation

In this paper, high power LED arrays for pulse and lock-in thermography are studied. Long pulse LED is compared to conventional flash thermographic and square wave lock-in LED excitation is compared to conventional lock-in approach.

3. Test specimen and data analysis

In this study, the experiment was tested on a CFRP laminate where 25 square defects between the different plies. The defects are composed of TeflonTM pieces which have dimensions ranging from 3 mm to 15 mm and are located at different depths ranging from 0.2 mm to 1 mm. Figure 1 shows the schematic of the specimen.

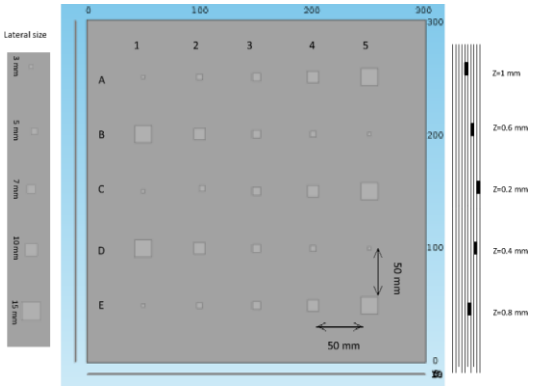

Figure 1. Schematic representation and defect location for specimen CFRP006

In this paper, the Tanimoto criterion was used to compare the capabilities of the different signal processing methods (DAC, PPT, PCT, TSR, PLST) for qualitative defect detection [10-12,19]. The Tanimoto criterion has been defined as follows:

$$T_c = \frac{N_{r.d} - N_{m.d}}{N_{r.d} + N_{f.d}} \qquad (3)$$

In this equation $N_{r.d}, N_{m.d}, N_{f.d}$ represent the numbers of true, missed and false defects which were detected by different data processing methods. In this study, the thermograms selected are summarized in the table 1:

Table 1 : Calculated Tanimoto criterion in different thermography algorithms

Excitation source	Signal processing method	The thermogram selected		Tanimoto criterion %
Pulsed thermography	RAW	t = 1.7159 s		64.2
Lock-in thermography	RAW	f = 100		58.6
		f = 200		60.7
		f = 300		55.6
		f = 400		53.5
		f = 700		51.8
		f = 1200		50.5
Vibrothermography	RAW	20kHz 0.125Hz 00-50 pct		52.0
		20kHz 0.250Hz 00-50 pct		48.0
		20kHz 0.250Hz 20-50 pct		52.0
		20kHz 0.500Hz 20-50 pct		50.0
		20kHz 0.500Hz 30-50 pct		53.8
Pulsed thermography	DAC	t = 1.109 s		66.7
LED (Pulsed thermography)	DAC	t = 0.98 s		16.0
Pulsed thermography	TSR	polynomial 4 and derivative 1		88.4
		polynomial 4 and derivative 2		75.0
LED (Pulsed thermography)	TSR	polynomial 4 and derivative 1		27.5
		polynomial 4 and derivative 2		25.0
Pulsed thermography	PCT	EOF4		76.9
Vibrothermography	PCT	20kHz 0.125Hz 00-50 pct	EOF3	60.7
		20kHz 0.250Hz 00-50 pct	EOF3	58.6
		20kHz 0.250Hz 20-50 pct	EOF3	64.2
		20kHz 0.500Hz 20-50 pct	EOF3	48.1
		20kHz 0.500Hz 30-50 pct	EOF4	50.0
Lock-in thermography	PCT	f = 100	EOF3	88.4
		f = 200	EOF4	84.6
		f = 300	EOF3	73.0

		f = 400	EOF3	80.0
		f = 700	EOF3	71.4
		f = 1200	EOF3	57.6
LED (Pulsed thermography)	PCT	EOF3		28.0
LED (Lock-in)	PCT	EOF2		16.0
Pulsed thermography	PPT	Phase image, f = 0.27 Hz		69.2
Vibrothermography	PPT	20kHz 0.125Hz 00-50 pct	Phase image: f = 0.055 Hz	60.7
		20kHz 0.250Hz 00-50 pct	Phase image: f = 0.165 Hz	60.7
		20kHz 0.250Hz 20-50 pct	Phase image: f = 0.055 Hz	62.9
		20kHz 0.500Hz 20-50 pct	Phase image: f = 0.183 Hz	46.4
		20kHz 0.500Hz 30-50 pct	Phase image: f = 0.165 Hz	57.1
Lock-in thermography	PPT	f = 100	Phase image: f = 0.110 Hz	88.4
		f = 200	Phase image: f = 0.165 Hz	66.6
		f = 300	Phase image: f = 0.165 Hz	69.2
		f = 400	Phase image: f = 0.110 Hz	50.0
		f = 700	Phase image: f = 0.110 Hz	57.6
		f = 1200	Phase image: f = 0.760 Hz	28.5
LED (Pulsed thermography)	PPT	f = 0.25 Hz		12.0
LED (Lock-in	PPT	f = 0.30 Hz		12.0
Pulsed thermography	PLST	4th PLS loading		92.3
Vibrothermography	PLST	20kHz 0.125Hz 00-50 pct	2nd PLS loading	60.7
		20kHz 0.250Hz 00-50 pct	2nd PLS loading	60.7
		20kHz 0.250Hz 20-50 pct	2nd PLS loading	58.6
		20kHz 0.500Hz 20-50 pct	2nd PLS loading	51.8
		20kHz 0.500Hz 30-50 pct	3rd PLS loading	48.1
Lock-in thermography	PLST	f = 100	3rd PLS loading	92.3
		f = 200	3rd PLS loading	92.0
		f = 300	3rd PLS loading	65.3
		f = 400	3rd PLS loading	60.0
		f = 700	3rd PLS loading	41.6
		f = 1200	3rd PLS loading	18.5
LED (Pulsed thermography)	PLST	2nd PLS loading		44.0
LED (Lock-in)	PLST	2nd PLS loading		28.0

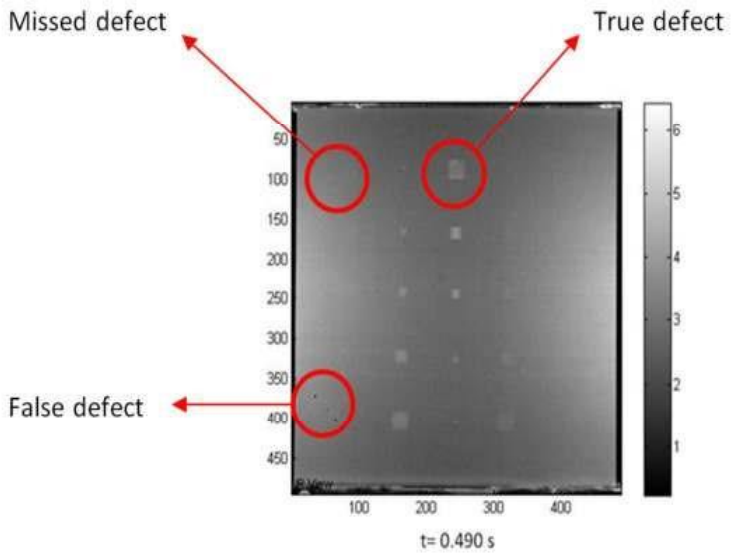

Figure 2. A typical raw image

In Table 1, t = 1.7159 s was selected because it corresponds to the best visibility time for a «maximum number of defects». The results of different methods are compared as below:

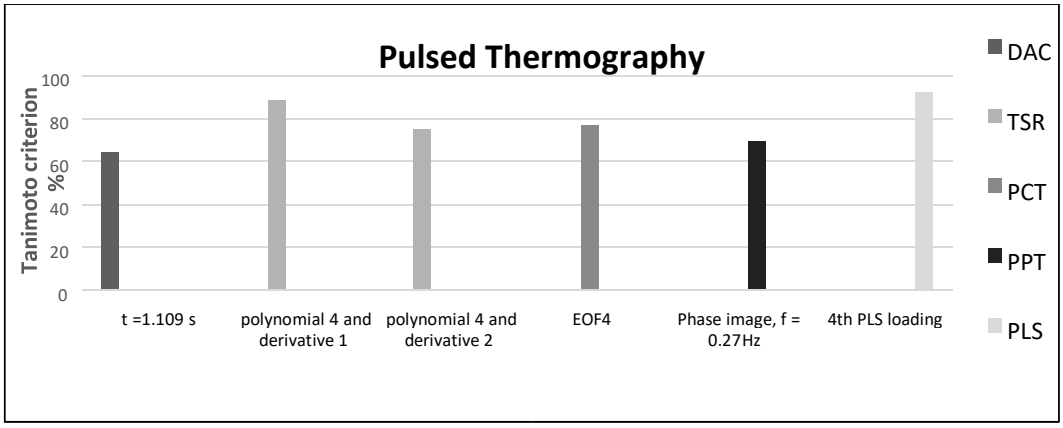

Figure 3.Diagram of compared results of different data processing techniques in pulsed thermography

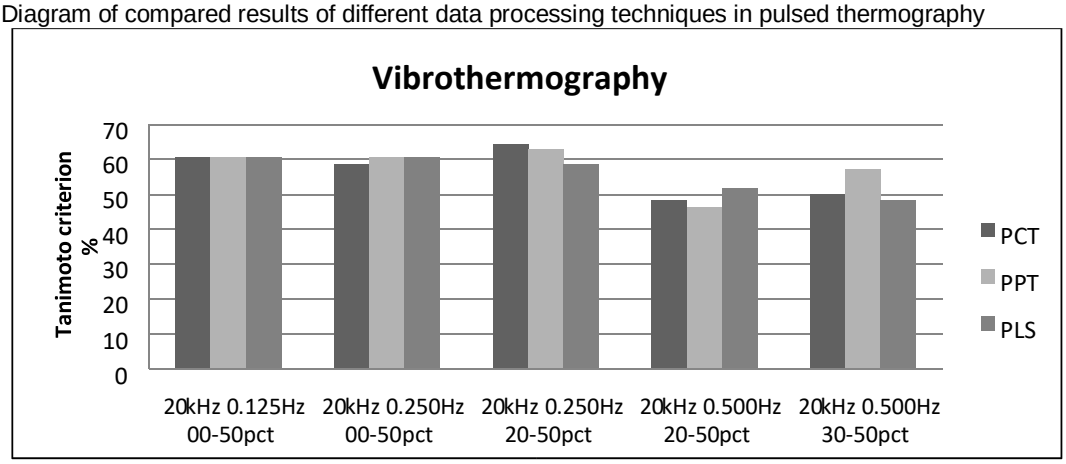

Figure 4. Diagram of compared results of different data processing techniques for Vibro-thermography

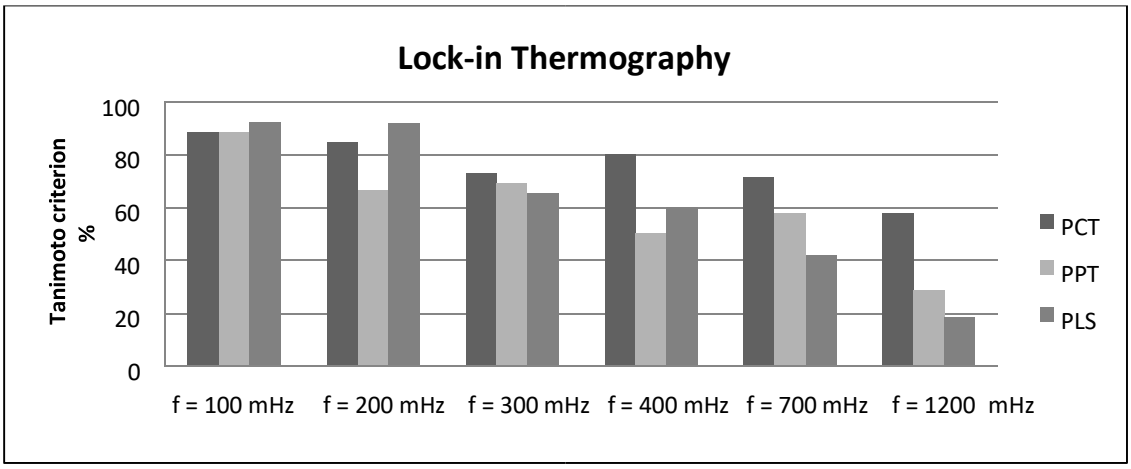

Figure 5.Diagram of compared results of different data processing techniques for lock-in thermography

4. Discussion

The important conclusion is that all used techniques have provided estimates of detection efficiency around 60 to 90 % by the Tanimoto criterion. For example, the best results (Tanimoto criterion ~ 90%) appeared in the case of lock-in thermography with PLST processing. However, we consider that not only the type of test procedure and/or the data processing algorithm used but also the power and rate of heating play a crucial role in ensuring detectable signals over hidden defects. In fact, this study simply confirms the fact that heating must be short and powerful (for this kind of CFRP laminates). This explains the surprisingly bad results obtained when applying LEDs (Tanimoto criterion values not exceeding 16 %). Even if reflected radiation was absent in this case, the energy input was fairly weak. For instance, continuous heating for 25 seconds resulted only in 8 °C of excess temperature while using a 500 W LED panel and the measured differential temperature signals (defect vs non-defect) were in order of centigrade fractions.Probably, the absorption coefficient was relatively low at the LED wavelength of about

0.6μm even if the CFRP laminate was visually black. Therefore, the rate of heat diffusion in defect areas was comparable if not higher than the heating rate elsewhere, thus «washing away» defect patterns.

5. Conclusion

It has been confirmed experimentally that infrared thermography is a useful tool in non-destructive testing of CFRP composite. There are different thermal NDT techniques of which efficiency depends on material characteristics test conditions. In this paper, four types of stimulating sources (pulse, lock-in, vibro and LED) have been applied to a CFRP laminate. The qualitative defect detection based on Tanimoto criterion was used to compare different signal processing methods.

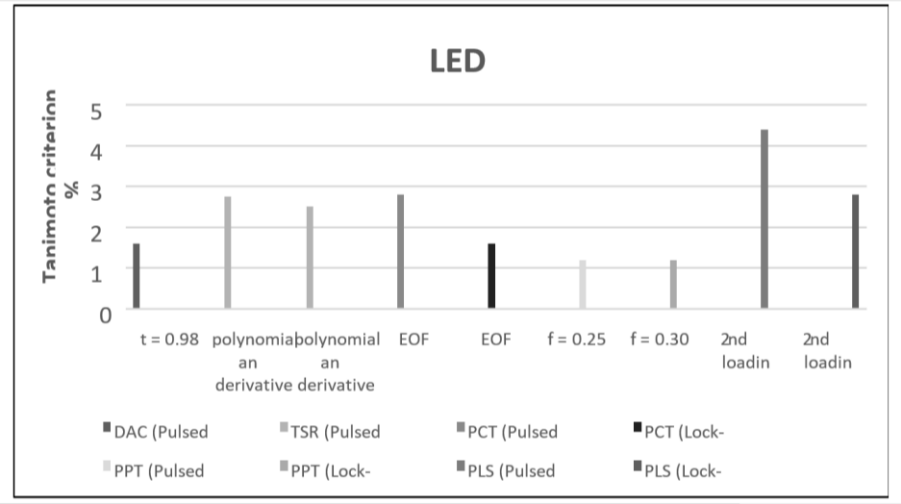

Figure 6.Diagram of compared results of different data processing techniques for LED

In the raw images, the defects which are large and near the surface are easily observed. To detect the defects which are smaller and deeper, signal processing techniques such as TSR, DAC, PPT,

PCT and PLST need to be used. Surprisingly, the results of using LED heating have not confirmed efficiency of this stimulation approach, probably, because of slow and low power input.

Reference

[1] Maldague, Xavier. "Theory and practice of infrared technology for nondestructive testing." (2001).
[2] Pickering, Simon, and Darryl Almond. "Matched excitation energy comparison of the pulse and lock-in thermography NDE techniques." *NDT & E International*41, no. 7 (2008): 501-509.
[3] Ibarra-Castanedo, Clemente, Marc Genest, Stéphane Guibert, Jean-Marc Piau, Xavier PV Maldague, and Abdelhakim Bendada. "Inspection of aerospace materials by pulsed thermography, lock-in thermography, and vibrothermography: a comparative study." In Defense and Security Symposium, pp. 654116-654116. International Society for Optics and Photonics, 2007.
[4] Szwedo, M., L. Pieczonka, and T. Uhl. "Application of vibrothermography in nondestructive testing of structures." In 6th European Workshop on Structural Health Monitoring. 2012.
[5] He, Yunze, Guiyun Tian, Mengchun Pan, and Dixiang Chen. "Impact evaluation in carbon fiber reinforced plastic (CFRP) laminates using eddy current pulsed thermography." Composite Structures 109 (2014): 1-7.
[6] Keo, Sam-Ang, Franck Brachelet, Florin Breaban, and Didier Defer. "Development of an Infrared Thermography Method with CO2 Laser Excitation, Applied to Defect Detection in CFRP." World Academy of Science, Engineering and Technology 80 (2013).
[7] Salski, Bartlomiej, Wojciech Gwarek, Przemyslaw Korpas, Szymon Reszewicz, Alvin YB Chong, Panagiotis Theodorakeas, Ieremias Hatziioannidis et al. "Non-destructive testing of carbon-fibre-reinforced polymer materials with a radio-frequency inductive sensor." Composite Structures 122 (2015): 104-112.
[8] Montanini, Roberto, and Fabrizio Freni. "Correlation between vibrational mode shapes and viscoelastic heat generation in vibrothermography." NDT & E International 58 (2013): 43-48.
[9] Mendioroz, A., A. Castelo, R. Celorrio, and A. Salazar. "Characterization and spatial resolution of cracks using lock-in vibrothermography." NDT & E International 66 (2014): 8-15.
[10] Duan, Yuxia, Stefanie Huebner, Ulf Hassler, Ahmad Osman, Clemente Ibarra-Castanedo, and Xavier PV Maldague. "Quantitative evaluation of optical lock-in and pulsed thermography for aluminum foam material." Infrared Physics & Technology 60 (2013): 275-280.
[11] VAVILOV, Vladimir P., and Arsenii O. CHULKOV. "Thermal NDT of Composites in the Aero Space Industry: A Quantitative Approach." [12] Vavilov, Vladimir P., Paolo G. Bison, and Ermanno G. Grinzato. "Statistical evaluation of thermographic NDT performance applied to CFRP." In Aerospace/Defense Sensing and Controls, pp. 174-177. International Society for Optics and Photonics, 1996.
[12] Lopez, Fernando, Clemente Ibarra-Castanedo, Xavier Maldague, and V. Nicolau. "Pulsed thermography signal processing techniques based on the 1D solution of the heat equation applied to the inspection of laminated composites." Mater. Eval 72 (2014): 91-102.
[13] Pickering, S. G., K. Chatterjee, D. P. Almond, and S. Tuli. "LED optical excitation for the long pulse and lock-in thermographic techniques." NDT & E International 58 (2013): 72-77.
[14] Vavilov, Vladimir. "Thermal NDT: historical milestones, state-of-the-art and trends." Quantitative InfraRed Thermography Journal 11, no. 1 (2014): 66-83.
[15] Ibarra-Castanedo, Clemente, Marc Genest, Jean-Marc Piau, Stéphane Guibert, Abdelhakim Bendada, and Xavier PV Maldague. "Active infrared thermography techniques for the nondestructive testing of materials." Capter XIV of the book:"Ultrasonic and Advanced Methods for Nondestructive Testing and Material Characterization", ed. Chen CH (2007): 325-348.
[16] Madruga, Francisco J., Clemente Ibarra-Castanedo, Olga M. Conde, José M. López-Higuera, and Xavier Maldague. "Infrared thermography processing based on higher-order statistics." NDT & E International 43, no. 8 (2010): 661-666.
[17] Genest, Marc, Clemente Ibarra-Castanedo, Jean-Marc Piau, Stéphane Guibert, Mirela Susa, Abdel Hakim Bendada, Xavier Maldague, and Abbas Fahr. "Comparison of Thermography Techniques for Inspection of CF-18 Honeycomb Structures}." In Aircraft Aging 2007 Conference}. 2007.
[18] LÓPEZ, Fernando, Vicente NICOLAU, Xavier MALDAGUE, and Clemente IBARRA-CASTANEDO. "Multivariate Infrared Signal Processing by Partial Least-Squares Thermography.", Proc. VIIth IWASPNDE, pp 29-34, Québec, Canada (2013).

Chapter VI

Optimization of the Inspection of Large Composite Materials Using Robotized Line Scan Thermography

6. 1. Résumé

La thermographie à balayage de ligne robotisée est l'une des méthodes dynamiques utiles qui sont employées pour l'inspection de composants de forme large et complexe. Dans cette technique, deux méthodes peuvent être utilisées: 1) la caméra IR et la source de chaleur sont installées sur le bras du robot. Ces composants se déplacent en tandem, tandis que l'échantillon reste fixe ou 2) la caméra infrarouge et la source sont fixes et l'échantillon est déplacé.

Pour régler tous les paramètres d'inspection tels que la vitesse de la source de chaleur, la distance entre la tête d'inspection et l'échantillon, le taux d'acquisition et la vitesse de balayage, un programme informatique fournissant les commandes du bras robotisé est utilisé.

La caméra IR enregistre le dépôt de chaleur dans le composant et le processus de refroidissement suivant. Les données acquises sont ensuite réorganisées en une séquence pseudo-statique (PSS) pour une analyse et un traitement plus poussés, de la même manière que dans la configuration statique. Dans cet article, la thermographie par balayage linéaire (LST) robotisée a été étudiée afin d'inspecter un grand spécimen de PRFC utilisé dans l'industrie aérospatiale.

La méthode LST robotisée présente certains avantages par rapport aux approches statiques. LST robotisé fournit une uniformité de chauffage et permet le traitement d'image qui améliore la probabilité de détection, permettant à un composant à grande échelle d'être inspecté sans perte de

résolution. En utilisant l'approche LST, il est possible d'inspecter de grandes surfaces à des vitesses de balayage élevées. De plus, les résultats d'inspection sont immédiatement disponibles pour analyse pendant que le processus de numérisation se poursuit. Des méthodes de traitement d'image sont employées pour augmenter la probabilité de détection de défauts. Le critère de probabilité de détection (PoD) a été utilisé pour comparer les algorithmes de traitement et la valeur de PoD a déterminé lequel d'entre eux est le plus approprié.

6. 2. Summary

Robotized line scanning thermography is one of the useful dynamic methods which is employed for the inspection of large and complex shaped components. In this technique, two methods can be used: 1) the IR camera and heat source are installed on the robot arm. These components move in tandem, while the specimen remains fixed or 2) the infrared camera and source are fixed and the specimen is moved.

To tune the all inspection parameters such as speed of the heat source, the distance between the inspection head and the specimen, acquisition rate, and the scanning velocity, a computer programme which provides the commands for the robotic arm is used.

The IR camera records the deposition of heat into the component and the subsequent cooling process. The acquired data is then reorganized as a pseudo-static sequence (PSS) for further analysis and processing in a similar way as is done in the static configuration. In this paper, robotized line scan thermography (LST) was investigated in order to inspect a large CFRP specimen which is used in the aerospace industry.

There are some advantage for the robotized LST method in comparison with the static approaches. Robotized LST provides heating uniformity and allows image processing which enhances the detection probability, allowing a large-scale component to be inspected without the loss of

resolution. Using the LST approach, it is possible to inspect large areas at high scan speeds. Also, the inspection results are immediately available for analysis while the scanning process continues. Image processing methods are employed to increase defect detection probability. The probability of detection (PoD) criterion has been used to compare processing algorithms and PoD value determined which of them is more suitable.

J Nondestruct Eval (2017) 36:32
DOI 10.1007/s10921-017-0412-x

Optimization of the Inspection of Large Composite Materials Using Robotized Line Scan Thermography

Fariba Khodayar[1] · **Fernando Lopez**[1] · **Clemente Ibarra-Castanedo**[1] ·Xavier Maldague[1]

Abstract

The emergence of composite materials has started a revolution in the aerospace industry. When using composite materials, it is possible to design larger and lighter components. However, due to their anisotropy, composite materials are usually difficult to inspect and detecting internal defects is a challenge. Line scan thermography (LST) is a dynamic thermography technique, which is used to inspect large components of metallic surfaces and composites,commonly used in the aerospace industry. In this paper, the robotized LST technique has been investigated on a large composite component which contains different types of internal defects located at a variety of depths. For theoretical analysis, the LST inspection was simulated using a mathematical formulation based on the 3D heat conduction equation in the transient regime in order to determine the optimum parameters. The solution of the model was performed using the finite element method. The LST parameters were adjusted to detect the deepest defects in the specimen. In order to validate the numerical results with experimental data, a robotized system in which the infrared camera and the heating source move in tandem, has been employed. From the experimental tests, it was noted that there are three sources of noise (non-uniform heating, unsynchronized frame rate with scanning speed and robot arm vibration) which affect the performance of the test. In this work, image processing techniques that were initially developed to be applied on pulse thermography have been successfully implemented. Finally, the performance of each technique was evaluated using the probability of detection approach.

Published online: 03 April 2017

Keywords Line scanning thermography, Finite element analysis,·Non-destructivetest,·Aerospace industry, Robotic inspection, Large composite

1 Introduction

Nowadays, composite materials, specifically carbon fiber reinforced polymers (CFRPs), play a dominant role in science as well as civil, nuclear, aerospace, renewable energy and automobile industries. These materials significantly improve the mechanical properties, providing high stiffness, higher strength, and improving the fatigue resistance [1,2]. Aerospace engineers prefer materials which are lighter and easier to shape. Advanced composites such as CFRPs have been increasingly utilized in aerospace structures such as aps, slats, spoilers, elevators, etc. CFRPs offer valuable properties to manufacture complex-shaped components with reduced manufacturing time [1,3,4]. Due to their interlaminar structure, CFRPs distribute the energy of impact over a large area using a polymeric matrix. This characteristic makes them more resistant against low velocity impacts, but it may increase the detection probability of internal defects that cannot be observed from the surface [1]. Therefore, due to the high probability of damaging composite materials, engineers must inspect and evaluate the components during the different steps of manufacturing, service and maintenance. In order to detect subsurface defects, non-destructive testing (NDT) techniques are employed. In the case of composite materials, a variety of NDT methods have been proposed in the literature to evaluate composite materials. Infrared thermography [5–8], ultrasonic [9] or thermosonics [10], SQUID magnetic response [1], and X-ray [11] are some of the methods used for the inspection of composite materials [12,13]. The final selection of an NDT technique depends on the defect type, material characteristics, accessibility, sensitivity required, as well as the time available to perform the inspection [14].

In this paper, robotized line scan thermography (LST) was investigated in order to inspect a large CFRP specimen which is used in the aerospace industry. This technique consists in heating the component, line-by-

line, while acquiring a series of thermograms with an infrared camera [15]. The robotic arm, which carries an infrared camera and the heating source moves along the surface while the specimen is motionless [15,16]. The robotized LST method provides advantages in comparison to the static approaches. Robotized LST provides heating uniformity and allows image processing which enhances the detection probability, allowing a large-scale component to be inspected with-out the loss of resolution. Using the LST approach, it is possible to inspect large areas at high scan speeds. Also, the inspection results are immediately available for analysis while the scanning process continues. In order to estimate the optimum inspection parameters, the heat transfer process that takes place during the LST inspection is simulated using the 3D-FEM approach.

COMSOL Multiphysics was the software used to model the problem and to solve the differential equations that govern the heat transfer process[17]. In this research, the CFRP specimen has been modeled using approximately 200K elements to achieve accurate results. An experimental LST inspection has been conducted in order to validate the numerical simulation and to verify the inspection parameters obtained through the finite element method (FEM) simulation. As per the obtained results, the main sources of noise that affect the LST inspection performance are the non-uniform heating, unsynchronized frame rate with scanning speed and the vibration produced by the robotic arm mechanism.

To compensate for the effects of the noise, data processing algorithms such as thermographic signal reconstruction (TSR), principal component thermography (PCA) and partial least square thermography (PLS) were employed. This paper investigates and evaluates the effect and performance of data processing algorithms in LST data. Finally, the performance of each data processing algorithm was evaluated using the probability of detection(PoD) criterion.

2 Robotized Line Scan Setup

Robotized line scanning thermography was proposed as a dynamic approach for the inspection of large and complex shaped components. The infrared camera and heat source are installed on the robot arm. These components move in tandem, while the specimen remains fixed (see Figure 1). Using a computer program

which provides the commands for the robotic arm, it is possible to tune all inspection parameters such as the speed of the inspection heat, the distance between the inspection head and the specimen, acquisition rate, and the scanning velocity.

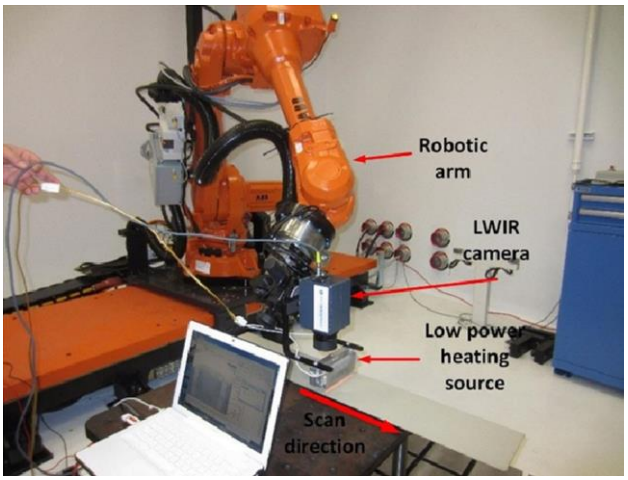

Figure 1 Robotized line scan thermography inspection with low power source

The specimen under study is a 900 mm×150 mm monolithic CFRP panel consisting of 10 sections (1–10 as indicated) with a variable number of CFRP layers (progressively increasing from 6 to 22 plies). Each section has 3 flat-bottomed holes of different diameters (6, 8 and 10 mm), for a total of 30 defects located at different depths (from0.425 to 6.09 mm). The characteristics of the specimen under study are shown in Figure 2. A relation of the depth and diameters of the defects is presented in Table 1, together with the diameter to depth ratios (D/z). A picture of the robotized line scanning setup is shown in Figure 1. The reference panel was positioned over a fixed table and the inspection head over the robot scanned the specimen surface while the camera and heat source moved on the reference panel. An uncooled micro-bolometer camera (Jenoptik IRTCM 384, LWIR 7.5– 14 μm; 384×288 pixels) was used during data acquisition and the specimen was heated using a low power heating line lamp.

3 Numerical Simulation of LST

Several models have been proposed in order to estimate the temperature distribution during the thermography process. In the case of LST thermography, there are some analytical models that are more precise than others. The following equation has been proposed for composite materials in 2008 [18].

$$T(x,t) = \frac{q}{\pi k} e^{-\frac{v|x-vt|}{2\alpha}} \left(K_0\left(\frac{v|x-vt|}{2\alpha}\right) \times 2\sum_{n=1}^{\alpha} K_0\left(\frac{v\sqrt{(x-vt)^2+4n^2L^2}}{2\alpha}\right)\right) \quad (1)$$

where the term K0(x) is a modified Bessel function of the second kind of order zero, v is the line-source velocity, L is the specimen thickness and q is the rate of heat emitted per unit length. This equation calculates the temperature on the specimen surface. It is considered that the material is homogenous and the input energy source should be identical for all points in the same line. In the case of CFRP materials, because of their porous structure, the preciseness of the analytical model is not sufficient enough in order to detect the small defects. Therefore, it is strongly suggested to employ the three-dimensional finite element approach in order to calculatetheheattransferinthematerialvolume.Itwillbemore time consuming, but the result will be close to the reality.

To simulate the LST inspection, the three-dimensional finite element method (3D-FEM) is employed to determine the thermal response of the composite specimen when a dynamic heat excitation is applied on its surface. The LST parameters must be adjusted to maximize the temperature variation on the material surface. COMSOL Multiphysics, was employed to model and simulate the LST inspection of the CFRP specimen. In order to simulate the LST thermography in COMSOL Multiphysics, the heat transfer module and multibody dynamics module isused. Thismodule allows the 3D transient energy equation to be modeled and solved in order to obtain the temperature distribution in the CFRP specimen that contains subsurface defects. The heat transfer modulus also provides different types of uniform and non-uniform time dependent heat sources[15].The proposed model in this work considers the heat transfer by conduction with in the specimen and heat transfer by convection and radiation between the sample surface and the ambient. Figure 3 shows the schematic of the heat fluxes considered in this work.

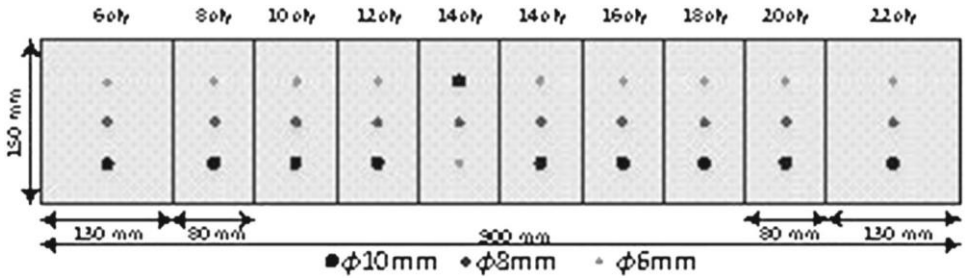

Figure 2 Defect map of the reference panel and corresponding depths

Table 1 Depths and diameter to depth ratios corresponding to the 30 at-bottom-holes of the reference panel

Section	1	2	3	4		6	7	8	9	10
D=6mm	0.88	0.86	0.63	0.69	0.94	0.99	0.42	0.86	0.54	0.65
	6.8	7.0	9.5	8.7	10.6	6.1	14.1	7.0	11.0	9.2
D=8mm	1.2	1.4	1.7	2.0	2.2	2.4	2.6	2.9	3.1	3.5
	6.5	5.7	4.7	4.1	3.6	3.3	3.1	2.7	2.6	2.3
D=10mm	1.5	2.1	2.6	3.2	3.5	3.7	4.2	4.9	5.5	6.1
	6.6	4.7	3.9	3.2	1.7	2.7	2.4	2.0	1.8	1.6

The 3D model geometry was defined as being the same as the experimental specimen. Figure 4 shows the 3D model which consists of 10 sections with various internal layers (progressively increasing from 6 to 22 plies). Also, the fiber orientations are shown in Figure 5. The number of layers, the defect position and size and the composite fiber direction are the most important parameters when developing the 3D model.

One of the key steps in the simulation process consists in generating the appropriate mesh size. There is a tradeoff between the accuracy of the results and the simulation time. A finer mesh size increases the accuracy; however, it also increases the simulation time and requires more computational resources. Figure 6 shows the generated mesh in COMSOL 3D. The simulation parameters as well as the thermophysical properties of the specimen are shown in Table 2.

4 Simulation Results

COMSOL solves the 3D heat conduction equation using the finite element method. To simulate the LST model using COMSOL, there are two procedures to implement that lead to the same results: (1) moving the specimen under the fixed heat source and camera (2) moving the heat source and camera with a fixed specimen.

In this work, because of some mechanical constraints in the experimental setup in order to move the specimen, the second strategy was chosen insimulation. Figure 7illustrates three defect lines which consist of all internal defects. In the results of the simulation, the sudden temperature change on thelinesindicatesthedefect position.To evaluate defectvisibility, the thermal contrast, which is defined as the difference of temperature between a non-defective and a defective area of the specimen, is used. There are various thermal contrast definitions such as the absolute contrast, running contrast, normalized contrast and standard contrast [19]. The absolute thermal contrast is the variable adopted to analyze the detectability of defects and is given by [7]:

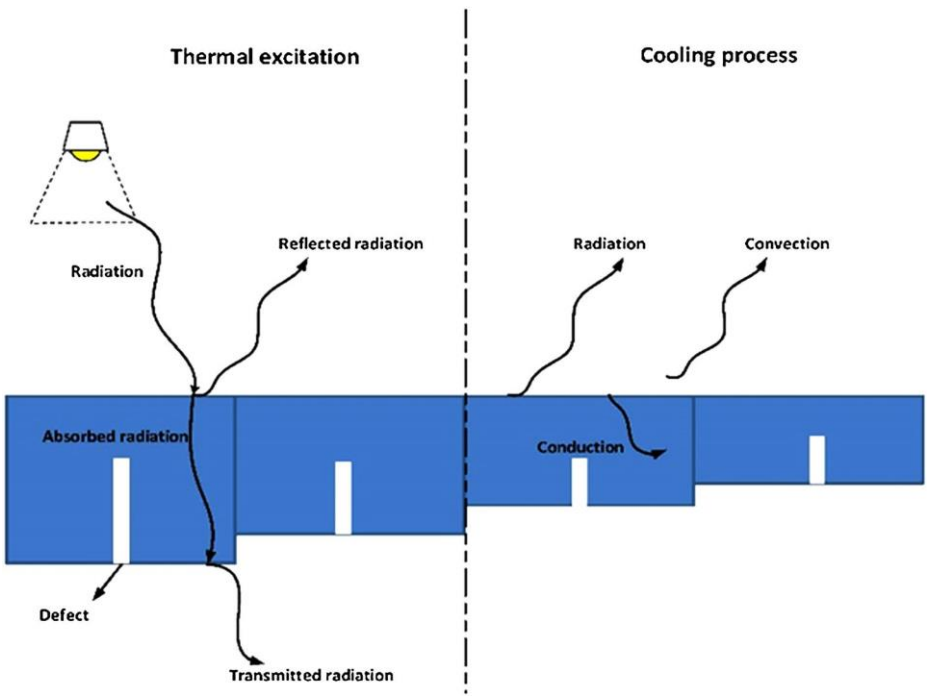

Figure 3 A schematic of the specimen with the heat fluxes participating

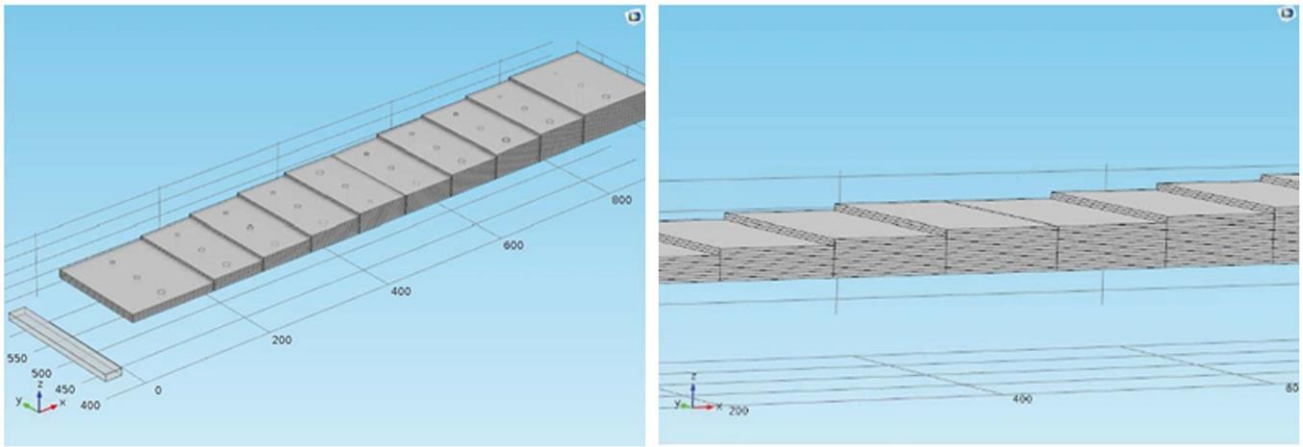

Figure 4 Computational geometry of the specimen developed in COMSOL

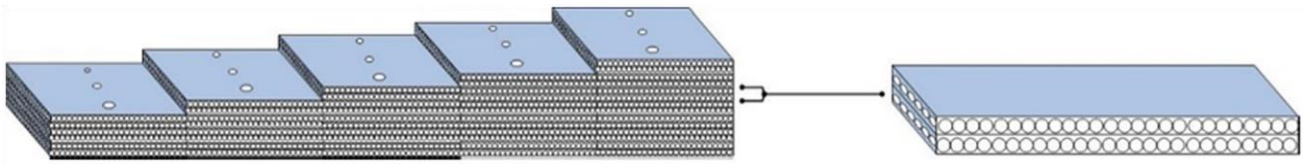

Figure 5 The specimen with bi-directional woven carbon fiber layers (in the photo on the *left*, half of the specimen is illustrated and in the photo on the *right*, two layers of the specimen are magnified)

Figure 6 The generated 3D mesh in COMSOL

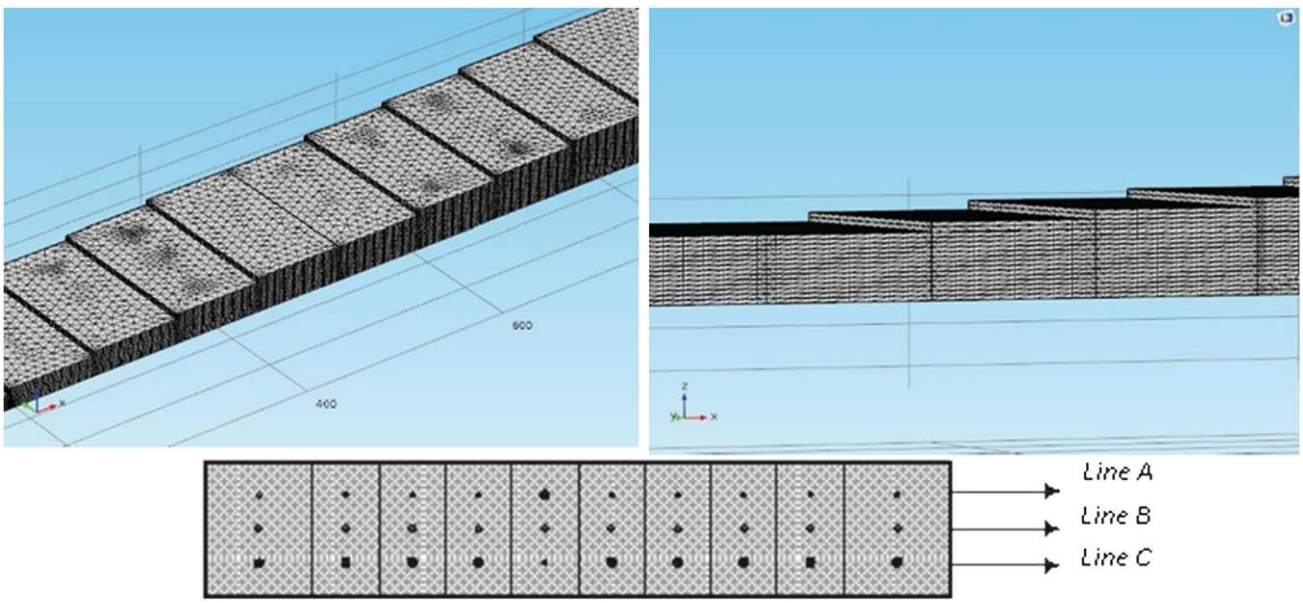

Figure 7 The defined defect lines

Table 2 Simulation parameters used in the numerical simulation

Symbol	Simulation parameters	Value
T_{amb}	Ambient temperature	293.15k
T_o	Initial temperature	293.15k
$H \times L \times W$	Specimen dimension	$H \times$ 900mm × 150mm
δ	Ply thickness	2 mm
H	Height of the specimen	δ × *number of layers*
u	Scan velocity	10mm/s
h	Convection heat transfer	9.1
ρ_{CFRP}	Density (CFRP)	1500kg/m^3
C_{PCFRP}	Specific heat (CFRP)	1000 J/(kgK)
K_{CFRP}	Thermal conductivity (fiber ‖)	7 W/(mK)
K_{CFRP} ρ_T	Thermal conductivity (fiber ⊥)	0.8 W/(mK)
	Density (Teflon)	2200 kg/m^3
C_{PT}	Specific heat (Teflon)	1050 J/(kgk)
K_T	Thermal conductivity (Teflon)	0.25 W/(mk)
ε	Emissivity	0.98

$$\Delta T\,(x, y, t) = T_d\,(x, y, t) - T_s(x, y, t) \qquad (2)$$

where Td is the temperature of a pixel or the average value of a group of pixels of a defective area, and Ts is the temperature at time t for the non-defective area [20].

In this paper, three scanning velocity speeds are considered: 10, 20 and 30 mm/s. The total power of the heating source is 500W. Figure 8 shows the temperature variation of three defect sizes (A4, B4 and C4) at two different scanning speeds (10 and 30mm/s) using a constant heat energy (500 W).

It can be observed from figure8 that the lower the scanning speed, the higher the thermal contrast (or the detectability level of the defects). This can be explained as follows lower speeds the specimen receives more energy from the line source, producing thus a higher thermal contrast between defective and non-defective areas. The scanning speed has an impact on the observation time as well as in the amount of energy that is delivered to the specimen. Thus, the observation time is dependent on the scanning speed. Since the scanning speed increases, the observation time decreases and the amount of

energy that is delivered to the specimen, decreases with a reduction in the observation time. The thermal contrasts of three defects (A4, B4 and C4) considering three scanning speeds are compared in Figure 9.

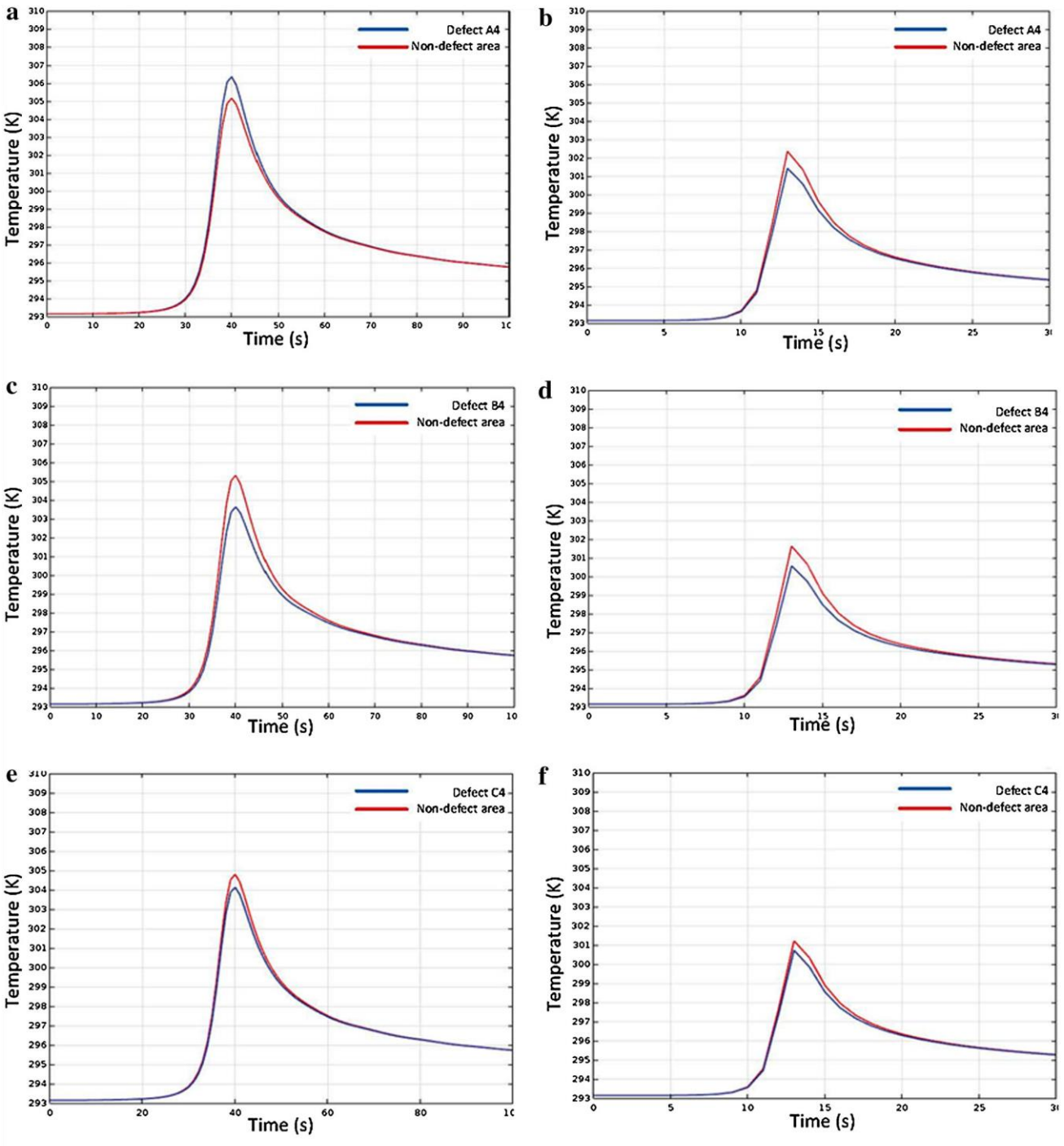

Figure 8 The thermal profiles of three defects (A4, B4 and C4) using two scanning speeds, 10 and 30 mm/s (from *left* to *right*) and a constant heating power of 500W

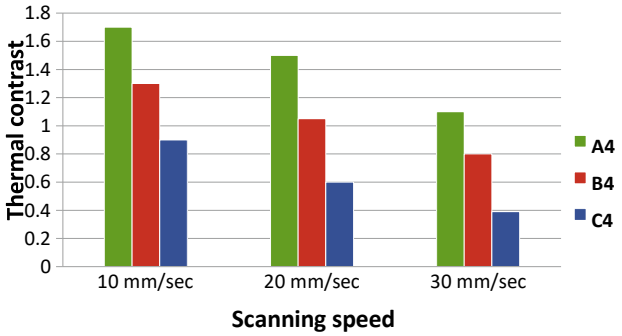

Figure 9 The comparison of maximum thermal contrasts (A4 with D/z=8.7, B4 with D/z=4.1 and C4 with D/z=3.2) with different scanning speeds

The maximum thermal contrast and its time of occurrence are dependent on the aspect ratio D/z of the defects (diameter to t depth ratio) [21]. It can be observed from the results

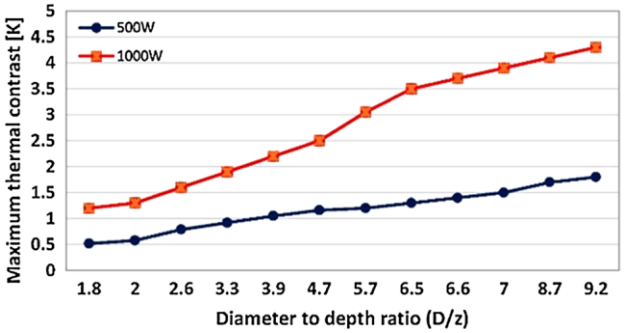

Figure 11 Comparison of the maximum thermal contrast values considering the 500 and 1000W heat source at 10 mm/s

obtained that defects with lower D/z require more energy (or lower scanning speed) to obtain a higher value of thermal contrast. Figure 10 illustrates the direct relationship between the maximum thermal contrast and the depth of defects (for three diameters) when the scanning speed is of 10mm/s.

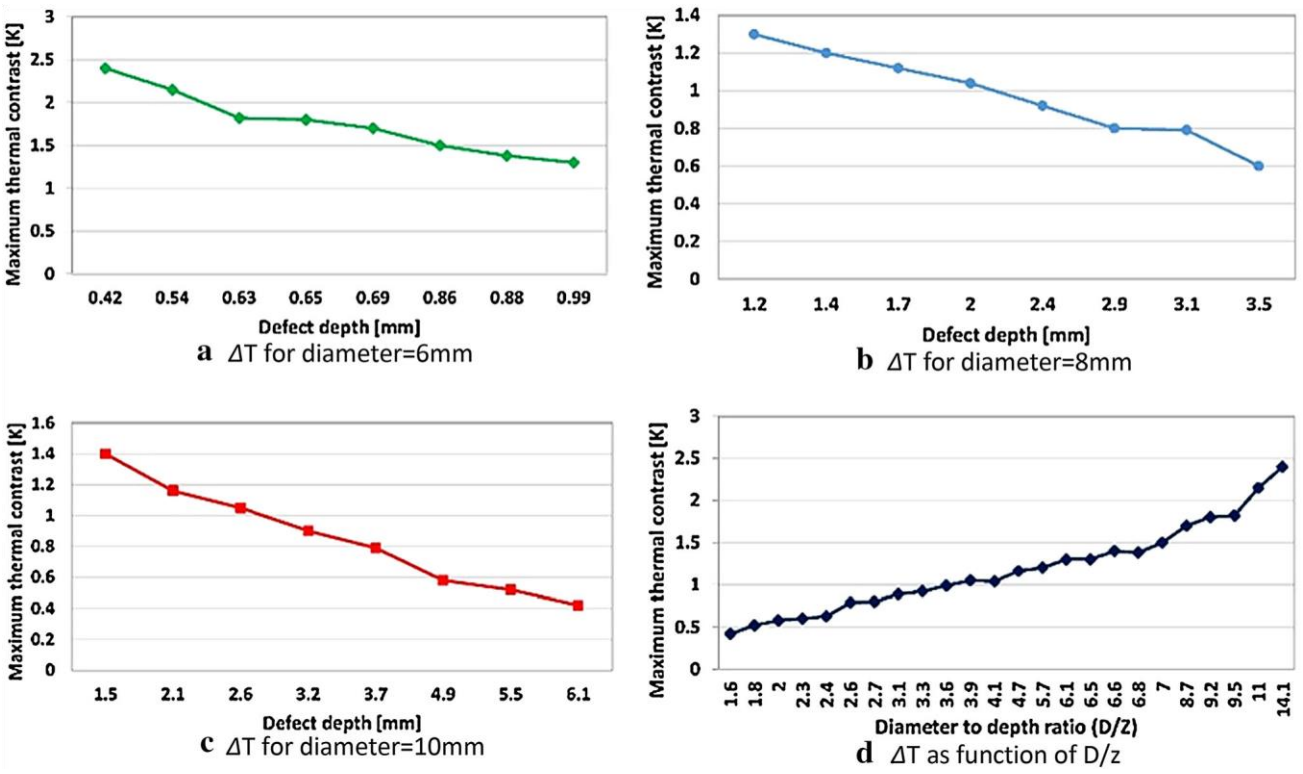

Figure 10 a–c Maximum thermal contrast as a function of depth for three different diameters, **d** maximum thermal contrast as a function of D/z ratio at 10 mm/s

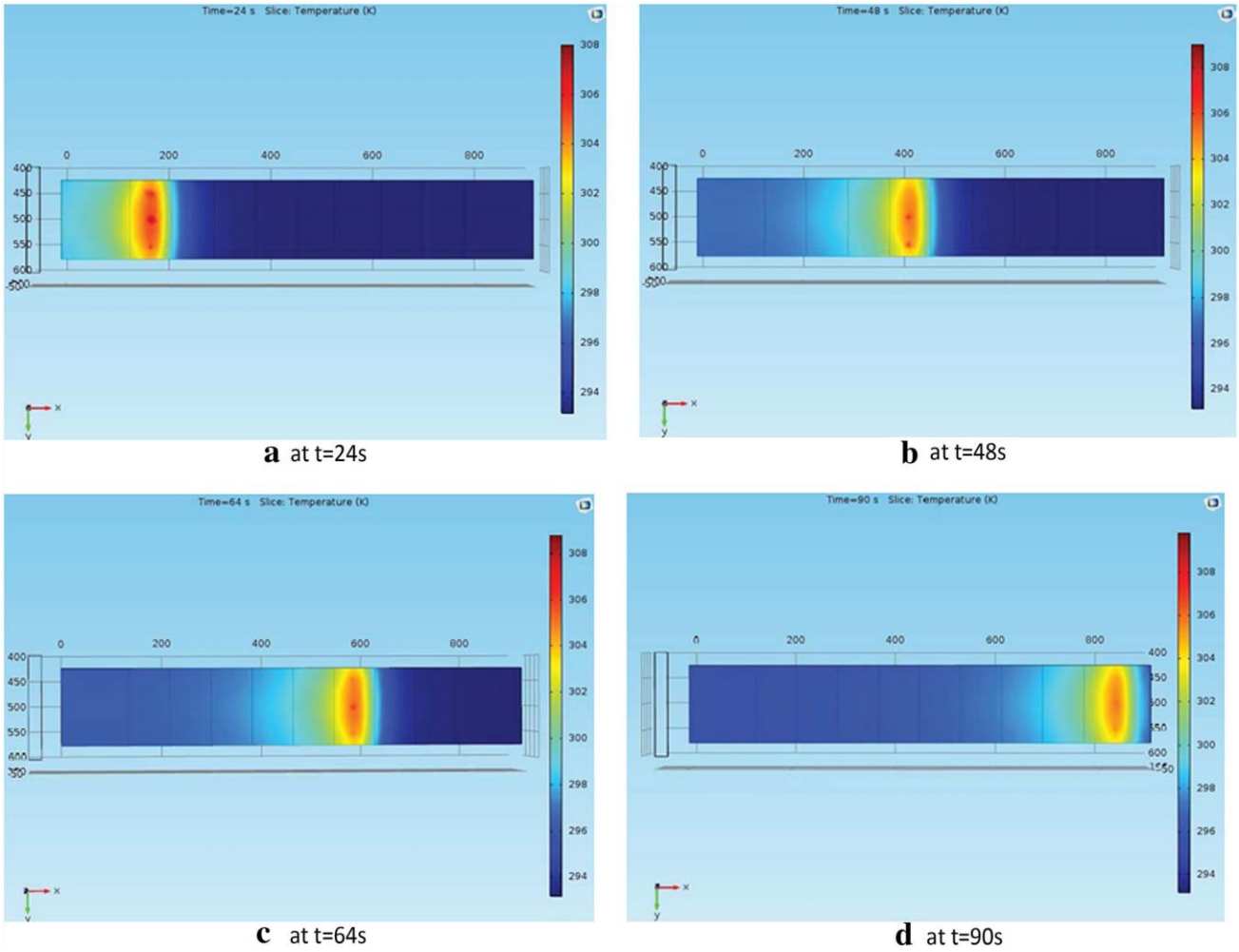

Figure 12 The surface temperature variation during the different simulation times at 10mm/s

The amount of energy has a significant effect on the detectability of the defects. To show the influence of the irradiation power density on the thermal contrast, another amount of energy is applied (1000W). Figure 11 shows the influence of the amount of energy on the maximum thermal contrast at a constant velocity. It can be observed that the visibility of the defects characterized in this work by the maximum thermal contrast can be improved by increasing the amount of the irradiation power density delivered to the specimen. And also, as shown in Figure 11, the simulation LST results indicate that the detection of the defects is a function of the aspect ratio of the defects (considering the same inspection parameters). Defects with a higher D/z ratio have higher detectability level.

Figure 12 shows 4 different thermal maps of the surface of the material at four different times of the inspection using a scanning speed of 10 mm/s. It is possible to observe that the thermal contrasts of the subsurface defects and the moment at which they become visible in the thermal map are functions of the depthand the lateral size of the defects. Data processing methods could help to increase the detection probability.

According to the simulation results, it is possible to detect almost all of the defects with a different level of visibility using the LST approach. The simulation results using different scanning speeds prove that a longer heating time (lower scanning speed) increases the PoD of the defects due to the time during which energy is delivered to the specimen surface

Table 3 Experimental parameters

Experimental parameters	Value
Heat source	500 W
Length of the source	150 mm
Width of the source	2 mm
Distance between source and sample	7 cm
Length of the projected line	950 mm
Velocity	10 mm/s

5 Experimental Setup

In the experimental setup, an uncooled microbolometer camera (Jenoptik IRTCM 384, LWIR 7.5–14 μm, 384×288 pixels) was used during data acquisition and the specimen was heated using a 500 W line source. The linear speed of the source on the specimen is 10mm/s. During the experimental implementation of LST, due to the specimen length, the infrared camera covered only a section of the specimen at a time. Therefore, the pseudo-static matrix reconstruction approach is utilized to produce a static image of the specimen, thus allowing a better analysis of

the produced data and the possibility to apply post-processing techniques to the acquired thermal images. The experimental parameters are shown in Table 3.

5.1 Validation of the Numerical Simulation

Figure 13 shows the thermal profiles of three defects (A1, B1 and C1) which were obtained from simulation and experimental results at a 10mm/s scanning speed. These profiles are the best criterion in order to validate and prove the accuracy of the simulation model. A comparison between the simulation profiles and experimental profiles confirms the validity of the simulation model, composite parameters and our analysis approach. However, because of the low frame rate of the camera, the resolution of the experimental profile is not high enough to compare with the simulation profiles. At the beginning of the heating process, the simulation and experimental results are in good agreement while in the cooling time, the cooling rate of the experimental data is higher. It could be dependent on the room temperature or data acquisition accuracy.

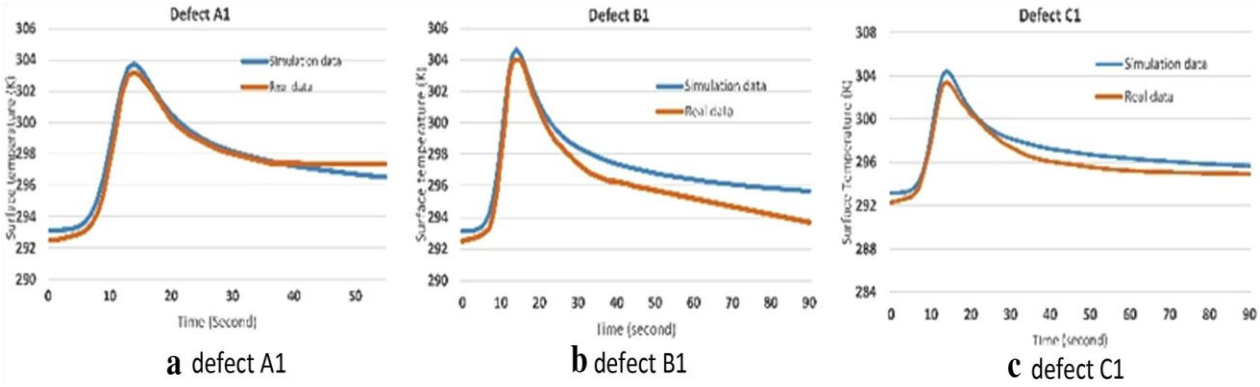

Figure 13 Thermal profiles of three defects in simulation and experimental data

5.2 Data Reconstruction

Figure 14 illustrates the methodology adopted to produce the pseudo-static matrix. The infrared camera captures the original sequence Pxi(t), frame by frame (through time t). The first line of the

image matrix at time t1,will be relocated as the first line of the reconstructed image matrix corresponding to a virtual time t1, that is $Px^1(t_1')$. The first line at the same position x1 but in the following frame (attimet2) is then relocated as the second line of the reconstructed matrix, and so on. At the end of this process, the sequence of lines at position x1 in the original sequence: Px1 (t1)... Px1(tn) is rearranged into a single image representing the first frame at the virtual time t1 which is defined as the time of the visibility of a specified specimen line for the camera.The same procedure is repeated for the remaining lines in the original sequence [15]. In order to construct the accurate pseudo matrix, the camera and heat source should move with a constant speed. In other words, the camera framerate must be perfectly synchronized with the scanning speed, which is difficult to achieve. To address this issue, an additional calibration procedure was proposed by Oswald-Tranta and Sorger [22]; or one can use a shifting correction procedure based on the interpolation between the initial and final positions of a reference pixel. In both cases, it is assumed that the camera and source move at a constant speed [15]. The observation time tobs (or time window), the time during which a given point (line) in the inspected object is observed at a given scanning speed ux, can be precisely calculated with the knowledge of the length of the FOV in the scanning direction X [15]:

$$t_{obs} = \frac{X}{u_x} \tag{3}$$

The virtual acquisition rate of the reconstructed sequence frate can then be estimated using the know number of pixels being scanned px during the observation time from tobs [15]:

$$f'_{rate} = \frac{px}{t_{obs}} = 1/\Delta t' \tag{4}$$

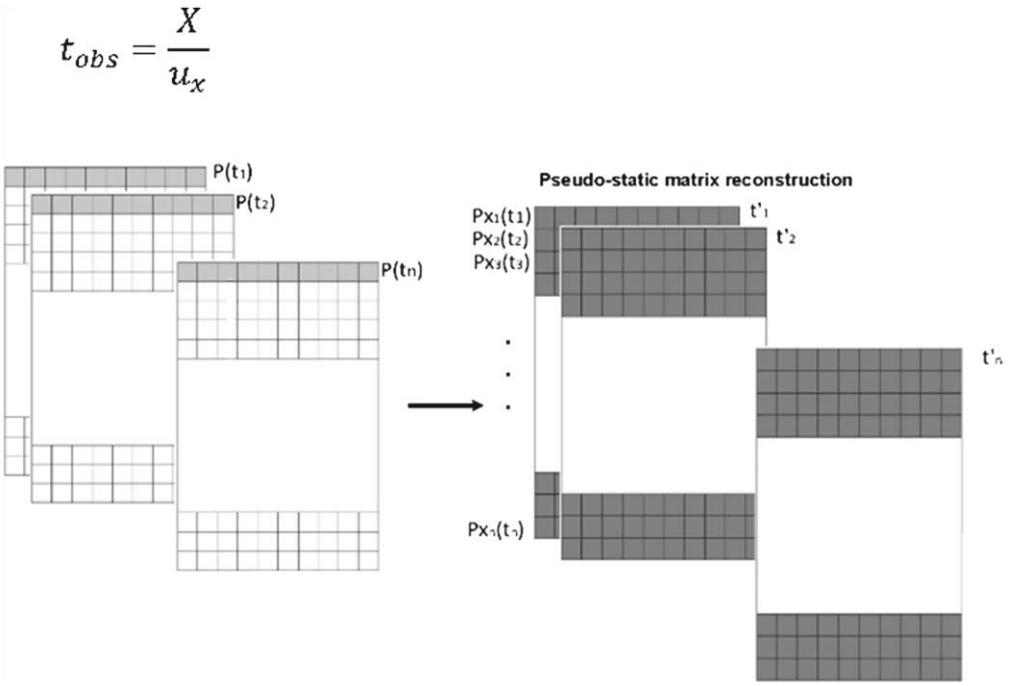

Figure 14 The algorithm is used to construct the pseudo matrix

Equations 3 and 4 are employed to reconstruct the pseudo static sequence from the dynamic matrix and to determine the observation time and frame rate for every pixel in the new sequence [15]. Figure 15 shows the reconstructed thermograms obtained using the robotized LST inspection. The reconstructed thermograms correspond to the virtual times 2.17, 3.03, 4.17 and 6.5s. As mentioned in the previous section, it is difficult to synchronize the mechanical motion speed and the acquisition frame rate of the IR camera. The mis-alignment is visible in the results caused by shifting the object position from one frame to the next. Several solutions have been proposed to reduce the effect of this problem, such as using the matching algorithms as iterative closest point (ICP), the interpolation between the initial and final positions of a reference pixel [22], or increasing the field of view (FOV). As per Figure 15 it is possible to observe that shallower defects (line A) were easy to detect by robotized LST. As times elapses, deeper defects are visible. In other words, deeper defects require more time to be detected, in a similar way as in the static inspection. In the last frame (at virtual time 6.5s), four defects in line B and the first defect in line C appeared. Therefore, without the data processing algorithms it is possible to detect the defects located close to the surface at a depth of 2mm and less. However, through the implementation of signal processing techniques it is possible to reduce the effects of different sources of noise and therefore, improve the detectability of the defects that are undetectable in raw images. The next section

discusses the implementation of some of the most commonly used techniques to process infrared thermal data.

6 Data Processing Algorithms

Currently in the literature one can find information on a wide selection of methods aimed at processing thermographic images. Some of the most commonly used techniques are: thermographic signal reconstruction (TSR) [23], thermal tomography [24], pulsed phase thermography (PPT) [5], Principal component thermography (PCT) [25,26] and Partial least square thermography (PLST) [27]. Data processing techniques in NDT enhance the defect detection probability, with the downside of increasing the computational time or requiring interactions with an operator to select algorithm parameters [26]. In this paper, these data processing algorithms have been used to increase the visibility of defects.

6.1 TSR

Thermographicsignalreconstruction(TSR)iswell-knownas an effective data processing technique for PT data. The most As its name implies, TSR

Figure 15 The robotized LST thermography experimental results

uses a low order polynomial function in order to reconstruct the temperature evolution curve which is obtained from a PT inspection [28]. Figure 16a shows the result of the TSR approach. It is clear that the TSR approach enhances the detection probability and makes it possible to locate deeper defects.

6.2 PCA

An interesting technique is principal component thermography (PCT) which is used to extract features and reduce the undesirable information in thermographic sequences. PCT is used in NDT

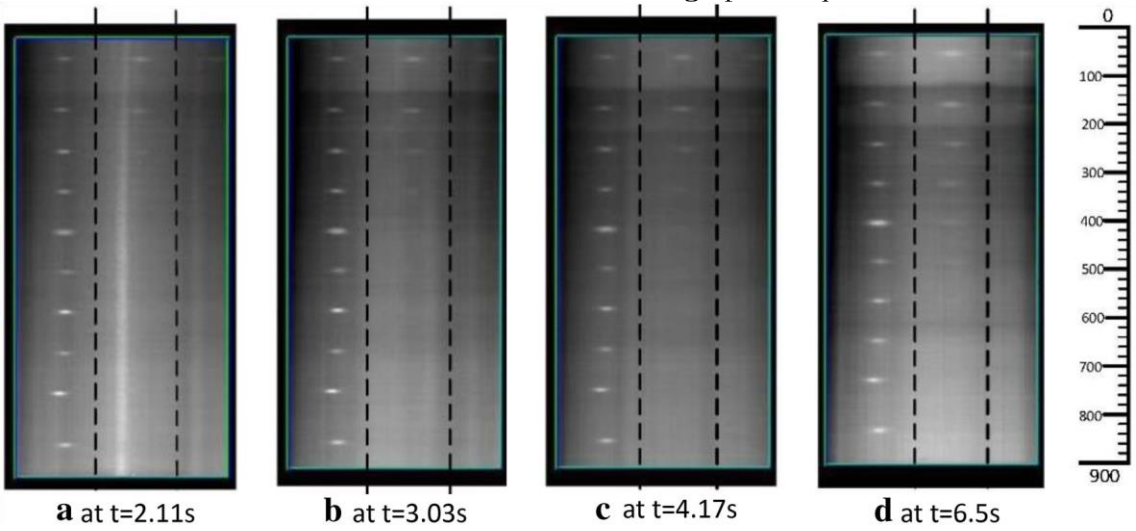

for defect detection and the estimation of depth of the detected subsurface defects [25]. PCT is based on the singular value decomposition (SVD) to extract the spatial (Empirical Orthogonal Functions or EOFs) and temporal (principal components PCs) information from thermal data. Each principal component is characterized by the variability level or its variance. Thus, the first component is the largest variance of all the components, followed by the second component and so on. Using the first few (most important) principal components helps to reduce the dimensionality of the data [29,30]. Figure 16b shows the results of using PCT on the robotized LST data. The PCT technique has a significant effect on raw data and enhances the detection capability of the test. In Figure 16c a combination of TSR and PCA techniques was employed, thereby improving the performance.

In this way, the TSR technique was used as a filter to reduce the noise and then PCA was applied to this sequence. The TSR is employed to suppress noise and in the next step PCT is carried out to improve defect detection. The combination of these signal processing techniques (TSR and PCT) effectively improves the result by combining the advantages of each technique.

6.3 PPT

The application of pulsed phase thermography to process thermographic data obtained from the LST inspection is also investigated in this work. PPT is based on the fact that any waveform can be approximated by the sum of harmonic waves at different frequencies through the Fourier Transform, which is used to extract a certain number of thermal waves from a thermal pulse [31], each one oscillating at a different frequency and having a different amplitude. The amplitude and phase maps obtained after the implementation of PPT to processing the thermographic LST data is shown in Figure 17a and b.

6.4 PLST

Partial least square (PLS) is composed of a wide class of methods in order to establish the relations between sets of observed variables by means of latent variables. This involves regression and classification tasks as well as dimension reduction techniques and modeling tools [32]. Using this method, irrelevant and unstable information is discarded and only the most relevant part of the thermal data is used for regression. Furthermore, since all variables are projected down to only a few linear combinations, simple plotting techniques can be used for analysis. As a regression method, PLSR seeks to model a dependent variable Y (predicted) in terms of an independent variable X (predictor) [27,33]. PLS generalizes and combines features of two techniques: prin cipal component regression (PCR) and multivariate linear regression (MLR) to achieve this aim [27,33]. The result of the partial least square thermography (PLST) technique is shown in Figure 17c. The PLS technique does not provide an appropriate performance for this data. In the next section, the performance of the different data processing approaches is compared.

7 Evaluation of Signal Processing Techniques

Concerning the signal processing algorithms, it is important to note that PPT and TSR were originally developed to be applied on static thermography, when the heat conduction regimes follow the solution of the 1D differential equations. For this reason, their performance could not be as expected.

Figure 16 The robotized LST results with the TSR and PCA approach

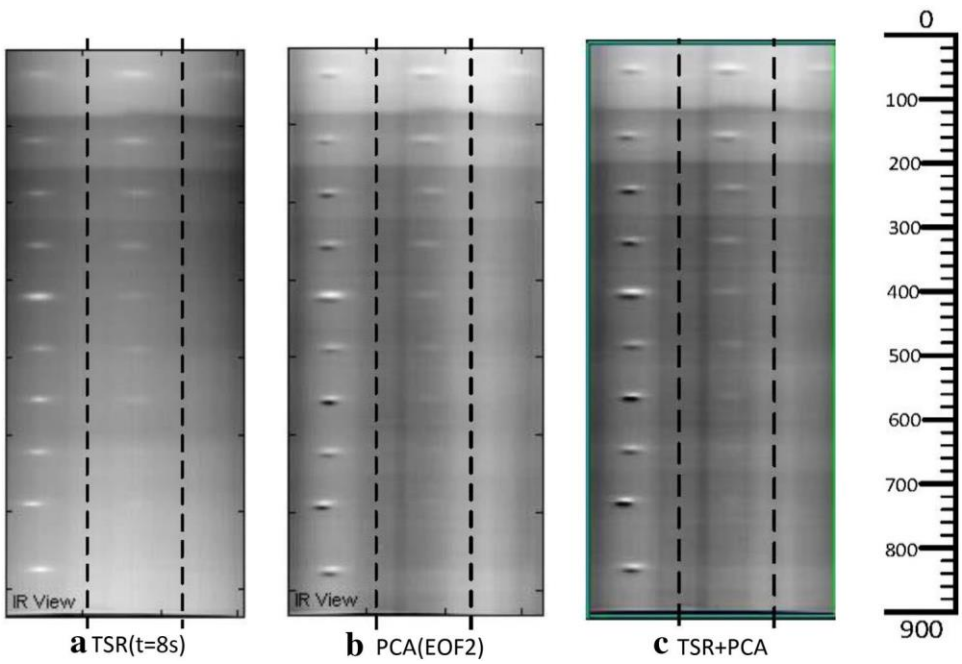

a TSR(t=8s) **b** PCA(EOF2) **c** TSR+PCA

Figure 17 The robotized LST results with PPTS and PLS

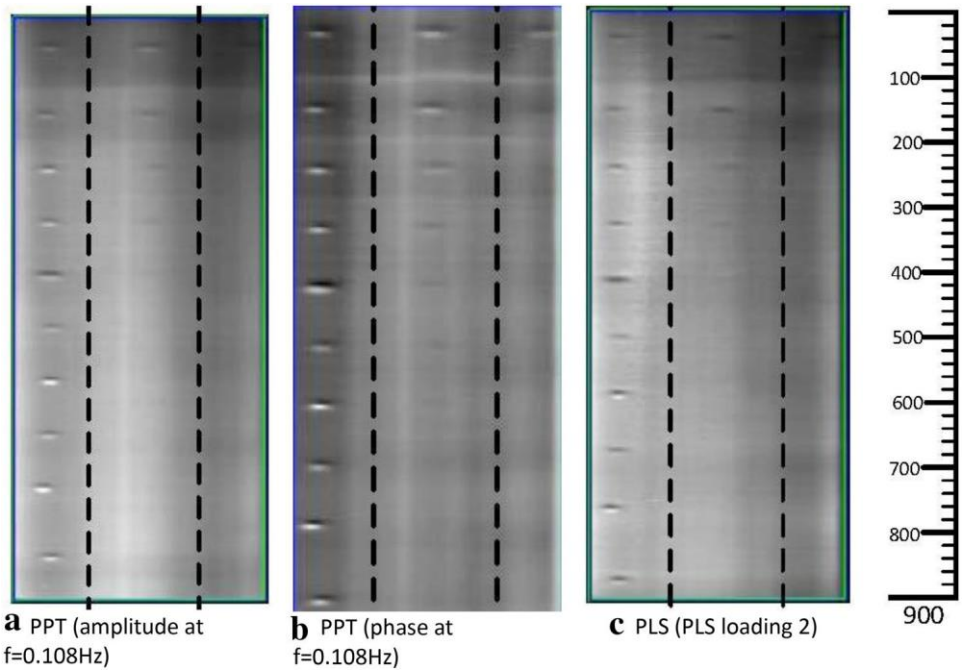

a PPT (amplitude at f=0.108Hz) **b** PPT (phase at f=0.108Hz) **c** PLS (PLS loading 2)

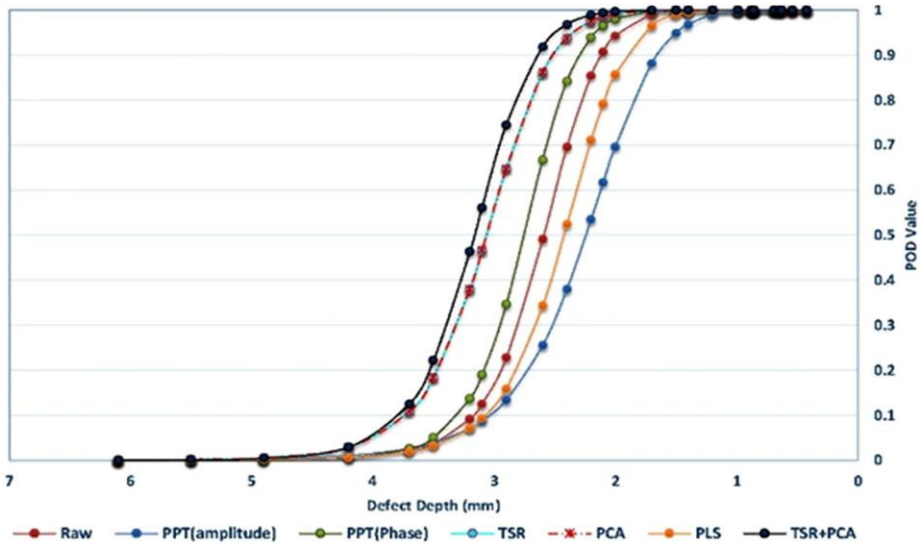

Figure 18 The calculated PoD value for different data processing techniques

since the thermal regime or the thermal process is not 1D anymore. In fact, the decay curve obtained from LST is very different from the one obtained from static thermography. Therefore, it is important to investigate and evaluate performance of the data processing algorithm in the new space. The performance evaluation provides a criterion to determine the capability of each algorithm to eliminate the noise and detect the deeper defects. The PoD is known as a powerful tool which is employed to estimate the performance of data processing algorithms [34–36].

In this research, the performance of the processing techniques has been evaluated quantitatively using the PoD approach. The PoD analysis is a quantitative measuring method used to evaluate the inspection quality and the reliability of a NDT&E technique. This criterion is widely used for traditional NDT&E techniques [30]. PoD tries to recognize the minimum aw depth that can be reliably detected by the NDT technique. This is best done by plotting the accumulation of flaws detected against the aw depth of all of the flaws "detected" or that produce a response over a threshold. Based on the PoD result, all defects which are deeper than a critical depth is not detected while others are detected. The tool most commonly used for PoD description is the PoD curve [37]. It was proven that the log-logistic distribution was the most acceptable [38]. The PoD curves can be produced from two types of data: (1) hit/miss data (the flaw is detected or not), (2) signal response data. The mathematical expression to describe the PoD function from hit/miss data is written below:

$$PoD(a) = \frac{e^{\frac{\pi}{\sqrt{3}}(lna-\mu)/\sigma)}}{1+e^{\frac{\pi}{\sqrt{3}}(lna-\mu)/\sigma)}} \qquad (5)$$

where a is the defect size, $\mu = -\frac{\alpha}{\beta}$ and$\sigma = \frac{\pi}{\beta\sqrt{3}}$ are the median standard deviation respectively. From Eq. 6, a direct relationship can be demonstrated between the log-odds PoD(a) and defect size:

$$\ln\left(\frac{PoD(a)}{1-PoD(a)}\right) = \alpha + \beta\, lna \qquad (6)$$

For signal response data, the following formula is commonly used to model the relation between a flaw size (a) and a quantitative response data (aˆ) [30,39]:

$$ln\,\hat{a} = \beta_0 + \beta_1 ln(a) \qquad (7)$$

where β0 and β1 are respectively the intercept and slope which can be estimated by maximum likelihood. The PoD(a) function will be calculated as:

$$PoD(a) = Probability(ln\hat{a} > ln\hat{a}_{dec}) \qquad (8)$$

Where $\hat{a}_{dec}$ is a decision concerning the threshold. Finally, the PoD function is written based on the continuous cumulative distribution function.

$$\begin{aligned} & PoD(a) \qquad (9)\\ & = 1 - F\left(\frac{ln\hat{a}_{dec} - \beta_0 + \beta_1 lna}{\sigma}\right)\\ & = F(\frac{ln(a) - \mu}{\sigma}) \end{aligned}$$

where F is the continuous cumulative distribution function which has the cumulative log-normal distribution. The values of β0, β1 and σ are calculated by Minitab software and represent the 95% lower confidence bound [30,39].

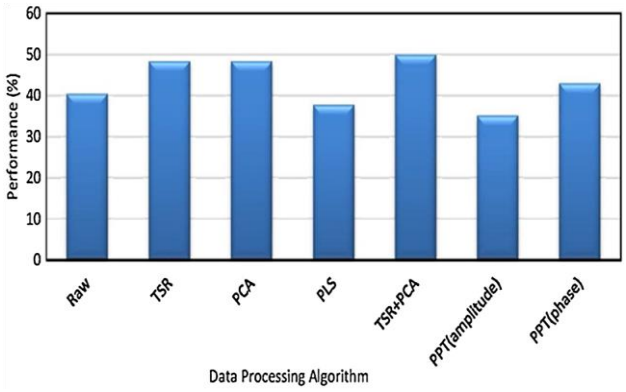

Figure 19 A comparison of the PoD value for different techniques

Figure 18 shows the 95% lower confidence bound of various data processing algorithms, which were calculated using Minitab. The PoD curves of each technique are shown in Figure 18. This result shows that PCA provides the highest probability to detect the deeper defects. In order to have a better comparison, the performance of each technique has been measured.The detection

performance of each approach is the area under the PoD curve divided by the total area. Figure 19 shows a comparison of the PoD value for different techniques which represents the capability to detect the deepest defects. PoD calculates the performance of each data processing algorithm based on the number of visible defects and their depth. In other words, PoD provides an appropriate criterion in order to determine the ranking of each algorithm. In this research, the results of raw data, TSR, PCA, PLS, TSR+PLS and PPT were evaluated and compared. The raw data has very low performance due to low camera resolution, camera vibration and Non-uniform motion of the camera and source. The TSR algorithm reduces the noise and significantly increases the number of visible defects. Unexpectedly, the PPT and PLSalgorithmshavelowerperformance. Incomparisonwith the static thermography, it can be concluded that these algorithms are sensitive to the motion noise and are not proper choices for LST application. PCA and TSR+PCA provide the highest performance in comparison to other techniques. This indicates that TSR, PCA and especially their combination is robust against the motion noise and are the bestchoices for LST.

8 Conclusion

In this research, the application of robotized Line Scan Thermography (LST) has been investigated for the nondestructive inspection of large and complex composite structures. All the experiments and theoretical analysis were conductedonacarbonfiberreinforcedpolymer(CFRP)specimen with defects located at different depths and diameters. For theoretical analysis, the heat transfer process that takes places within the material during the LST inspection was simulated using COMSOL Multiphysics.The developed thermal model also considered different parameters associated with the LST setup, such as the amount of energy delivered to the specimen and the speed at which the IR camera and heating source move. It is important to mention that the developed thermal model can be used not only to study the heat transfer process in the LST inspection, but also as a technical tool that can be employed for training of technicians and specialists. Furthermore, the model can be used as a prescreening tool to obtain inspection parameters and to verify the reliability of the LST before being applied in real tests. A parametric study was conducted to analyze the influence of the irradiation density and the scanning speed on the thermal contrast (or the defectivity level) of the defects. From this study, it was observed that the simulated thermal curves of the defects with respect to time follow a similar behavior as that observed inpulse thermography. Furthermore,theresults indicate that there is a direct relation between the scanning speed and the maximum thermal contrast of the defects due to the amount of heat energy delivered to the specimen. Based on the results obtained from numerical simulation, a comprehensive analysis of several image processing techniques (TSR, PCT, PCT+TSR, PPT and PLST) commonly used to improvethequalityofPTdatawereimplementedonthethermal maps obtained from the inspection by the robotized line scan thermography system.After processing, the results were evaluated in terms of the PoD criteria, allowing to conclude that principal components thermography and thermographic signal reconstruction provided an improvement of the depth probing capabilities of LST. In both cases, it was possible to detect defects up to a depth of 2.1 mm from the surface of the specimen. Further investigations are focused on the implementation of machine learning methods to go beyond the current limit of 2.1 mm depth.

Acknowledgements The authors are thankful for the support of the following organizations which help to fund our research activities: Natural Science and Engineering Research Council of Canada, Canada Research Chair Secretariat, Ministre des Relations Internationales du QuebecandQuebec-Wallonia/Brussels Program, Visioimage Ltd.,Centre.

References

1. Bonavolonta, C., Valentino, M., Peluso, G., Barone, A.: Nondestructive evaluation of advanced composite materials for aerospace application using hts squids. IEEE Trans. Appl. Supercond. **17**(2), 772–775 (2007). doi:10.1109/TASC.2007.897193
2. Hull, D., Clyne, T.: An Introduction to Composite Materials. Cambridge University Press, New York (1996)
3. Matthews, D.F., Rawlings, R.D.: Composite Materials: Engineering and Science. Elsevier (1999)
4. Soutis, C.: Fibre reinforced composites in aircraft construction.Prog. Aerosp. Sci. **41**(2), 143–151 (2005)
5. Lopez, F., Ibarra-Castanedo, C., Maldague, X., Nicolau, V.: Pulsedthermography signal processing techniques based on the 1d solution of the heat equation applied to the inspection of laminated composites. Mater. Eval. **72**, 91–102 (2014)
6. Ibarra-Castanedo,C.,Gonzalez,D.,Klein,M.,Pilla,M.,Vallerand,S., Maldague, X.: Infrared image processing and data analysis. Infrared. Phys. Technol. **46**(1), 75–83 (2004)
7. Ibarra-Castanedo, C., Genest, M., Servais, P., Maldague, X., Bendada, A.: Qualitative and quantitative assessment of aerospace structures by pulsed thermography. Nondestruct. Test. Eval. **22**(2– 3), 199–215 (2007)
8. Ibarra-Castanedo, C., Avdelidis, N.P., Grinzato, E.G., Bison, P.G.,Marinetti,S.,Plescanu,C.C.,Bendada,A.,Maldague,X.P.:Delamination detection and impact damage assessment of glare by active thermography. Int. J. Mater. Prod. Technol. **41**(1–4), 5–16 (2011)
9. Dillenz, A., Zweschper, T., Busse, G.: Progress in ultrasound phasethermography. In: Aerospace/Defense Sensing, Simulation, and Controls. International Society for Optics and Photonics, pp. 574– 579 (2001)
10. Favro, L., Han, X., Ouyang, Z., Sun, G., Sui, H., Thomas, R.: Infrared imaging of defects heated by a sonic pulse. Rev. Sci. Instrum. **71**(6), 2418–2421 (2000)
11. McCann, D., Forde, M.: Review of ndt methods in the assessmentof concrete and masonry structures. NDT & E Int. **34**(2), 71–84 (2001)
12. Ibrahim, M.: Nondestructive evaluation of thick-section composites and sandwich structures: a review. Compos. A Appl. Sci. Manuf. **64**, 36–48 (2014)
13. Gholizadeh, S.: A review of non-destructive testing methods ofcomposite materials. Procedia Struct. Integr. **1**, 50–57 (2016)
14. Ley,O.,Godinez-Azcuaga,V.:Linescanningthermographyanditsapplication inspecting aerospace composites. In: 5th International Symposium on NDT in Aerospace, Singapore
15. Ibarra-Castanedo, C., Servais, P., Ziadi, A., Klein, M., Maldague,X.: RITA-Robotized Inspection by Thermography and Advanced processing for the inspection of aeronautical components. In: 12th International Conference on Quantitative InfraRed Thermography (2014)
16. Woolard, D.F., Cramer, K.E.: Line scan versus ash thermography: comparative study on reinforced carbon-carbon. In: Defense and Security, International Society for Optics and Photonics, pp. 315– 323 (2005)
17. Aieta, N.V., Das, P.K., Perdue, A., Bender, G., Herring, A.M.,Weber, A.Z., Ulsh, M.J.: Applying infrared thermography as a quality-control tool for the rapid detection of polymer-electrolytemembrane-fuel-cell catalyst-layer-thickness variations. J. Power Sources **211**, 4–11 (2012)
18. Kaltmann, D.: Quantitative line-scan thermographic evaluation ofcomposite structures, Masters by Research, Aerospace, Mechanical and Manufacturing Engineering, RMIT University
19. Benitez, H., Ibarra-Castanedo, C., Bendada, A., Maldague, X.,Loaiza, H., Caicedo, E.: Modified differential absolute contrast using thermal quadrupoles for the nondestructive testing of finite thickness specimens by infrared thermography. In: Electrical and Computer Engineering, 2006. CCECE'06. Canadian Conference on, IEEE, 2006, pp. 1039–1042
20. Ibarra-Castanedo, C., Benitez, H., Maldague, X., Bendada, A.: Review of thermal-contrast based signal processing techniques for the nondestructive testing and evaluation of materials by infrared thermography. In: Proceedings of the International Workshop on Imaging NDE (Kalpakkam, India, 25–28 April 2007), pp. 1–6 (2007)
21. Lopez, F., de Paulo Nicolau, V., Ibarra-Castanedo, C., Maldague,X.: Thermal numerical model and computational simulation of pulsed thermography inspection of carbon fiber reinforced composites. Int. J. Therm. Sci. **86**, 325–340 (2014)
22. Oswald-Tranta, B., Sorger, M.: Scanning pulse phase thermography with line heating. Quant. InfraRed Thermogr. J. **9**(2), 103–122 (2012)
23. Ibarra-Castanedo, C., Bendada, A., Maldague, X.: Thermographicimage processing for NDT. In: IV Conferencia Panamericana de END, vol. 79. Citeseer (2007)
24. Vavilov, V., Nesteruk, D., Shirayev, V., Ivanov, A.: Some novelapproaches to thermal tomography of CFRP composites. In: Proceedings of the 10th International Conference on Quantitative Infrared Thermography, FIE du CAO, pp. 433–440 (2010)
25. Vahid, P.H., Hesabi, S., Maldague, X.: The effect of pre-processingtechniques in detecting defects of thermal images

26. Fariba, K., Saeed, S., Maldague, X.: Infrared thermography andNDT: 2050 horizon, QIRT
27. Lopez, F., Nicolau, V., Maldague, X., Ibarra-Castanedo, C.: Multivariate infrared signal processing by partial least-squares thermography. In: ISEM Conference (2013)
28. Lopez, F., Ibarra-Castanedo, C., Maldague, X., de Paulo Nicolau,V.: Analysis of signal processing techniques in pulsed thermography. In: SPIE Defense, Security, and Sensing, International Society for Optics and Photonics, 2013, pp. 87050W–87050W
29. Ibarra-Castanedo, C., Avdelidis, N.P., Grenier, M., Maldague, X.,Bendada, A.: Active thermography signal processing techniques for defect detection and characterization on composite materials. In: SPIE Defense, Security, and Sensing, International Society for Optics and Photonics, 2010, pp. 76610O–76610O
30. Duan, Y.: Probability of detection analysis for infrared nondestructive testing and evaluation with applications including a comparison with ultrasonic testing, Ph.D. thesis, Universite Laval (2014)
31. Castanedo, C.I.: Quantitative subsurface defect evaluation bypulsed phase thermography: depth retrieval with the phase, Ph.D. thesis, Universite Laval (2005)
32. Rosipal, R., Kramer, N.: Overview and recent advances in partialleast squares. In: Subspace, Latent Structure and Feature Selection. Springer, pp. 34–51 (2006)
33. Lopez, F., Ibarra-Castanedo, C., de Paulo Nicolau, V., Maldague,X.: Optimization of pulsed thermography inspection by partial least-squares regression. NDT & E Int. **66**, 128–138 (2014)
34. Duan, Y., Servais, P., Genest, M., Ibarra-Castanedo, C., Maldague,X.P.: Thermopod: A reliability study on active infrared thermography for the inspection of composite materials. J. Mech. Sci. Technol. **26**(7), 1985–1991 (2012)
35. Junyan, L., Yang, L., Fei, W., Yang, W.: Study on probability ofdetection (pod) determination using lock-in thermography for nondestructive inspection (ndi) of cfrp composite materials. Infrared Phys. Technol. **71**, 448–456 (2015)
36. Wehling, P., LaBudde, R.A., Brunelle, S.L., Nelson, M.T.: Probability of detection (pod) as a statistical model for the validation of qualitative methods. J. AOAC Int. **94**(1), 335–347 (2011)
37. Duan, Y., Huebner, S., Hassler, U., Osman, A., Ibarra-Castanedo,C., Maldague, X.P.: Quantitative evaluation of optical lock-in and pulsed thermography for aluminum foam material. Infrared Phys. Technol. **60**, 275–280 (2013)
38. Georgiou, G.A.: Probability of detection (pod) curves: derivation,applications and limitations. Jacobi Consulting Limited Health and Safety Executive Research Report 454
39. Muller, C., Elaguine, M., Bellon, C., Ewert, U., Zscherpel, U.,Scharmach, M., Redmer, B., Ryden, H., Ronneteg, U.: Pod (probability of detection) evaluation of NDT techniques for cu-canisters for risk assessment of nuclear waste encapsulation. In: Proceedings of the 9th European Conference on NDT, Berlin, German, Sept, 2006, pp. 25–29

Chapter VII

Implementation of Advanced Signal Processing Techniques on Line-Scan Thermography Data

7. 1. Résumé

Dans de nombreuses industries, le matériau composite joue un rôle important en raison de ses propriétés, telles qu'une résistivité élevée à la fatigue et une résistance plus élevée. Le composite de type sandwich est un composite utile qui est largement utilisé dans les industries principales. Les composites de type sandwich se composent de deux couches minces, généralement en aluminium, fibre de verre ou fibre de carbone, et un noyau en nid d'abeilles léger. La qualité des composites de type sandwich peut être compromise par plusieurs types de défauts internes, tels que des délaminations, des vides, des bulles d'air et des rides. Dans cet article, la thermographie par balayage linéaire (LST) est étudiée en tant que technique NDT visant à détecter les défauts de subsurface dans un grand échantillon composite sandwich, et des algorithmes de traitement de données sont implémentés pour réduire le bruit dans les images brutes. La performance des algorithmes de traitement de données pour éliminer le bruit et détecter les défauts plus profonds est comparée par le rapport signal sur bruit.

7. 2. Summary

In the many industries, composite material has a significant role due to their properties, such as high resistivity to fatigue and higher strength. Sandwich-type composites is a useful composite which is widely employed in main industries. Sandwich-type composites consist of two thin layers, commonly of aluminum, fiberglass or carbon fiber, and a lightweight honeycomb core. The quality of the sandwich-type composites may be compromised by several types of internal defects, such

as delaminations, voids, air bubbles and wrinkles. In this paper, line scan thermography (LST) is investigated as a NDT technique aimed to detect subsurface defects in a large sandwich composite specimen, and data processing algorithms are implemented to reduce the noise in raw images. The performance of data processing algorithms to eliminate the noise and detect the deeper defects are compared by signal to noise ratio.

Implementation of Advanced Signal Processing Techniques on Line-Scan Thermography Data

Fariba Khodayar Fernando Lopez Clemente Ibarra- Castanedo Xavier Maldague

Department of Electrical and Computing Engineering, Laval University

Abstract— In the last few years, composite materials have found an important niche of application in several industries, mainly because of their improved mechanical properties (higher stiffness, strength and resistance to fatigue). In this context, sandwich-composites, a special class of composite materials – are commonly used in the aerospace industry to manufacture lighter components. The increasing use of this type of materials in the aerospace sector has opened the necessity of inspection methods to evaluate its physical integrity and quality. Line Scan Thermography (LST) is one of the emerging technologies aimed to detect and evaluate subsurface defects present in the sandwiches composite structures. As a non-destructive testing and evaluation (NDT&E) technique, LST is a dynamic technique suited to inspect large and complex aerospace components. However, its performance to detect deeper and smaller defects is negatively affected due to the different sources of noise present in the collected thermal images. In this paper is studied the application of advanced signal processing techniques on LST data obtained from the inspection of a large composite component, which contains different types of internal defects located at a variety of depths. To evaluate the ability of each technique to reduce the noise, the signal-to-noise ratio (SNR) at the maximum signal contrast of each defect has been computed for further analysis.

Keywords: non-destructive testing, line scan thermography, signal processing, statistical analysis

I. INTRODUCTION

Composite materials play a significant role in the manufacturing industry of aerospace components due to their improved mechanical properties, such as high resistivity to fatigue and higher strength

[1]. Sandwich-type composites - materials under concern in this work, consist of two thin layers, commonly of Aluminum, fiberglass or carbon fiber, and a lightweight honeycomb core [2].

As already known, the physical integrity and quality of the manufactured aerospace components is one of the major concerns in this industry. The quality of the sandwich-type composites may be compromised by several types of internal defects, such as delaminations, voids, air bubbles and wrinkles [1] [2]. Non-destructive testing (NDT) techniques represent the front line to detect and characterize subsurface defects present in the manufactured components. Currently, a wide spectrum of NDT techniques exists, each one having its strengths and limitations as a function of the physical properties of the material under study, the size and depth of the defects size and the shape of the specimens and component under investigation [3]. Infrared thermography (IR) [4, 5], eddy current thermography [6], ultrasound thermography [7] or thermosonics [8], microwave [9], SQUID magnetic response [1], and X-ray [10], are some of the methods currently used to inspect composite materials [11, 12] .

In this paper, line scan thermography (LST) is investigated as a NDT technique aimed to detect subsurface defects in the a large sandwich composite specimen. LST is a dynamic active thermography technique and one of the emerging technologies aimed to solve key problems in the inspection of complex component (for instance, non-uniform heating due to the irregular shape of the surface under inspection).

In LST the inspection is performed by heating the component, line-by-line, while acquiring a series of thermograms with an IR camera. The inspection head – comprised of the IR camera and the line-heating source - move in tandem, while the field of view (FOV) of the IR camera records the deposition of heat into the component and the subsequent cooling process. The acquired data is then reorganized as a pseudo-static sequence (PSS) for further analysis and processing in a similar

way as is done in the static configuration. Despite this configuration enables to shorten the inspection process, several limitations arise when reorganizing the data in the PSS. It is well-known that without further post processing, the thermographic inspection is limited to near-surface defects and the quantitative analysis using raw data is a difficult – if not impossible – task. In this context, traditional signal processing techniques based on heat conduction models haven been proven to not be suitable to processing the data acquired during the LST inspection.

In this work an alternative way is proposed and is based on the application of advanced statistical algorithms and the Fourier Transforms as signal processing techniques. This paper study the implementation of pulsed phase thermography (PPT) [13], principal components thermography (PCT) [14, 15]and partial least squares thermography (PLST) [16] on the acquired thermal data via LST. After reorganizing the thermal data into the pseudo-static sequence, the above-mentioned algorithms are implemented as signal processing techniques to reduce the noise content in the raw data and improve the depth probing capabilities of the inspection by LST. The signal-tonoise ratio (SNR) at maximum signal contrast is the variable adopted to discuss the capabilities and limitations of each technique.

II. ROBOTIZED LINE SCAN SETUP

Figure 1 depicts the robotic line scanning thermography system used in the research to inspect the sandwich-composite specimen. The NDT system presented herein represents a typical configuration currently used in the aerospace industry. As is shown in Figure 1, the infrared camera and the heat source are both installed on the robot arm.

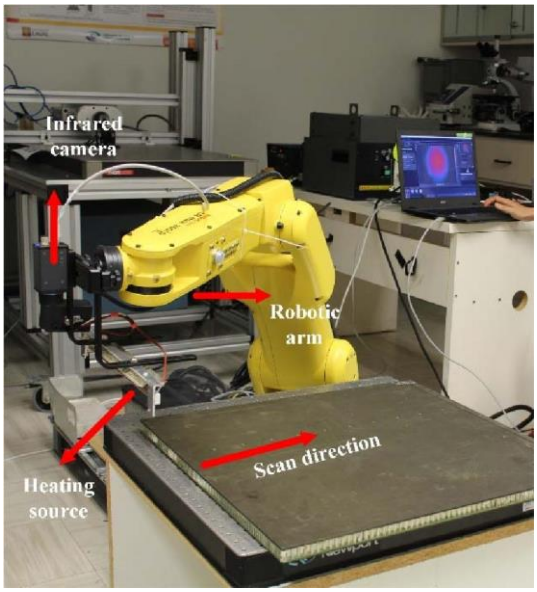

Figure 1. Robotized line scan thermography inspection with low power source

One of the main advantages of this configuration is the ability to provide an uniform heating to the specimen, reducing this way one of the major source of noises (non-uniform heating) that affect the detection of smaller and deeper defects.

The LST inspection system is controlled via a computer software. Through this control software it is possible to adjust all inspection parameters, such as the scanning speed, the distance between the inspection head and the specimen and the acquisition rate. Figures 2 shows the configuration of the specimen studied in this work, along with the position, size and depth of the different artificial defects present in the specimen. The defects are Teflon inserts – which have similar thermophysical properties than the air – and are located between the layers of the composite, simulating delaminations at the interface of the plies. Table 1 shows in details the size and position of the 15 defects contained in the sample test.

The specimen was positioned over a fixed table while the inspection head (comprised by the IR camera and the heat source) scanned the specimen surface. An uncooled microbolometer camera (FLIR A35, LWIR 7.5-13 µm, 320 x 256 pixels) was employed to capture the temperature data and the specimen was heated using a heating line lamp.

In the experimental setup, a 750 W line source was used as a heating unit. The linear speed of the source on the specimen (scanning speed) was 60 mm/sec and the distance between the line source and the surface of the specimen was approximately 10 cm. Once the totality of the specimen is scanned, the acquired thermal data is reorganized into the pseudo-static matrix for further processing.

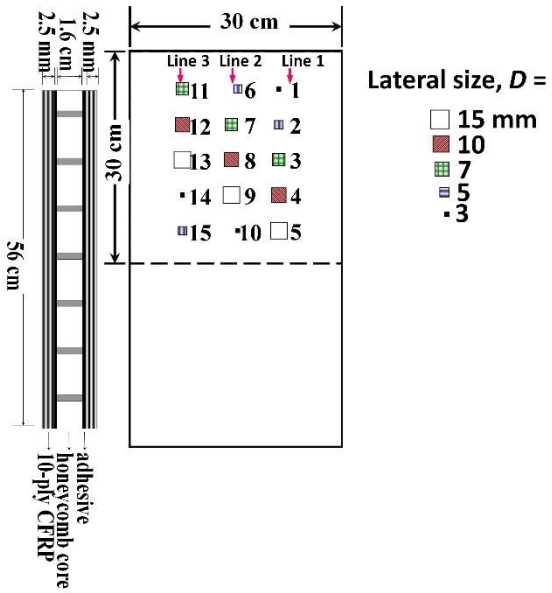

Figure 2. Defect map of the specimen and corresponding depths

TABLE. I. The number of defects and their locations

Defect No.	Depth of defect	Defect No.	Depth of defect	Defect No.	Depth of defect
1	0.25 mm	6	1.5mm	11	0.25mm
2	0.5mm	7	1.75mm	12	0.5mm
3	0.75mm	8	2mm	13	0.75mm
4	1mm	9	2.25mm	14	1mm
5	1.25mm	10	2.25mm	15	1.25mm

III. EXPERIMENTAL RESULTS

Figure 3 shows the reconstructed thermograms (at three different virtual times: 0.33, 2.73 and 3.1 seconds) obtained after the inspection of the composite specimen via LST. The reconstructed raw

images show a misalignment of the position of the defects caused by shifting the object position from one frame to the next. To overcome the effects of misalignment, it has been proposed the implementation of matching algorithms such as iterative closest point (ICP), the interpolation between the initial and final positions of a reference pixel [15].

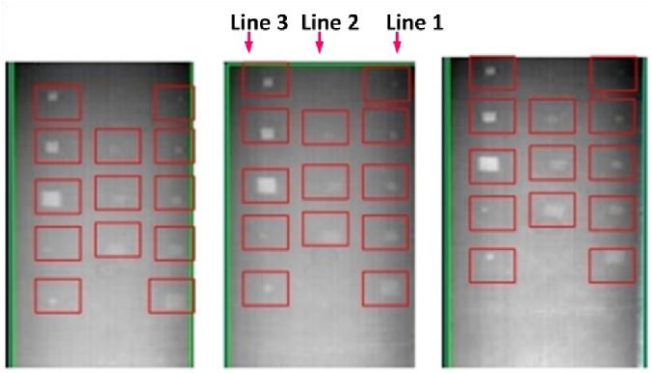

a) At time=0.33 b) at time=2.73 c) at time=3.1

Figure 3. The robotized LST thermography experimental results (raw reconstructed thermograms)

Figure 3 also shows that – without post-processing, it is possible to detect the defects with larger aspect ratio (D/z) and as time elapses, deeper defects can be visible, following a transient heat transfer process. In other words, deeper defects require more time to be detected as in the conventional static NDT configuration. Despite most of the defects are detectable, the quality of the images can be improved by implementing signal processing techniques, allowing to reduce the effects of the different sources of noise that affect the defects, specially those having smaller aspect ratio. Next section provides the fundamentals concepts of PPT, PCT and PLST, which are the techniques subject of investigation in this work.

IV. ADVANCED SIGNAL PROCESSING TECHNIQUES

Thermographic signal processing is a topic that has been widely investigated. In this regard, several algorithms based on the solution of the 1D equation for heat conduction (for instance, thermographic signal reconstruction and differential absolute contrast) have been proposed to

enhance defect visibility [1]. In the other hand, pulsed phase thermography (PPT) is one of the techniques based on space transformation. Based on the discrete Fourier transform (DFT), in PPT the data is transformed from the time domain to the frequency domain. Principal component thermography (PCT) [14, 15] and partial least squares thermography (PLST) [16] are both statistical regression techniques which are based, respectively, on the singular-value and basic latent component

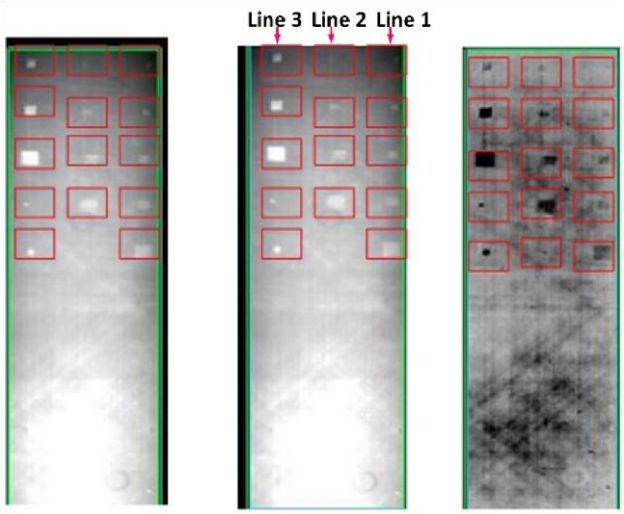

a) PCT(EOF1) b) PPT (amplitude) c) PLS (xloading1)

Figure 4. Results of the implementation of the signal processing techniques on the data acquired via the robotic LST inspection system

decomposition of a predictor (e.g., the thermal data) and predicted (e.g., a time series vector) matrices into a combination of loadings, scores and residuals. The main attraction of these methods is the ability to decompose the thermal data matrix into a set of factors. Each factor is orthogonal to each other and are characterized by its variance; through a carefully analysis of each factor it is possible to associate them to different phenomena that take place during the heating and cooling regime processes of the LST inspection. Thus, it is possible to separate from the regressed sequence those factors associated with noise and with unstable information and keep the most relevant part of the original data. Additionally, these techniques can often be complemented with

quantitative inversion procedures to retrieve defect parameters such as depth, size and material properties [17]. Figure 4 shows the results after the implementation of PCT, PPT and PLST on the thermal data obtained through the inspection of the sandwich composite. It is important to mention that in figure 4c (processed thermogram with PLST), the defects appear in black because of the slope of the temperature decay, which is negative due to the cooling process.

V. SIGNAL TO NOISE RATIO

In this works, the signal-to-noise (SNR) ratio is the variable adopted to evaluate the ability of the processing techniques to reduce the noise content present on the thermographic images. The SNR is a measurement of the physical sensitivity of an imaging system and is used to measure the relationship between the desired signal and the level of background noise [18]. The following expression is used to calculate the SNR [19]:

$$SNR = \frac{Defect\ contrast\ (S_{def} - S_{sa})}{Standard\ deviation\ of\ a\ reference\ area\ (\sigma_{sa})} \qquad (1)$$

This variable allows to determine ability to reduce the noise of each technique based on the inspection parameters, the thermal properties of the material and the aspect ratio of the defects [4, 17, 20]. Figure 5 depicts the computed SNR as a function of the defect number.

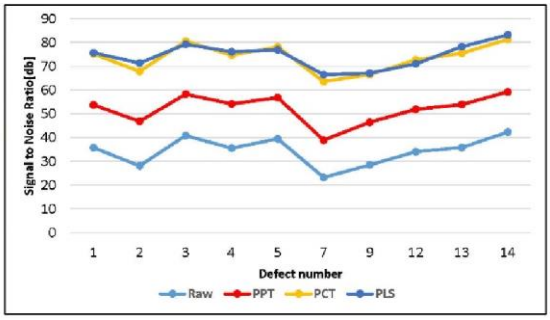

Figure 5. Comparison of SNR for different data processing methods

The results showed that the SNR – and consequently the visibility of the defects, can be increased substantially by implementing the processing techniques discussed in earlier sections. In general,

the SNR values obtained by PLST and PCT are similar. Both techniques are statistical regression techniques, however PCT decomposes the data in empirical orthogonal functions while PLST reconstruct the data using latent components. In the other hand, PPT allows an enhancement in the SNR values but it provides lower effect in comparison with the PLST and PCT.

VI. CONCLUSION

In this paper, the principles of line scan thermography as a non-destructive testing and evaluation technique have been presented as well as its implementation to inspect a large composite material. As pointed out in the first section, LST as an NDT, is well suited to inspect large and complex aerospace components due to its ability provide an uniform heating of the specimen under study in as fast and straightforward manner. Furthermore, this work has presented the implementation of advanced signal processing techniques aimed to reduce the noise content and increase the detectability level. To obtain quantitative insights on the performance of each processing technique, the signal-to-noise ratio at maximum signal contrast was computed for each of the 15 defects of the specimen. The results showed that both multivariate statistical methods – PCT and PLST – provide a substantial improve of the SNR over raw data. It is important to mention that since LST is considered a new approach in NDT (compared with the IR static configurations), the development and implementation of signal processing techniques is a subject currently under investigation.

References

[1] C. Bonavolonta, M. Valentino, G. Peluso, and A. Barone, "Non destructive evaluation of advanced composite materials for aerospace application using HTS SQUIDs," *IEEE Transactions on Applied Superconductivity*, vol. 17, pp. 772-775, 2007.

[2] "Aviation Maintenance Technician Handbook—Airframe " *the United States Department of Transportation, Federal Aviation Administration, Airman Testing Standards Branch, Oklahoma City*, vol. Volume 1, p. Chapter 7, 2012.

[3] S. Sojasi, F. Khodayar, F. Lopez, C. Ibarra-Castando, X. MALDAGUE, V. P. VAVILOV, *et al.*, "Infrared testing of CFRP components: comparisons of approaches using the Tanimoto criterion," in *NDT in Canada 2015 Conference, Edmonton, Canada*, 2015, pp. 1-8.

[4] F. Lopez, C. Ibarra-Castanedo, and X. Maldague, "Pulsed thermography signal processing techniques based on the 1D solution of the heat equation applied to the inspection of laminated composites," *Materials Evaluation*, vol. 72, 2014.

[5] C. Ibarra-Castanedo, N. P. Avdelidis, E. G. Grinzato, P. G. Bison, S. Marinetti, C. C. Plescanu, *et al.*, "Delamination detection and impact damage assessment of GLARE by active thermography," *International Journal of Materials and Product Technology*, vol. 41, pp. 5-16, 2011.

[6] Y. He and R. Yang, "Eddy current volume heating thermography and phase analysis for imaging characterization of interface delamination in CFRP," *IEEE Transactions on Industrial Informatics*, vol. 11, pp. 1287-1297, 2015.

[7] A. Dillenz, T. Zweschper, and G. Busse, "Progress in ultrasound phase thermography," in *Aerospace/Defense Sensing, Simulation, and Controls*, 2001, pp. 574-579.

[8] L. Favro, X. Han, Z. Ouyang, G. Sun, H. Sui, and R. Thomas, "Infrared imaging of defects heated by a sonic pulse," *Review of scientific instruments*, vol. 71, pp. 2418-2421, 2000.

[9] A. Foudazi, M. T. Ghasr, and K. M. Donnell, "Application of active microwave thermography to inspection of carbon fiber reinforced composites," in *2014 IEEE AUTOTEST*, 2014, pp. 318-322.

[10] I. Amenabar, A. Mendikute, A. López-Arraiza, M. Lizaranzu, and J. Aurrekoetxea, "Comparison and analysis of non-destructive testing techniques suitable for delamination inspection in wind turbine blades," *Composites Part B: Engineering*, vol. 42, pp. 1298-1305, 2011.

[11] M. Ibrahim, "Nondestructive evaluation of thick-section composites and sandwich structures: A review," *Composites Part A: Applied Science and Manufacturing*, vol. 64, pp. 36-48, 2014.

[12] S. Gholizadeh, "A review of non-destructive testing methods of composite materials," *Procedia Structural Integrity*, vol. 1, pp. 50-57, 2016.

[13] C. Soutis, "Fibre reinforced composites in aircraft construction," *Progress in Aerospace Sciences*, vol. 41, pp. 143-151, 2005.

[14] D. Kaltmann, "Quantitative line-scan thermographic evaluation of composite structures," 2008.

[15] H. Benítez, X. Maldague, C. Ibarra-Castanedo, H. Loaiza, A. Bendada, and E. Caicedo, "Modified differential absolute contrast using thermal quadrupoles for the nondestructive testing of finite thickness specimens by infrared thermography," in *2006 Canadian Conference on Electrical and Computer Engineering*, 2006, pp. 1039-1042.

[16] C. Ibarra-Castanedo, H. Benítez, X. Maldague, and A. Bendada, "Review of thermal-contrast-based signal processing techniques for the nondestructive testing and evaluation of materials by infrared thermography," in *Proc. Int. Workshop on Imaging NDE (Kalpakkam, India, 25–28 April 2007)*, 2007, pp. 1-6.

[17] F. Khodayar, S. Sojasi, and X. Maldague, "Infrared Thermography and NDT: 2050 Horizon," *Quantitative InfraRed Thermography Journal,Taylor & Francis*, vol. 13, pp. 210-231, 2016.

[18] F. Lopez, C. Ibarra-Castanedo, V. de Paulo Nicolau, and X. Maldague, "Optimization of pulsed thermography inspection by partial least-squares regression," *NDT & E International*, vol. 66, pp. 128-138, 2014.

[19] C. Ibarra-Castanedo, J.-M. Piau, S. Guilbert, N. P. Avdelidis, M. Genest, A. Bendada, *et al.*, "Comparative study of active thermography techniques for the nondestructive evaluation of honeycomb structures," *Research in Nondestructive Evaluation*, vol. 20, pp. 1-31, 2009.

[20] P. Albendea, F. J. Madruga, A. Cobo, and J. M. López-Higuera, "Signal to noise ratio (SNR) comparison for pulsed thermographic data processing methods applied to welding defect detection," in *X International Conference on Quantitative InfraRed Thermography*, 2010.

Chapter VIII

Parameter Optimization of Robotize Line Scan Thermography for CFRP Composite Inspection

8. 1. Résumé

Les matériaux composites jouent un rôle important dans de nombreuses industries en raison de leurs propriétés comme une résistivité élevée à la fatigue et supérieure à la force. En raison de leur structure interlaminaire, les composites distribuent l'énergie de l'impact sur une grande surface en utilisant une matrice polymérique. Cette caractéristique les rend plus résistants aux impacts à faible vitesse, mais elle peut augmenter la probabilité de détection de défauts internes qui ne peuvent pas être observés depuis la surface. La thermographie infrarouge est une méthode intéressante en raison de ses avantages qui sont utilisés pour l'inspection de l'échantillon afin de détecter les défauts. Dans cet article, la méthode LST est employée pour détecter les défauts dans un grand spécimen aérospatial. Certains algorithmes de traitement de données sont utilisés sur les images brutes pour améliorer les résultats (PCA, PPT et PLST). Les critères signal à bruit sont travaillés pour comparer les performances de traitement des données à la réduction du bruit et augmenter la capacité de détection des défauts. Certains paramètres importants contribuent de manière significative à l'amélioration des résultats tels que la vitesse, la source de chaleur, la distance entre la source de chaleur et l'échantillon, etc. La méthode des éléments finis 3D est utilisée pour trouver les paramètres optimaux. Pour ce faire, COMSOL Multiphysics est utilisé pour simuler le modèle. Les résultats expérimentaux sont utilisés pour valider les résultats de la simulation 3D. Après optimisation, le signal sur bruit est amélioré jusqu'à 95% et la profondeur maximale détectée est augmentée à 3,5 mm.

978-1-5090-5538-8/17/$31.00 ©2017 IEEE

8. 2. Summary

Composites materials play an important role in many industries due to their properties as a high resistivity to fatigue and higher than strength. Due to their interlaminar structure, composites distribute the energy of the impact over a large area using a polymeric matrix. This characteristic makes them more resistant to low-velocity impacts, but it may increase the detection probability of internal defects that cannot be observed from the surface. Infrared thermography is an interesting method due to its advantages which is used for the inspection of the specimen to detect the defects. In this paper, LST method is employed to detect the defects in a large aerospace specimen. Some data processing algorithms are employed on the raw images to enhance the results (PCA, PPT and PLST). Signal to noise criteria is worked to compare the data processing performance to noise reduction and increase the defect detection ability. There are some important parameters that have a significant contribution to improving the results such as velocity, heat source, distance between heat source and specimen, and etc. The 3D finite elements method is utilized to find the optimum parameters. For this aim, COMSOL Multiphysics is used to simulate the model. The experimental results are used to validation the results of 3D simulation. After optimization, the signal to noise is enhanced up to 95% and maximum detected depth is increased to 3.5mm.

J Nondestruct Eval September (Published on January 2018)

Parameter Optimization of Robotize Line Scan Thermography for CFRP Composite Inspection

Fariba Khodayar[1], Fernando Lopez[1], Clemente Ibarra-Castanedo[1], Xavier Maldague[1],

[1] MIVIM Laboratory, Electircal Engineering department, Laval University, Quebec, Canada

Abstract. Demands to Composite materials is increasing more and more because of their specific mechanical properties, especially in aerospace industry. Due to the porous structure of composite material, there is the negligible probability of breaking up and defects in the internal structure. Detection of deep defects is a challenging subject in the field of Non-destructive testing. Due to the large size of composite components in the aerospace industry, line scanning thermography (LST) coupled with a robot arm is used to inspect large composite materials. In this paper, an innovative optimization procedure has been employed using analytical model, 3-D simulation using COMSOL Multiphysics, experimental setup and signal processing algorithms. The goal is to maximize the detection depth and signal to noise value as the criteria to evaluate the inspection quality and performance. the proposed algorithm starts searching to find the optimization variables of robotized LST such as scanning speed, source power and distance considering all technical and mechanical constraints. The optimal values are dependent on the material structure, thermal specifications of the composite, defect shape and infrared camera resolution. Using the proposed optimization algorithm, the detection depth was increased to 3.5 mm in the carbon fiber reinforced polymer (CFRP) and the signal to noise ratio was enhanced to 95%.

Keywords: Line scan thermography, Finite Element, Optimization, signal to noise.

1 Introduction

Nowadays, composite materials are widely used in different industries as civil, nuclear, aerospace, renewable energy and automobile industries [1]. Composites can be divided into two groups based on their structure: laminates and sandwich panels. Sandwich-type composites consist of two thin layers, commonly made of Aluminum, fiberglass or carbon fiber, and a lightweight honeycomb core [2]. Laminates are stacked and bonded as fiber-reinforced sheets. These materials play a significant role in today's world due to their improved mechanical properties, such as high resistivity to fatigue and higher strength [3]. Composites offer valuable properties to manufacture complex shaped components with reduced manufacturing time [3]. Due to their interlaminar structure, composites distribute the energy of the impact over a large area using a polymeric matrix. This characteristic makes them more resistant to low-velocity impacts, but it may increase the detection probability of internal defects that cannot be observed from the surface [1]. Therefore, due to the high probability of damaging composite materials, engineers must inspect and evaluate the components during the different steps of manufacturing, service, and maintenance [2, 4].

Non-destructive testing (NDT) techniques are wildly used to detect and characterize sub-surface defects present in the manufactured components. Currently, a variety of NDT techniques exists such as infrared thermography (IR) [5, 6], eddy current thermography [7], ultrasound thermography [8] or thermosonics [9], microwave [10], SQUID magnetic response [4], and X-ray [11], are some of the methods currently used to inspect composite materials [12, 13]. Each one has its strengths and limitations as a function of the physical properties of the material under study, the size, and depth of the defects size and the shape of the specimens and component under investigation [14].

In this paper, parameter optimization of robotized line scan thermography (LST) was investigated in order to maximize the inspection performance of a large CFRP specimen which is used in the aerospace industry. In this technique, a large specimen warms up by a mobile heat source, while acquiring a series of thermograms with an infrared camera [15]. The robotic arm - which carries an infrared camera and the heating source - moves along the surface while the specimen is motionless [15] [16]. Robotized LST method provides some advantages compared to the static thermography. Robotized LST provides heating uniformity through a large specimen and allows image processing to enhance the detection probability, and allows a large-scale component to be inspected without loss of resolution. Using the LST approach, it is possible to inspect large areas at high scan speeds. Also, the inspection results are immediately available for analysis while the scanning process continues [15, 17]. Figure 1 shows the robotized LST scanning setup which was used to scan a large CFRP specimen.

To analyze the LST method, various approaches were proposed in the literature. Researchers employed analytical thermal model, finite element method and compound methods to analyze the LST and increase the performance of the test. In order to estimate the optimum inspection parameters, the heat transfer process that takes place during the LST inspection is simulated using the 3D-FEM approach. COMSOL Multiphysics was the software used to model the problem and to solve the differential equations that govern the heat transfer process [18].

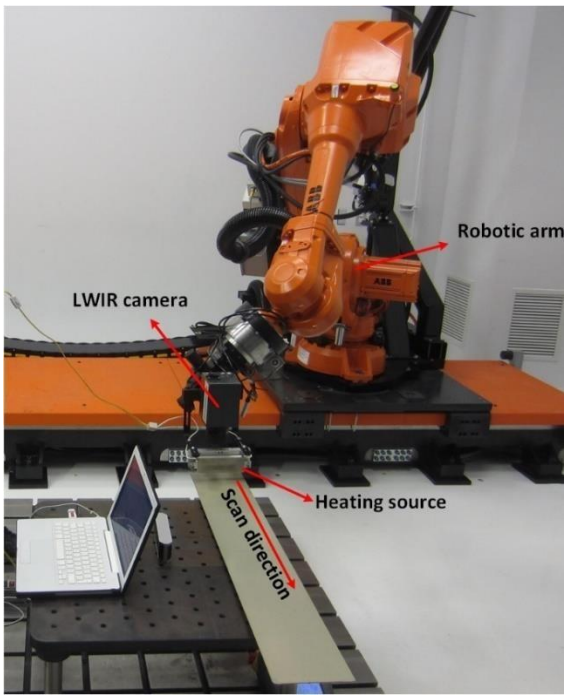

Figure 1. Robotized line scan thermography inspection with low power source

CFRP composites are popular high-technology material, which is widely used in the aerospace industry. The effectiveness of LST is dependent on various parameters such as scanning speed, heat source power, the distance between heat source and specimen, camera resolution, robot driving system etc. In this research, a novel approach has been proposed and developed in order to determine the optimal LST parameters to maximize the thermography performance. To increase the detection probability of defects, several image-processing algorithms are employed. It was proven that the principal component thermography (PCT) provides among the best result in the case of LST issues [19]. In this paper, a combination of analytical model, 3-D finite element analysis, and experimental data was employed to find the optimal LST parameters in term of CFRP scanning. Also, a signal to noise approach was employed as a criterion to estimate the thermography performance. Using optimal parameters, the maximum detected depth increases to 3.5mm, and the signal to noise value enhances to 95%.

2 Robotized Line Scan Setup

Robotized line scanning thermography is made up of a robotized arm, infrared camera and a heat source which provides a dynamic approach for the inspection of large and complex shaped components. The infrared camera and heat source are installed on the robot arm. These components move in tandem, while the specimen remains fixed (see Figure 1). Using a computer program which provides the commands for the robotic arm, it is possible to tune all inspection parameters such as the speed of the inspection heat, the distance between the inspection head and the specimen, acquisition rate, and the scanning velocity. The specimen under study is a 900 mm×150 mm monolithic CFRP panel consisting of 10 sections (1–10 as indicated) with a variable number of CFRP layers (progressively increasing from 6 to 22 plies). Each section has 3 flatbottomed holes of different diameters (6, 8 and 10 mm), for a total of 30 defects located at different depths (from 0.425 to 6.09 mm). The characteristics of the specimen under study are shown in Figure 2. A relation of the depth and diameters of the defects is presented in Table 1, together with the diameter to depth ratios (D/z). A picture of the robotized line scanning setup is shown in Figure 1.

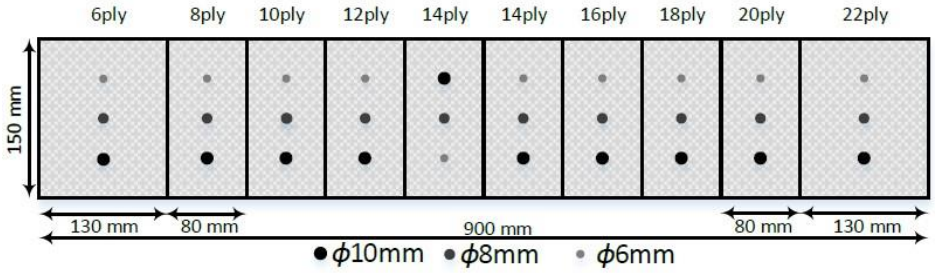

Figure 2. Defect map of the reference panel and corresponding depths

Table 1. Depths and diameter to depth ratios corresponding to the 30 at-bottom-holes of the reference panel

section		1	2	3	4	5	6	7	8	9	10
D=6mm	depth	0.88	0.86	0.63	0.69	0.94	0.99	0.42	0.86	0.54	0.65
	d/z	6.8	7.0	9.5	8.7	10.6	6.1	14.1	7.0	11.0	9.2
D=8mm	depth	1.2	1.4	1.7	2.0	2.2	2.4	2.6	2.9	3.1	3.5
	d/z	6.5	5.7	4.7	4.1	3.6	3.3	3.1	2.7	2.6	2.3
D=10mm	depth	1.5	2.1	2.6	3.2	3.5	3.7	4.2	4.9	5.5	6.1
	d/z	6.6	4.7	3.9	3.2	1.7	2.7	2.4	2.0	1.8	1.6

3 Analytical model

Analytical model is an effective tool to estimate the thermal distribution and determine the effect of each parameter. Several analytical models have been proposed in order to compute the temperature distribution during the thermography process. In the case of LST thermography, there are some analytical models that are more precise than others. The following equation has been proposed for composite materials in 2008 [20].

$$T(x,t) = \frac{q}{\pi k} e^{-\frac{v(x-vt)}{2\alpha}} \left(K_0\left(\frac{v|x-vt|}{2\alpha}\right) 2 \sum_{n=1}^{\alpha} K_o\left(\frac{v\sqrt{(x-vt)^2+4n^2L^2}}{2\alpha}\right)\right) \quad (1)$$

where the term $K_0(x)$ is a modified Bessel function of the second kind of order zero, v is the line-source velocity, L is the specimen thickness, α is thermal diffusivity, t is the observation time and q is the rate of heat emitted per unit length. This equation calculates the temperature on the specimen surface. It is considered that the material is homogenous and the input energy source should be identical for all points in the same line [20]. In the case of CFRP materials, because of their porous structure, the preciseness of the analytical model is not sufficient in order to detect the small defects. Therefore, it is strongly suggested to employ the three-dimensional finite element approach in order to calculate the heat transfer in the material volume. It will be more time consuming, but the result will be closer to the reality.

4 Numerical Simulation of LST

In this research, the robotized LST was simulated using three-dimensional finite element method (3D-FEM). The most important parts are the dynamic heat excitation, CFPR component and mechanical movement that must be simulated. The LST parameters must be tuned to maximize the temperature variation on the material surface and increase the detection probability. COMSOL Multiphysics (thermal module), a powerful simulation software, was employed to study the LST inspection of the CFRP specimen.

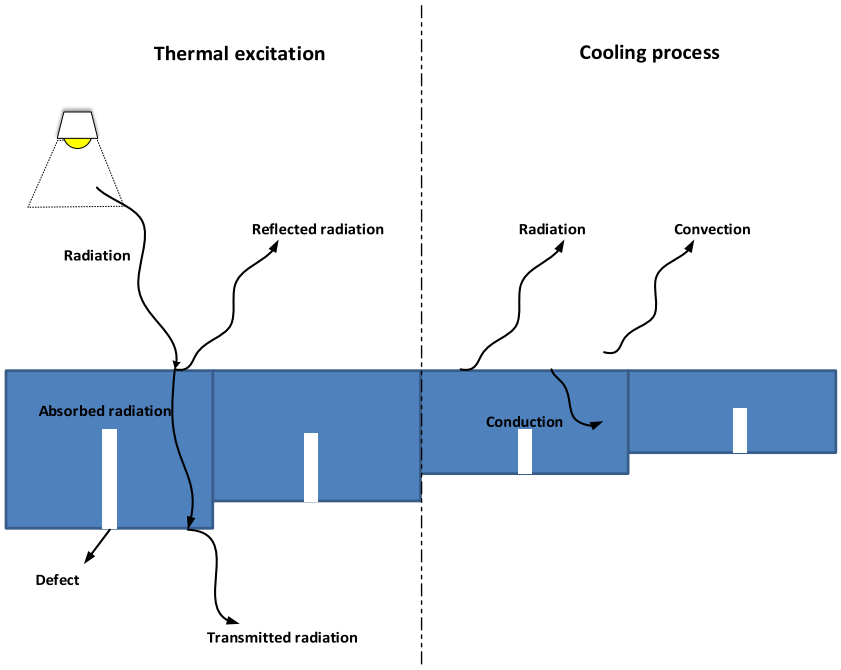

Figure 3. A schematic of the specimen with the heat fluxes participating

In order to simulate the LST thermography in COMSOL Multiphysics (thermal module), the heat transfer module and multi-body dynamics module are used. The heat transfer module is intended to solve the 3D transient energy equation and obtain the temperature distribution in the interlaminar structure of CFRP that contains subsurface defects. The heat transfer module also provides different types of uniform and non-uniform time dependent heat sources [15]. In this

model, the influences of heat conduction, convection, and radiation (surface-to-surface and surface to ambient) are considered and simulated. Figure 3 shows the schematic of the specimen with participating of the heat fluxes. The external excitation is applied by radiation heat transfer. Part of the incident energy is absorbed and the rest is reflected by the material surface. Due to the sudden increase in temperature caused by the thermal excitation, a thermal front is created and this propagates through the rest of the material by heat conduction. Heat transfer by convection and radiation also take places between the material surfaces and the environment. Internal discontinuities are resistive defects: regions of the material with different thermal properties which affect the heat flux rate [21]

The reference panel was positioned over a fixed table and the inspection head over the robot scanned the specimen surface while the camera and heat source moved on the reference panel. An uncooled micro-bolometer camera (Jenoptik IRTCM 384, LWIR 7.5– 14 μm; 384×288 pixels) was used for data acquisition and the specimen was heated using a low power heating line lamp of 500-2000 W.

4.1 Geometry and meshing

Because of the complexity of composite structure, the simulation of CFRP specimen is known as the most important part of LST simulation [22]. The 3D model geometry was designed the same as the CFRP specimen. Figure 4 shows the specimen which consists of 10 sections with various internal layers (progressively increasing from 6 to 22 plies). The number of layers, the defect position, the size and the composite interlaminar direction are most important parameters in the implementation.

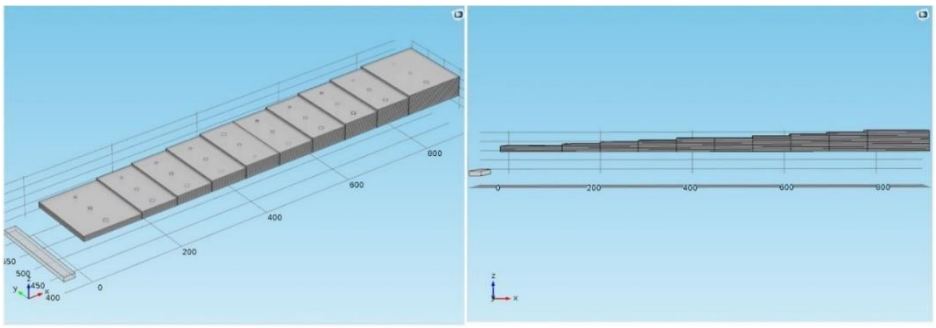

Figure 4. Geometry of the specimen that consists of 10 sections with various layers

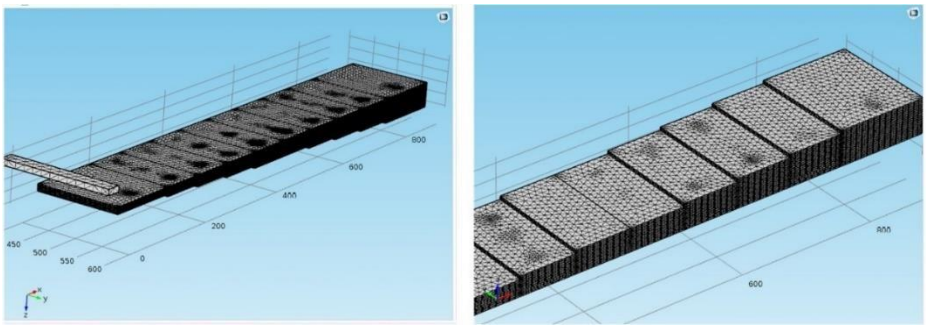

Figure 5. The generated 3D mesh in COMSOL

The next step is to generate the appropriate mesh size. An important step to solve the differential equations is to choose the optimal mesh size. There is a trade-off concerning the accuracy of the results and the simulation time. A finer mesh size increases the accuracy; however, it increases simulation time and requires more computational resources. Due to the interlaminar structure of composite material, it may be difficult to generate the mesh in the intersections and therefore it may be difficult to achieve convergence [23]. Due to the motion of the specimen and the generated mesh, the final data volume may be too large and thus impossible to store before the completion of the simulation. Considering all constraints, the generated mesh consists of 196848 tetrahedral elements and the mesh size is finer in the intersections, defect walls and between the composite layers. Figure 5 shows the generated mesh in COMSOL 3D.

4.2 Governing Equations

The transient heat transfer and temperature distribution in the 3D geometry are described by differential equations. The mathematical model for heat transfer in solids is [24, 25]:

$$\rho C_p \frac{\partial T}{\partial t} = \left[\frac{\partial}{\partial x}\left(k_{xx}\frac{\partial T}{\partial x}\right) + \frac{\partial}{\partial y}\left(k_{yy}\frac{\partial T}{\partial y}\right) + \frac{\partial}{\partial z}\left(k_{zz}\frac{\partial T}{\partial z}\right)\right] \quad (2)$$

where ρ is density, C_p is specific heat capacity, T is the temperature field at coordinates x, y and z and t is the variable time. The thermal conductivity is given by k, to simplify the calculation of thermal conductivity of an anisotropic sample that is related to the orientations of the principal axes of the thermal conductivity tensor (k_{xx}, k_{yy}, k_{zz}), it can be given as [22]:

$$k = \sqrt{k_{xx}k_{yy}cos^2\gamma + k_{xx}k_{zz}cos^2\beta + k_{yy}k_{zz}cos^2\theta} \quad (3)$$

where θ, β, γ are, respectively angles between the line source axis and the principal axes of thermal conductivity x, y and z [22]. In this paper it, was assumed that $k_{xx} = k_{yy} = k_{zz}$ .Considering that at the beginning of the LST inspection the entire specimen was at ambient temperature, the initial condition is given by the following expression [25]:

$$T(x, y, z, t_0) = T_{amb} \quad (4)$$

The following equation presents the heat transfer by convection and radiation between the surfaces of the specimen and the ambient temperature [24, 25]:

$$n.(k\nabla T) = h_{conv}(T_{amb} - T) + \sigma\varepsilon({T_{amb}}^4 - T^4) \quad (5)$$

where h_{conv} is the convective heat transfer coefficient, ε is the emissivity of the material and σ is the Stefan-Boltzmann constant. The simulation parameters as well as the thermophysical properties of the specimen as shown in table 2. The important parameters of LST setup are the source power, scanning speed and the distance between the specimen and the source. To find the

optimal value, the simulation has been done utilizing a range of value for each parameter. Figure 6 Shows the results of 3-D simulation in different scanning speeds at different time.

Table 2. Simulation parameters used in the numerical simulation

Symbol	Simulation parameters	value
T_{amb}	Ambient temperature	293.15 K
T_0	Initial temperature	293.15 K
$H \times L \times W$	Specimen dimension	$(\delta \times$ number of layers$) \times 900mm \times 150mm$
δ	Ply thickness	2 mm
u	Velocity	10 mm/sec
h	Convection heat transfer	9.1
ρ_{CFRP}	Density (CFRP)	1500 kg/m^3
C_{pCFRP}	Specific heat (CFRP)	1000 J/(kg.K)
k_{CFRP}	Thermal conductivity (CFRP) $(k_{xx} = k_{yy} = k_{zz})$	24 W/(m.K)
ρ_T	Density (Teflon)	2200 kg/m^3
C_{pT}	Specific heat (Teflon)	1050 J/(kg.K)
k_T	Thermal conductivity (Teflon)	0.25 W/(m.K)
ε	Emissivity	0.98

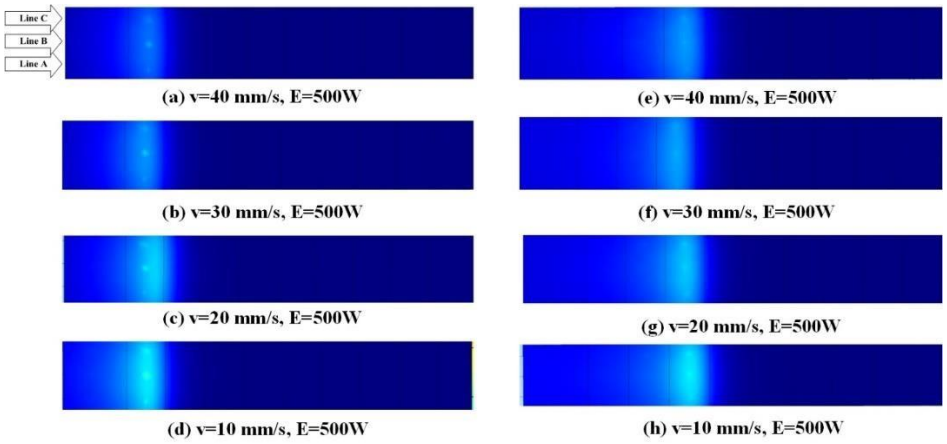

Figure 6. The surface temperature variation in the different scanning speed (simulation)

5 Experimental Setup

Robotized linear scanning thermography tests have been done to evaluate and prove the reliability of the theoretical models. The experimental results were employed achieving two different goals. The first goal was to evaluate and verify the 3-D simulation and correct the proposed model. The

second goal is to find the optimal parameters of LST setup in case of the inspection of CFRP materials. The linear speed of the source on the specimen, the power of the source and the distance between the source and specimen were selected from a range in order to find the optimal parameters. During the experimental implementation of LST, due to the specimen length, the infrared camera covered only a part of the specimen at a time. Therefore, the pseudostatic matrix reconstruction approach is utilized to produce a static image of the specimen, thus allowing a better analysis of the produced data and the possibility to apply post-processing techniques to the acquired thermal images [19] [15]. The experimental parameters are shown in Table 3.

Table 3. Experimental parameters

Experimental Parameter	Value
Heat source	500-2000W
Length of heat source	150 mm
Width of heat source	2 mm
Distance between source and specimen	7 cm
Length of projected line	950 mm
Velocity	5-40 mm/sec

The variation ranges are selected based on the simulation results. Figure 7 and 8 show the results of LST thermography versus the scanning velocity and source power, respectively. These results were provided from the pseudo-static matrix reconstruction approach and PCT filter [15].

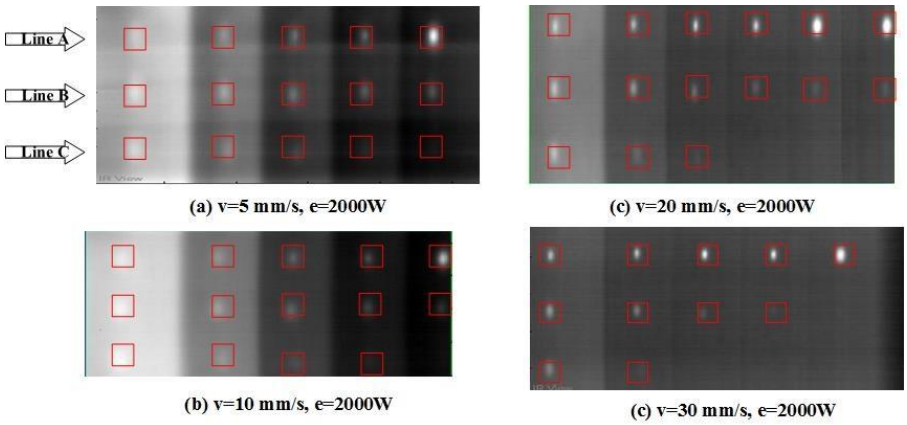

Figure 7. The robotized LST results in different scanning speed

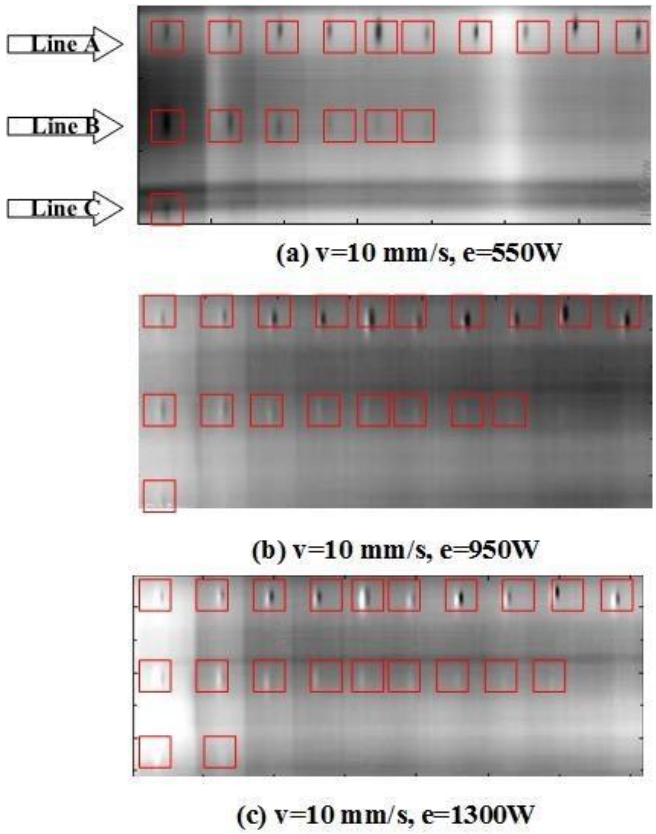

Figure 8. The robotized LST results in different source power

6 Result Analysis and Optimization

Figure 9 shows the algorithm of optimization including optimization variables, constraints and goal function and mathematical model. The optimization variables are source power, velocity, and

distance from the specimen. Constraints are a limitation of source power such as the maximum power of the source and its power supply, mechanical limitation of robot arms such as velocity, linear range, and vibration that depend on robot arm design. There is a limited range for each robot arm that can work with constant speed without any vibration. The goal function is to maximize the inspection performance to detect deeper and smaller defects.

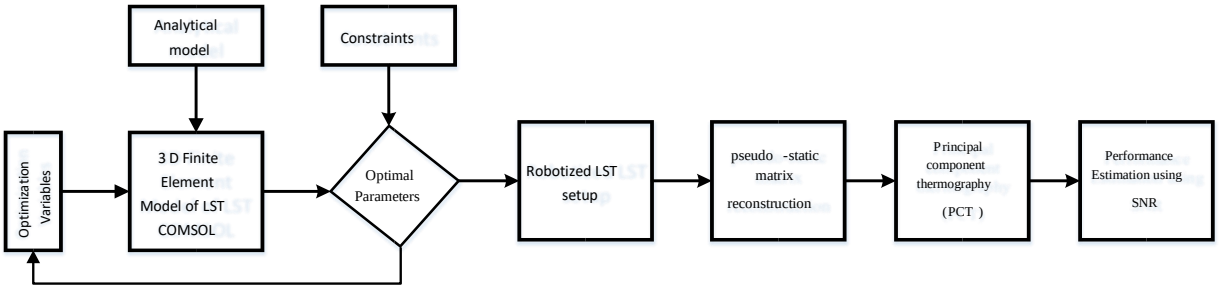

Figure 9. Proposed optimization algorithm of robotized line scan thermography

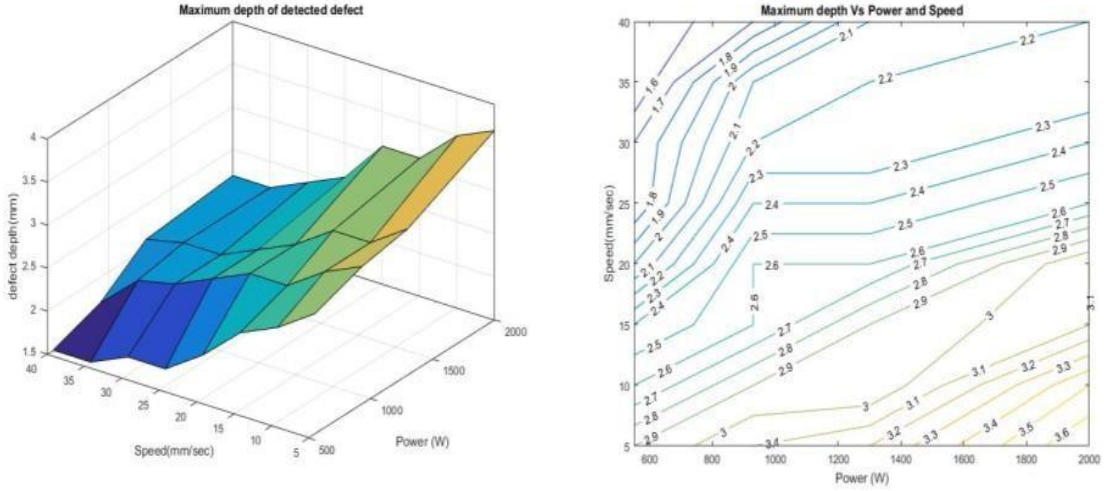

a) Maximum detected depth Vs speed b) Contour of detected depth Vs and power speed and power

Figure10. The maximum detected defect's depth versus scanning speed and source power

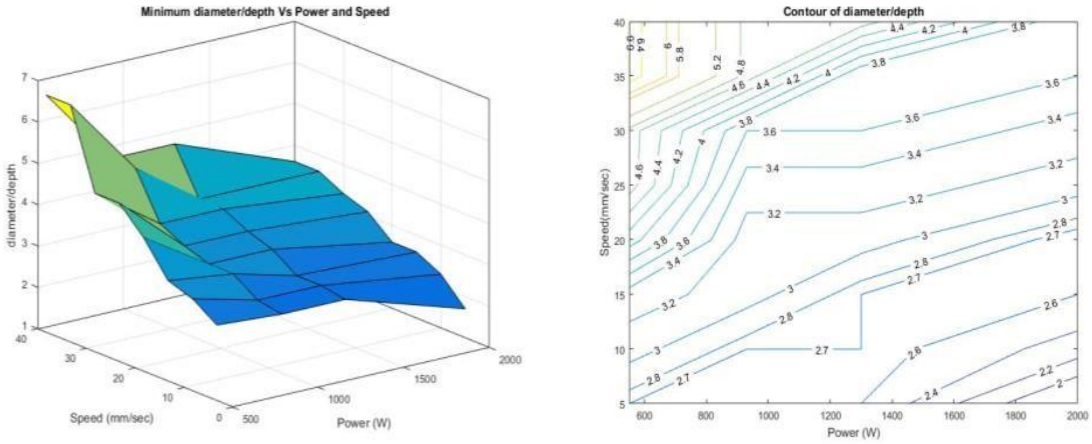

a) Diameter/depth Vs speed and power b) Contour of diameter/depth Vs speed and power

Figure 11. The minimum diameter per depth versus scanning speed and source power

The performance of LST inspection was evaluated using three criteria. In the case of CFRP material, increasing the defect depth strongly affects the inspection quality that is evaluated using several criteria such as maximum detected depth, minimum diameter, and signal to noise ratio. Also, the defect diameter per depth is a popular criterion to evaluate the inspection quality. To find the optimal point, the performance of LST inspection is calculated versus the source power and linear speed. Therefore, 3D curve and contour of the inspection criteria are calculated. Figure 10 shows the 3D curve and contour of maximum detected depth versus the scanning speed and source power. Increasing the source power enhances the detection probability while increasing the scanning speed decreasing the maximum detected depth. The contour shows that to find the deeper defects, larger source power is needed. On the other hand, it should be considered that utilizing higher power to increase the possibility of saturation in shallow defects.

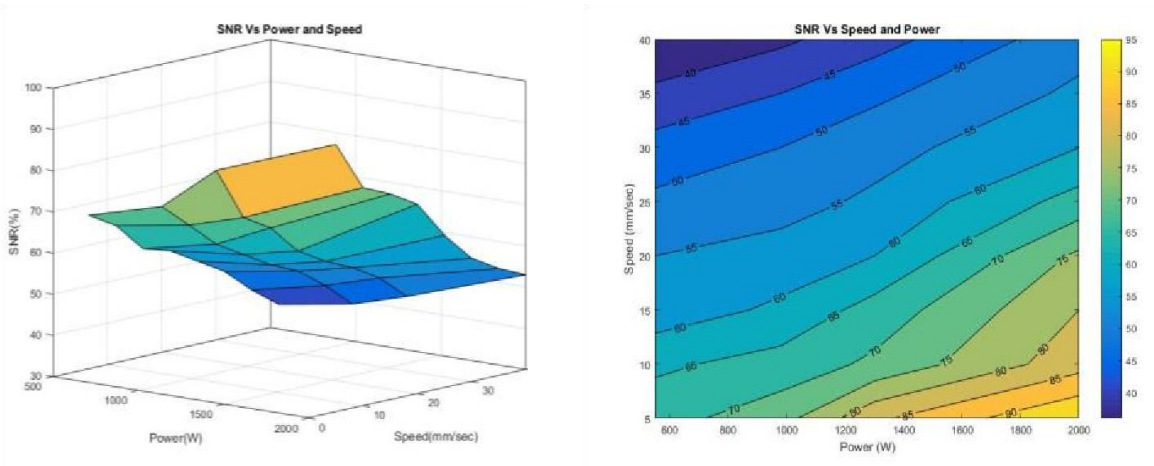

a) SNR Vs scanning speed and b) Contour of SNR Vs scanning speed power and power

Figure 12. The SNR value versus scanning speed and source power

Depth parameter is not a perfect criterion to evaluate the test performance. Therefore, the diameter per depth of defect was defined as a criterion to compute the LST performance. Figure 11 shows the 3D curve and contour of minimum diameter/depth versus scanning speed and source power. The diameter per depth provides more information about inspection quality. This criterion strongly is sensitive to scanning speed. On the other words, the inspection sensitivity against the scanning speed is more than the source power. It is possible to use this criterion with lower source power to avoid saturation effect.

One of the most popular factors, which is used to show the inspection quality, is the signal to noise (SNR) ratio. The SNR value shows the probability of defect detection in LST inspection. Also, it shows the performance of image processing algorithms such as PCT which are used to reduce the noise and enhance the inspection quality. Table 4 shows SNR value for experimental data.

Table 4. SNR value for experimental data

speed / power	550 W	930 W	1300 W	2000W
5 mm/sec	67.5	72.8	82.9	95
10 mm/sec	64	67	71	89
20 mm/sec	65.3	56.2	58.3	76
30 mm/sec	46.5	48.7	52.5	60

Experimental data Calculated using 3D FEM

Figure 12 shows the 3D curve and contour of SNR value versus scanning speed and source power. Using optimal values and PCT filter, the value of SNR increased up to 95%.

7 Conclusion

In this paper, a novel systematic algorithm has been proposed and developed in order to optimize the parameters of robotized LST thermography of CFRP materials. Due to the porous structure of CFRP, detection of the deeper defect is complex and challenging in NDT field. The performance of LST inspection depends on various parameters such as scanning speed, heat source power, distance from specimen and camera resolution. The analytical model of LST was employed to initialize the three-dimensional finite element simulation using COMSOL Multiphysics (thermal module). The optimal parameters of the simulation are used by experimental setup and the results are utilized to correct the simulation parameters of CFRP and LST parameters. Signal processing algorithm such as PCT was employed to eliminate the noise and increase the detection probability. The maximum depth per diameter and signal to noise ratio were used as the criteria to evaluate the inspection performance. After optimization, the detection depth in CFRP material increased up to 3.5 mm and the signal to noise ratio was enhanced up to 95%.

Acknowledgements: The authors are thankful for the support of the following organizations which help to fund our research activities: Natural Science and Engineering Research Council of Canada, Canada Research Chair Secretariat, Ministre des Relations Internationales du Quebec and Quebec-Wallonia/Brussels Program, Visioimage Ltd., Centre.

References

[1] C. Bonavolontà, M. Valentino, C. Meola, G. Carlomagno, R. Volponi, and I. Rosca,"Non-destructive testing of a carbon-nanotube-reinforced composite using HTSSQUID and electromagnetic techniques," *Superconductor Science and Technology,* vol. 22, p. 095001, 2009.

[2] "Aviation Maintenance Technician Handbook—Airframe " the United States Department of Transportation, Federal Aviation Administration, Airman Testing Standards Branch, Oklahoma City, vol. Volume 1, p. Chapter 7, 2012."

[3] C. Soutis, "Fibre reinforced composites in aircraft construction," *Progress in Aerospace Sciences,* vol. 41, pp. 143-151, 2005.

[4] C. Bonavolonta, M. Valentino, G. Peluso, and A. Barone, "Non destructive evaluation of advanced composite materials for aerospace application using HTS SQUIDs," *IEEE Transactions on Applied Superconductivity,* vol. 17, pp. 772-775, 2007.

[5] F. Lopez, C. Ibarra-Castanedo, and X. Maldague, "Pulsed thermography signal processing techniques based on the 1D solution of the heat equation applied to the inspection of laminated composites," *Materials Evaluation,* vol. 72, 2014.

[6] C. Ibarra-Castanedo, N. P. Avdelidis, E. G. Grinzato, P. G. Bison, S. Marinetti, C. C. Plescanu, *et al.*, "Delamination detection and impact damage assessment of GLARE by active thermography," *International Journal of Materials and Product Technology,* vol. 41, pp. 5-16, 2011.

[7] Y. He and R. Yang, "Eddy current volume heating thermography and phase analysis for imaging characterization of interface delamination in CFRP," *IEEE Transactions on Industrial Informatics,* vol. 11, pp. 1287-1297, 2015.

[8] A. Dillenz, T. Zweschper, and G. Busse, "Progress in ultrasound phase thermography," in *Proc. SPIE,* 2001, pp. 574-579.

[9] L. Favro, X. Han, Z. Ouyang, G. Sun, H. Sui, and R. Thomas, "Infrared imaging of defects heated by a sonic pulse," *Review of scientific instruments,* vol. 71, pp. 24182421, 2000.

[10] A. Foudazi, M. T. Ghasr, and K. M. Donnell, "Application of active microwave thermography to inspection of carbon fiber reinforced composites," in *AUTOTESTCON, 2014 IEEE,* 2014, pp. 318-322.

[11] I. Amenabar, A. Mendikute, A. López-Arraiza, M. Lizaranzu, and J. Aurrekoetxea, "Comparison and analysis of non-destructive testing techniques suitable for delamination inspection in wind turbine blades," *Composites Part B: Engineering,* vol. 42, pp. 1298-1305, 2011.

[12] M. Ibrahim, "Nondestructive evaluation of thick-section composites and sandwich structures: A review," *Composites Part A: Applied Science and Manufacturing,* vol. 64, pp. 36-48, 2014.

[13] S. Gholizadeh, "A review of non-destructive testing methods of composite materials," *Procedia Structural Integrity,* vol. 1, pp. 50-57, 2016.

[14] S. Sojasi, F. Khodayar, F. Lopez, C. Ibarra-Castando, X. MALDAGUE, V. P. VAVILOV, *et al.*, "Infrared testing of CFRP components: comparisons of approaches using the Tanimoto criterion," in *NDT in Canada 2015 Conference, Edmonton, Canada,* 2015, pp. 1-8.

[15] C. Ibarra-Castanedo, P. Servais, A. Ziadi, M. Klein, and X. Maldague, "RITARobotized Inspection by Thermography and Advanced processing for the inspection of aeronautical components," in *12th International Conference on Quantitative InfraRed Thermography,* 2014.

[16] D. F. Woolard and K. E. Cramer, "Line scan versus flash thermography: comparative study on reinforced carbon-carbon," in *Defense and Security*, 2005, pp. 315-323.

[17] F. Khodayar, F. Lopez, C. Ibarra-Castanedo, and X. Maldague, "Implementation of advanced signal processing techniques on Line-Scan Thermography data," in *Electrical and Computer Engineering (CCECE), 2017 IEEE 30th Canadian Conference on*, 2017, pp. 1-4.

[18] N. V. Aieta, P. K. Das, A. Perdue, G. Bender, A. M. Herring, A. Z. Weber, *et al.*, "Applying infrared thermography as a quality-control tool for the rapid detection of polymer-electrolyte-membrane-fuel-cell catalyst-layer-thickness variations," *Journal of Power Sources,* vol. 211, pp. 4-11, 2012.

[19] F. Khodayar, F. Lopez, C. Ibarra-Castanedo, and X. Maldague, "Optimization of the Inspection of Large Composite Materials Using Robotized Line Scan Thermography," *Journal of Nondestructive Evaluation,* vol. 36, p. 32, 2017.

[20] D. Kaltmann, "Quantitative line-scan thermographic evaluation of composite structures," 2008.

[21] F. d. J. L. Rodríguez, "Detecção e caracterização de defeitos internos por termografia infravermelha pulsada," 2014.

[22] R. Sweeting and X. Liu, "Measurement of thermal conductivity for fibre-reinforced composites," *Composites Part A: applied science and manufacturing,* vol. 35, pp. 933938, 2004.

[23] A. M. Thiele, A. Kumar, G. Sant, and L. Pilon, "Effective thermal conductivity of three-component composites containing spherical capsules," *International Journal of Heat and Mass Transfer,* vol. 73, pp. 177-185, 2014.

[24] V. Pasquale, M. Verdoya, and P. Chiozzi, *Geothermics: heat flow in the lithosphere*: Springer, 2014.

[25] "Multiphysics C. Heat Transfer Module User's Guide. Comsol AB Group. 2006:1-222."

Conclusion and future works

1. Conclusion

In this thesis, the theorical model, simulation, implementation and optimization of line scan thermography applied to the large composite material were presented, investigated and developed. This dissertation is composed of eight chapters. Chapters 1 and 2 presented a literature review on the popular NDT methods and their applications, Composite materials and specifications, instruments and infrared camera, and the horizons of thermography in 2050. Also, line scan thermography was introduced as an effective and fast approach to inspect the large composite material spcially in the sensitive industries such as aerospace and military. Chapter 2 is composed of a published literature review paper which was published in Quantitative Infrared Themrography Journal by Taylor & Francis Publications.

Chapter 3 presented a review on the most popular data processing algorithms in thermography applications. Thermographic signal reconstruction (TSR), Differential absolute contrast (DAC), Pulse Phase Thermography (PPT), Principal component analysis (PCA), and Partial least square Thermography (PLST) are the most important data processing algorithms which were investigated in terms of theory, application, effectiveness, properties, and advantages. Also, three evaluation criteria were introduced and investigated to evaluate and estimate the performance of data processing algorithms on the raw data.

Chapter 4 presented the step by step procedure to simulate the line scan thrermography using numerical approach in COMSOL Multiphysics. COMSOL Multiphysics employed finite element approach to solve the derivative equations. The simulation procedure includes geometry definition,

material selection, mesh generation, solving, and result analysis. The most complex parts of the simulation is to define the CFRP material, light heat source, and linear motion of the source and camera. The results of 3-D simulation of line scan thermography were investigated in order to find the optimal value of the inspection parameters.

Chapter 5 investigated the performance of data processing and algorithms were evaluated and compared using Tanimoto criterion in the case of static thermography. This chapter includes a conference paper which was published in NDT in Canada 2015 Conference.

In chapter 6, the effect of different data processing algorithms in LST thermography were investigated and compared. The procedure of reconstructed raw matrix of LST was presented and used to generate the static data from LST data. The performance of of various data processing algorithms such as PPT, TSR, PCT, and PLSR were evaluated using PoD criterion. This chapter includes an original research paper which was published in the Journal of Nondestructive Evaluation (Springer).

In chapter 7, various data processing algorithms such as PPT, TSR, PCT and PLSR were employed to enhance the LST inspection quality. Different experimental data of LST was employed to evaluate the performance of data processing algorithms. To determine the performance of algorithms, signal to noise (SNR) criterion was used. This chapter includes a research paper which was published in 30th IEEE Canadian Conference on Electrical and Computer Engineering (CCECE).

In chapter 8, a systematic approach was proposed and developed to find the optimal parameters of LST inspection using a composition of analytical model, 3-D finite element simulation and experimental data. After parameter optimization, the signal to noise value was enhanced to 95%. Also, the detection depth in CFRP material increased up to 3.5 mm under the surface. This chapter

includes an original research paper which was published to the Journal of Nondestructive Evaluation (Springer).

As results, the contributions of this thesis are listed below:

1- Investigation of CFRP material and its numerical model
2- Investigation of LST thermography, properties, advantages and disadvantages
3- Investigation of Analytical thermal model of LST for CFRP materials
4- Three-dimentional finite element thermal simulation of LST thermography including CFRP model, light source and movement using COMSOL multiphysics.
5- Implementation of robotized line scan thermography testing a CFRP specimen including different size of defect with different depths.
6- Implementation of data processing methods on the LST data to enhance the performance of the test
7- Evaluation of the LST performance different criteria such as signal to noise (SNR), probability of detection (PoD), and Tanimoto criterion
8- Parameter optimization of LST thermography using a composition of analytical model, 3D finite element simulation and experimental data
9- Utilizing the optimal parameters, the maximum detected depth in CFRP material was increased up to 3.5 mm under the surface. Also, the signal to noise criterion was enhance up to 95%.

2. Future works

As future works, it is recommended to make the optimization of the LST parameters according to the material and shape of specimen and defects. Hence, the optimization parameters should be

increased and more data is needed for evaluation. On the other hand, it is strongely recommended to work on the mesh optimization in order to reduce the simulation time and increase the accuracy. There are other data processing algorithm such as wavelet, modified PCT which could be employed for LST data. Also, It should be noted that the optimal parameters are calculated according to the CFRP properties. The optimiazation could be repeated for other materials.

3. Acknowledgments

Since I started working in MIVIM laboratory as PhD student, I received the support from many people. I would like to express my appreciation to my supervisor, Professor Xavier Maldague, for his great guidance and encouragement.

I would like to extend myappreciation to the Jury members for their great comments and assist to enrich the quality of this thesis.

I would like to thanks Dr. Clemente Ibarra-Castanedo, who had a great contribution to gather the robotized LST inspection data. Also, I would like to thanks Dr. Fernando Lopez who helped to analyze the LST data and mesh optimization of 3D simulation.

Finally, I am thankful for the support of the following organizations which help to fund our research activities: Natural Science and Engineering Research Council of Canada, Canada Research Chair Secretariat, Ministre des Relations Internationales du Quebec and Quebec-Wallonia/Brussels Program, Visioimage Ltd.

References

[1] S. Bagavathiappan, B. Lahiri, T. Saravanan, J. Philip, and T. Jayakumar, "Infrared thermography for condition monitoring–a review," *Infrared Physics & Technology*, vol. 60, pp. 35-55, 2013.

[2] "Preventive and Predictive Maintenance. Web [cited 2016 Feb 15]. Available from: https://www.lce.com/pdfs/The-PMPdM-Program-124.pdf."

[3] "Predictive Maintenance Technologies. Web [cited 2016 Feb 15]. Available from: https://www1.eere.energy.gov/femp/pdfs/om_6.pdf."

[4] "About ASNT. Introduction to nondestructive testing. Web [cited 2015 Apr 12]. Available from:https://www.asnt.org/MinorSiteSections/AboutASNT/Intro-to-NDT."

[5] "NDT and Training. N D T and NDT online training – 218-270-3182 – Hutchinson and Brainerd and MN NDT and training, N D T and NDT online training – 218-270-3182 – Hutchinson and Brainerd and MN. Web [cited 2015 Apr 12]. Available from: http://trainingndt.com."

[6] S. Sojasi, F. Khodayar, F. Lopez, C. Ibarra-Castando, X. MALDAGUE, V. P. VAVILOV, *et al.*, "Infrared testing of CFRP components: comparisons of approaches using the Tanimoto criterion," in *NDT in Canada 2015 Conference, Edmonton, Canada*, 2015, pp. 1-8.

[7] "Introduction to Nondestructive Testing." NDT Resource Center. Web. 29 July 2015.."

[8] F. Khodayar, S. Sojasi, and X. Maldague, "Infrared thermography and NDT: 2050 horizon," *Quantitative InfraRed Thermography Journal*, vol. 13, pp. 210-231, 2016.

[9] X. Maldague, "Theory and practice of infrared technology for nondestructive testing," 2001.

[10] A. Karim and J. Y. Andersson, "Infrared detectors: Advances, challenges and new technologies," in *IOP Conference Series: Materials Science and Engineering*, 2013, p. 012001.

[11] S. Ness, C. N. Sherlock, P. O. Moore, and P. McIntire, *Nondestructive testing overview*: American Society for Nondestructive Testing, 1996.

[12] A. Rogalski, "Infrared detectors: status and trends," *Progress in quantum electronics*, vol. 27, pp. 59-210, 2003.

[13] F. Lopez, C. Ibarra-Castanedo, and X. Maldague, "Pulsed thermography signal processing techniques based on the 1D solution of the heat equation applied to the inspection of laminated composites," *Materials Evaluation*, vol. 72, 2014.

[14] C. Ibarra-Castanedo, M. Genest, J.-M. Piau, S. Guibert, A. Bendada, and X. P. Maldague, "Active infrared thermography techniques for the nondestructive testing of materials," *Ultrasonic and advanced methods for nondestructive testing and material characterization*, pp. 325-348, 2007.

[15] C.-H. Chen, *Ultrasonic and advanced methods for nondestructive testing and material characterization*: World Scientific, 2007.

[16] J. García-Martín, J. Gómez-Gil, and E. Vázquez-Sánchez, "Non-destructive techniques based on eddy current testing," *Sensors*, vol. 11, pp. 2525-2565, 2011.

[17] N. K. Anuar, W. T. Wui, D. K. Ghodgaonkar, and M. N. Taib, "Use of microwave nondestructive testing (NDT) technique to characterize the film for applications in transdermal drug delivery system," in *Sensors and the International Conference on new Techniques in Pharmaceutical and Biomedical Research, 2005 Asian Conference on*, 2005, pp. 31-33.

[18] C. Ibarra-Castanedo, J.-M. Piau, S. Guilbert, N. P. Avdelidis, M. Genest, A. Bendada, *et al.*, "Comparative study of active thermography techniques for the nondestructive evaluation of honeycomb structures," *Research in Nondestructive Evaluation*, vol. 20, pp. 1-31, 2009.

[19] M. Tarin and R. Rotolante, "NDT in Composite Materials with Flash, Transient, and Lock-in Thermography," *FLIR Systems, Inc*, pp. 1-4, 2011.

[20] N. Avdelidis, T. Gan, C. Ibarra-Castanedo, and X. Maldague, "Infrared thermography as a non-destructive tool for materials characterisation and assessment," *SPIE Defense, Security, and Sensing*, pp. 801313-801313, 2011.
[21] C. Meola and G. Carlomagno, "The role of infrared thermography in NDT," in *Nondestructive Testing of Materials and Structures*, ed: Springer, 2013, pp. 91-96.
[22] R. Montanini and F. Freni, "Correlation between vibrational mode shapes and viscoelastic heat generation in vibrothermography," *NDT & E International*, vol. 58, pp. 43-48, 2013.
[23] A. Mendioroz, A. Castelo, R. Celorrio, and A. Salazar, "Characterization and spatial resolution of cracks using lock-in vibrothermography," *NDT & E International*, vol. 66, pp. 8-15, 2014.
[24] "Aviation Maintenance Technician Handbook—Airframe " the United States Department of Transportation, Federal Aviation Administration, Airman Testing Standards Branch, Oklahoma City, vol. Volume 1, p. Chapter 7, 2012.."
[25] C. Bonavolonta, M. Valentino, G. Peluso, and A. Barone, "Non destructive evaluation of advanced composite materials for aerospace application using HTS SQUIDs," *IEEE Transactions on Applied Superconductivity*, vol. 17, pp. 772-775, 2007.
[26] F. L. Matthews and R. D. Rawlings, *Composite materials: engineering and science*: Elsevier, 1999.
[27] C. Soutis, "Fibre reinforced composites in aircraft construction," *Progress in Aerospace Sciences*, vol. 41, pp. 143-151, 2005.
[28] C. Ibarra-Castanedo, P. Servais, A. Ziadi, M. Klein, and X. Maldague, "RITA-Robotized Inspection by Thermography and Advanced processing for the inspection of aeronautical components," in *12th International Conference on Quantitative InfraRed Thermography*, 2014.
[29] D. F. Woolard and K. E. Cramer, "Line scan versus flash thermography: comparative study on reinforced carbon-carbon," in *Defense and Security*, 2005, pp. 315-323.
[30] "Automated Thermography in Production Chain." DLR Portal, www.dlr.de/dlr/en/desktopdefault.aspx/tabid-10660/1147_read-4484/.".
[31] C. I. Castanedo, "Quantitative subsurface defect evaluation by pulsed phase thermography: depth retrieval with the phase," Université Laval, 2005.
[32] C. Ibarra-Castanedo, H. Benítez, X. Maldague, and A. Bendada, "Review of thermal-contrast-based signal processing techniques for the nondestructive testing and evaluation of materials by infrared thermography," in *Proc. Int. Workshop on Imaging NDE (Kalpakkam, India, 25–28 April 2007)*, 2007, pp. 1-6.
[33] N. Rajic, "Principal component thermography for flaw contrast enhancement and flaw depth characterisation in composite structures," *Composite Structures*, vol. 58, pp. 521-528, 2002.
[34] D. Kaltmann, "Quantitative line-scan thermographic evaluation of composite structures," 2008.
[35] H. Benítez, X. Maldague, C. Ibarra-Castanedo, H. Loaiza, A. Bendada, and E. Caicedo, "Modified differential absolute contrast using thermal quadrupoles for the nondestructive testing of finite thickness specimens by infrared thermography," in *Electrical and Computer Engineering, 2006. CCECE'06. Canadian Conference on*, 2006, pp. 1039-1042.
[36] F. d. J. L. Rodríguez, "Detecção e caracterização de defeitos internos por termografia infravermelha pulsada," 2014.
[37] N. V. Aieta, P. K. Das, A. Perdue, G. Bender, A. M. Herring, A. Z. Weber, *et al.*, "Applying infrared thermography as a quality-control tool for the rapid detection of polymer-electrolyte-membrane-fuel-cell catalyst-layer-thickness variations," *Journal of Power Sources*, vol. 211, pp. 4-11, 2012.
[38] V. P. VAVILOV and A. O. CHULKOV, "Thermal NDT of Composites in the Aero Space Industry: A Quantitative Approach."
[39] C. Ibarra-Castanedo, A. Bendada, and X. Maldague, "Thermographic image processing for NDT," in *IV Conferencia Panamericana de END*, 2007.
[40] S. M. Shepard, "System for generating thermographic images using thermographic signal reconstruction," ed: Google Patents, 2004.

[41] M. Pilla, M. Klein, X. Maldague, and A. Salerno, "New absolute contrast for pulsed thermography," in *Proc. QIRT*, 2002.
[42] F. Lopez, C. Ibarra-Castanedo, X. Maldague, and V. de Paulo Nicolau, "Analysis of signal processing techniques in pulsed thermography," *SPIE Defense, Security, and Sensing, International Society for Optics and Photonics*, pp. 87050W-87050W, 2013.
[43] F. Lopez, X. Maldague, and C. Ibarra-Castanedo, "Enhanced image processing for infrared non-destructive testing," *Opto-Electronics Review*, vol. 22, pp. 245-251, 2014.
[44] H. D. Benítez, C. Ibarra-Castanedo, A. Bendada, X. Maldague, H. Loaiza, and E. Caicedo, "Definition of a new thermal contrast and pulse correction for defect quantification in pulsed thermography," *Infrared Physics & Technology*, vol. 51, pp. 160-167, 2008.
[45] X. Maldague and S. Marinetti, "Pulse phase infrared thermography," *Journal of applied physics*, vol. 79, pp. 2694-2698, 1996.
[46] "Fourier Transform".www. homepages.inf.ed.ac.uk/rbf/HIPR2/fourier.htm. Retrieved July 30, 2015."
[47] X. Maldague, F. Galmiche, and A. Ziadi, "Advances in pulsed phase thermography," *Infrared physics & technology*, vol. 43, pp. 175-181, 2002.
[48] C. Ibarra-Castanedo, D. Gonzalez, F. Galmiche, X. Maldague, and A. Bendada, "Discrete signal transforms as a tool for processing and analyzing pulsed thermographic data," in *Proc. SPIE*, 2006, pp. 620514-620525.
[49] C. Ibarra-Castanedo and X. Maldague, "Defect depth retrieval from pulsed phase thermographic data on plexiglas and aluminum samples," in *Proc. SPIE*, 2004, pp. 348-356.
[50] C. Ibarra-Castanedo, N. P. Avdelidis, and X. Maldague, "Quantitative pulsed phase thermography applied to steel plates," *Thermosense XXVII*, vol. 5782, p. 222, 2005.
[51] C. Ibarra-Castanedo, M. Genest, P. Servais, X. P. Maldague, and A. Bendada, "Qualitative and quantitative assessment of aerospace structures by pulsed thermography," *Nondestructive Testing and Evaluation*, vol. 22, pp. 199-215, 2007.
[52] S. Marinetti, E. Grinzato, P. G. Bison, E. Bozzi, M. Chimenti, G. Pieri, *et al.*, "Statistical analysis of IR thermographic sequences by PCA," *Infrared Physics & Technology*, vol. 46, pp. 85-91, 2004.
[53] N. Rajic, "Principal component thermography," DEFENCE SCIENCE AND TECHNOLOGY ORGANISATION VICTORIA (AUSTRALIA) AERONAUTICAL AND MARITIME RESEARCH LAB2002.
[54] P. H. Vahid, S. Hesabi, and X. Maldague, "The Effect of Pre-processing Techniques in Detecting Defects of Thermal Images," in *Proceedings of the VIIth International Workshop on Advances in Signal Processing for Non Destructive Evaluation of Materials*, 2013, pp. 53-54.
[55] C. Ibarra-Castanedo, N. Avdelidis, M. Grenier, X. Maldague, and A. Bendada, "Active thermography signal processing techniques for defect detection and characterization on composite materials," *Ralph B. Dinwiddie and Morteza Safai*, vol. 7661, p. 76610O, 2010.
[56] P. Hedayati, "Automatic Defect Detection and Depth Estimation Using Pulsed Thermography," Master of Electrical Engineering, Université Laval, 2014.."
[57] D. Yuxia, "Probability of Detection Analysis for Infrared Nondestructive Testing and Evaluation with Applications Including a Comparison with Ultrasonic " Doctorat en Génie électrique, Université Laval, 2014.."
[58] R. Parvataneni, "Principal component thermography for steady thermal perturbation scenarios," 2009.
[59] H. Abdi, "Partial least square regression (PLS regression)," *Encyclopedia for research methods for the social sciences*, vol. 6, pp. 792-795, 2003.
[60] R. Rosipal and N. Krämer, "Overview and recent advances in partial least squares," *Lecture notes in computer science*, vol. 3940, p. 34, 2006.
[61] F. Lopez, V. Nicolau, X. Maldague, and C. Ibarra-Castanedo, "Multivariate infrared signal processing by partial least-squares thermography," in *international symposium on applied electromagnetics and mechanics. Québec City, Canada*, 2013, pp. 661-666.

[62] F. Lopez, C. Ibarra-Castanedo, V. de Paulo Nicolau, and X. Maldague, "Optimization of pulsed thermography inspection by partial least-squares regression," *NDT & E International*, vol. 66, pp. 128-138, 2014.
[63] P. Bison, A. Bortolin, G. Cadelano, G. Ferrarini, L. Finesso, F. Lopez, *et al.*, "Evaluation of frescoes detachments by partial least square thermography," in *12th International Conference on Quantitative Infrared Thermography, Bordeaux (France)*, 2014, pp. 07-11.
[64] F. López, C. Ibarra-Castanedo, V. Nicolau, and X. Maldague, "Comparative study of Thermographic signal reconstruction and partial least-squares thermography for detection and evaluation of subsurface defects," in *12th International Conference on Quantitative Infrared Thermography, Bordeaux, France*, 2014.
[65] V. P. Vavilov, P. G. Bison, and E. G. Grinzato, "Statistical evaluation of thermographic NDT performance applied to CFRP," in *Thermosense XVIII: An International Conference on Thermal Sensing and Imaging Diagnostic Applications*, 1996, pp. 174-177.
[66] V. Vavilov, X. Maldague, B. Dufort, F. Robitaille, and J. Picard, "Thermal nondestructive testing of carbon epoxy composites: detailed analysis and data processing," *NDT & E International*, vol. 26, pp. 85-95, 1993.
[67] Y. Duan, "Probability of detection analysis for infrared nondestructive testing and evaluation with applications including a comparison with ultrasonic testing," Université Laval, 2014.
[68] Y. Duan, S. Huebner, U. Hassler, A. Osman, C. Ibarra-Castanedo, and X. P. Maldague, "Quantitative evaluation of optical lock-in and pulsed thermography for aluminum foam material," *Infrared Physics & Technology*, vol. 60, pp. 275-280, 2013.
[69] G. A. Georgiou, "PoD curves, their derivation, applications and limitations," *Insight-Non-Destructive Testing and Condition Monitoring*, vol. 49, pp. 409-414, 2007.
[70] G. Georgiou, "Probability of detection (PoD) curves. Derivation, application and limitations, Jacobi Consulting Limited," Research Report 4542006.
[71] C. Müller, M. Elaguine, C. Bellon, U. Ewert, U. Zscherpel, M. Scharmach, *et al.*, "Pod (probability of detection) evaluation of NDT techniques for cu-canisters for risk assessment of nuclear waste encapsulation," in *5Th International Conference on NDE in Relation to Structural Integrity for Nuclear and Pressurized Components, San Diego, CA*, 2006.
[72] G. P. Tran, "Crack Inspection and simulations with Eddy Current Thermography for the Aerospace Industry," Université Laval, 2013.
[73] "COMSOL 4.2 Tutorial,www.che.wsu.edu,2015."
[74] M. Susa, "Numerical modeling of pulse thermography experiments for defect characterisation purposes," Citeseer, 2009.
[75] C. Meola, G. M. Carlomagno, and L. Giorleo, "The use of infrared thermography for materials characterization," *Journal of materials processing Technology*, vol. 155, pp. 1132-1137, 2004.